2008

INVESTIGATING THE TRANSIENT EFFECTS OF TWO-PHASE FLOW IN POROUS MEDIA

Geremy Wayne Camps-Roach

INVESTIGATING THE TRANSIENT EFFECTS OF TWO-PHASE FLOW IN POROUS MEDIA

(Spine title: Transient Two-Phase Flow)

(Thesis format: Monograph)

by

Geremy W. Camps-Roach

Graduate Program in Engineering Science
Department of Civil and Environmental Engineering

A thesis submitted in partial fulfillment
of the requirements for the degree of
Master of Engineering Science

The School of Graduate and Postdoctoral Studies
The University of Western Ontario
London, Ontario, Canada

THE UNIVERSITY OF WESTERN ONTARIO
SCHOOL OF GRADUATE AND POSTDOCTORAL STUDIES

CERTIFICATE OF EXAMINATION

Supervisors	Examiners
Dr. Denis O'Carroll	Dr. Jason Gerhard
Dr. Timothy Newson	Dr. Sean Hinchberger
	Dr. Madhumita Ray

The thesis by

Geremy Wayne Camps-Roach

entitled:

Investigating the Transient Effects of Two-phase Flow in Porous Media

is accepted in partial fulfillment of the
requirements for the degree of
Master of Engineering Science

Date_____

_____
Chair of the Thesis Examination Board

Abstract

Two-phase flow occurs in the unsaturated zone and in aquifers contaminated with non-aqueous phase liquids. The macroscopic flow equations used to predict two-phase flow typically utilizes a capillary pressure-saturation relationship determined under equilibrium conditions. Theoretical and experimental evidence have indicated that this relationship may not be unique, but may depend on the saturation rate. To quantify this dependency, direct measurements of equilibrium and dynamic capillary pressure-saturation relationships were made. For a given saturation, capillary pressure measured under dynamic conditions was shown to be larger than capillary pressure measured under equilibrium conditions, consistent with thermodynamic theory [1]. The damping coefficient τ, was shown to be dependant on porous media properties and the desaturation rate, and independent of the domain size. This implies that two-phase flow simulators should account for dynamic flow when saturation rates are high and for porous media with low intrinsic permeability and high air entry pressures.

Key words: Capillary pressure; Saturation; Two-phase flow; Dynamic effects; Porous media; Unsaturated zone; Volume averaging; Macro scale; Dynamic effect coefficient.

Acknowledgements

Firstly, I thank God the creator for life, health and fortunate circumstances. I sincerely thank my advisors Dr. D. O'Carroll and Dr. T. Newson for all that they have done for me during my studies here at Western. I am thankful for the constant optimism, inspiring ideas and constructive insights which they have shared with me.

I would like to thank the members of my thesis committee for their time and interest in my research. A special thanks to Dr. T. Sakaki. and Dr. M. Celia for their advice and useful discussions on "Dynamic Effects". With a heart full of gratitude, I would like to thank my friends Gaurav ("G-unit") and Stephanie ("SD") for their assistance with experimental work and formatting the thesis. Finally, I would like to thank my family for their continued love and support throughout my life.

Table of Contents

INVESTIGATING THE TRANSIENT EFFECTS OF TWO-PHASE FLOW IN POROUS MEDIA ____ *i*

CERTIFICATE OF EXAMINATION ____ *ii*

Abstract ____ *iii*

Acknowledgements ____ *iv*

List of Tables ____ *vii*

List of Figures ____ *viii*

Glossary of Terms ____ *xi*

Chapter 1 - Introduction ____ *1*

1.0 Aims of the Thesis ____ **5**

Chapter 2 - Literature Review ____ *6*

2.0 Introduction ____ **6**

2.1 Unsaturated Groundwater Flow ____ **6**

2.2 DNAPL Subsurface Contamination ____ **7**

2.3 The Challenge of Multiphase Subsurface Modeling ____ **9**

2.4 Soil Constitutive Relationships ____ **10**

2.5 Relative Permeability ____ **11**

2.6 Capillary Pressure ____ **12**

2.6.1 The Static P_c-S_w Relationship ____ 14

2.6.2 The Dynamic P_c-S_w Relationship ____ 16

2.7 Experimental Evidence of Dynamic Effects in P_c-S_w ____ **19**

2.7.1 The Direct Measurement Method ____ 19

2.7.2 The Inverse Modeling Method ____ 23

2.8 Conclusions ____ **28**

Chapter 3 - Methods and Materials ____ *30*

3.0 Introduction ____ **30**

3.1 Solid, Non-Wetting and Wetting Phases ____ **30**

3.2 1-D Pressure Cell ____ **32**

3.3 P_c-S_w Measurement Instruments ____ **33**

3.3.1 Wetting Phase Tensiometer (WPT) ____ 34

3.3.2 Non-Wetting Phase Tensiometer ____ 35

3.4 FP2000 Pressure Transducer ____ **36**

3.4.1 Pressure Transducer Calibration Procedure ____ 36

3.5 EC-5 Soil Moisture Probe ____ **37**

3.5.1 EC-5 Calibration Procedure ____ 37

3.6 Dry Packing and Saturation Procedure 38
3.7 Saturated Hydraulic Conductivity Measurements 39
3.8 Static and Dynamic Outflow Experiments 42
Chapter 4 - Results *45*
4.0 Introduction 45
4.1 Static Drainage Experiments 46
4.2 Dynamic Drainage Experiments 48
4.3 Statistical Analysis of Measured Static and Dynamic P_c-S_w Curves 60
4.4 Direct Quantification of τ : Method 1 62
4.5 Upscaling Pressures and Saturations 69
4.6 Direct Quantification of τ : Method 2 76
Chapter 5 - Discussion *80*
5.0 Introduction 80
5.1 Desaturation Rate Effects on the Measured P_c-S_w Relationship 80
5.2 Desaturation Rate Effects on τ 86
5.3 Upcaling Effects on τ 86
5.4 Porous Media Property Effects on τ 88
5.5 The Experimentally Determined dP_c vs. dS_w/dt Relationship 89
Chapter 6 - Summary and Conclusions *92*
6.0 Conclusions 92
6.1 Future Work 94
Bibliography *96*
Appendix A: Measured Drainage Parameters *102*
Appendix B: Investigating the Relationship between dP_c and dS_w/dt *117*
Appendix C: EC-5 Soil Moisture Probe Calibration Comparison *128*
Appendix D: Saturated Hydraulic Conductivity Example *135*
VITA *136*

List of Tables

Table 2.1. Common DNAPL contaminants [27, 29, 30] 9

Table 2.2. Summary of τ determined from experimental data 23

Table 3.1. Physical properties of fluids at 20°C 31

Table 4.1. Summary of unsaturated experimental results 46

Table 4.2. A comparison of the measured desaturation rate (dS_w/dt) and residual saturations (S_{rw}) for dynamic drainage experiments 50

Table 5.1. Comparison of the cumulative outflow at the time desaturation first occurs at Level 1. 84

Table 5.2. A comparison of the magnitude of τ and soil properties for dynamic or transient experiments. 88

List of Figures

Figure 2.1. Multiphase flow scenario 8
Figure 2.2. An illustration of the Relative permeability – Saturation relationship [39] ... 12
Figure 2.3. Young's Equation – air-water interfacial tension [4] 13
Figure 2.4. The hysteretic equilibrium P_c-S_w relationship [25] 15
Figure 3.1. Grain size distribution of F35-F50 and F70 Ottawa sand. 31
Figure 3.2. The soil chamber, fitted with ports for P_c-S_w measurement instruments 32
Figure 3.3. Side view of soil chamber 33
Figure 3.4. Cross-sectional view of soil chamber (A-A") 33
Figure 3.5. Ceramic porous cup attached to Swaglok fittings. 34
Figure 3.8. Hydraulic conductivity experimental setup 40
Figure 3.9. Outflow experimental setup 43
Figure 4.1. Measured experimental parameters at levels 1, 2 and 3 for F32-F50 Static Experiment 2: cumulative outflow, tensiometric air pressures (A1, A2 and A3), tensiometric water pressures (W1, W2 and W3) and saturations (S1, S2 and S3) vs. time 47
Figure 4.2. Measured experimental parameter at levels 1, 2 and 3 for F32-F50 Dynamic Experiment 5 (Pair=135 cm): outflow, tensiometric water pressures (W1, W2 and W3) and saturations (S1, S2 and S3) vs. time 49
Figure 4.3. Measured experimental parameters at levels 1, 2 and 3 for F70 Dynamic Experiment 7: outflow, tensiometric water pressures (W1, W2 and W3) and saturations (S1, S2 and S3) vs. time 51
Figure 4.4. Measured experimental parameters at levels 1, 2 and 3 for F70 Dynamic Experiment 3: outflow, tensiometric air pressures (A1, A2 and A3), tensiometric water pressures (W1, W2 and W3) and saturations (S1, S2 and S3) vs. time 52
Figure 4.5. Comparison of P_c-S_w Curves measured at three different levels for F32-50 Static Experiment 2 56
Figure 4.6. Comparison of Pc-S_w curves for Dynamic Experiment 7 (Pair=214cm water) 57
Figure 4.7. A comparison of the normalized effective cumulative outflow vs. time for dynamic experiments conducted at constant upper boundary air pressure of 135 cm water 59
Figure 4.8. A comparison of the normalized effective cumulative outflow vs. time for dynamic experiments conducted at a constant upper boundary air pressure of 214 cm water 59

Figure 4.9. A comparison of the normalized effective cumulative outflow vs. time for F70 dynamic experiments conducted at an initial upper boundary air pressure of 135 cm water..... 60

Figure 4.10. Comparison of the F32-F50 mean static, F32-F50 mean dynamic (upper boundary = 135cm water) and F32-F50 mean dynamic (upper boundary air pressure = 215cm water) measured capillary pressure-saturation curves. Error bars indicate the 95% confidence intervals about the mean..... 61

Figure 4.11. Statistical analysis of drainage experiments conducted on F70 sand. Static and dynamic (initial upper boundary air pressure = 135 cm water) primary drainage capillary pressure-saturation curves show 95% confidence intervals of the mean static and dynamic curves. 62

Figure 4.12. Comparison of dP_c vs. saturation measured at three different levels during F32-F50 Dynamic experiment 7. 64

Figure 4.13. Comparison of the mean F32-F50 dP_c vs. saturation 64

Figure 4.14. Comparison of dS_w/dt vs. time measured at three different levels during Dynamic Experiment 7. Data points represent dS_w/dt calculated from consecutive saturation readings taken 15 seconds apart (2 point smooth). Solid lines represents dS_w/dt calculated from the 7 point moving polynomial smoothing routine [64]..... 66

Figure 4.15. Comparison of dS_w/dt vs. saturation measured at three different levels during Dynamic Experiment 7..... 67

Figure 4.16. Comparison of the dynamic effect coefficient (τ) vs. wetting phase saturation (S_w) for mean F70 and F32-F50 dynamic experiments (Upper boundary air pressure of 135 cm) and mean F32-F50 dynamic experiments (Upper boundary air pressure = 214cm). 68

Figure 4.17. A comparison of τ vs S_w determined from either point measurements or from averaged pressures and saturations for F32-F50 Dynamic experiment 5. 71

Figure 4.18. A comparison of τ vs S_w determined from either point measurements or from averaged pressures and saturations for F32-F50 Dynamic experiment 7. 72

Figure 4.19. A comparison of τ vs S_w determined from either point measurements or from averaged pressures and saturations for F32-F50 Dynamic experiment 8. 73

Figure 4.20. A comparison of τ vs S_w determined from either point measurements or from averaged pressures and saturations for F70 Dynamic experiment 1..... 74

Figure 4.21. A comparison of τ vs S_w determined from either point measurements or from averaged pressures and saturations for F70 Dynamic experiment 2..... 75

Figure 4.22. A comparison of τ vs S_w determined from either point measurements or from averaged pressures and saturations for F70 Dynamic experiment 3..... 76

Figure 4.23: A comparison of τ vs. S_w between Direct Measurement Method 1 and Direct measurement Method 2 for F70 Dynamic experiments 1, 2 and 3. 78

Figure 4.24: A comparison of τ vs. S_w between Direct Measurement Method 1 and Direct Measurement Method 2 for F32-F50 Dynamic experiments 7 and 8. 78

Figure 4.25: A comparison of τ vs. S_w between Direct Measurement Method 1 and Direct Measurement Method 2 for F32-F50 Dynamic experiment 5. 79

Glossary of Terms

Symbol	*Definition*	*Units*
τ	Damping coefficient	($kg.m^{-1}.s^{-1}$)
P_c	Capillary pressure	(cm water)
S_w	Wetting phase saturation	($cm^3.cm^{-3}$)
k_r	Relative permeability	-
S_{rw}	Residual water saturation	($cm^3.cm^{-3}$)
P_{nw}	Non wetting phase pressure	(cm water)
P_w	Wetting phase pressure	(cm water)
S_{eff}	Effective water saturation	($cm^3.cm^{-3}$)
P_d	Entry pressure for P_c-S_w after BROOKS AND COREY (1964)	(cm water)
$P_c^{dynamic}$	Dynamic capillary pressure	(cm water)
P_c^{static}	Static capillary pressure	(cm water)
dS_w/dt	Saturation rate	(1/sec)
dP_c	The difference between dynamic and static capillary pressure	(cm water)

Symbol	*Definition*	*Units*
ϕ	Porosity	($cm^3.cm^{-3}$)
k	Intrinsic permeability	(m^2)
$\langle S_w \rangle$	Volume averaged water saturation	($cm^3.cm^{-3}$)
$\langle P_c \rangle$	Volume averaged capillary pressure	(cm water)
$\langle P_w \rangle$	Volume averaged water pressure	(cm water)
PCE	Perchloroethylene	-
DNAPL	Dense non-aqueous phase liquid	-
MCL	Maximum contaminant level	-

Chapter 1 - Introduction

Two-phase flow occurs in numerous natural and engineered systems. In the natural environment, the unsaturated zone is composed of porous media. Within the pore spaces of this media, both air and water coexists as separate phases. The flow of water and air in the unsaturated zone needs to be understood to determine the movement of dissolved solutes and pesticides from surface sources into aquifers, to develop conservative irrigation schedules and to determine the ground water recharge rate. Engineered scenarios such as the remediation of non aqueous phase liquids (NAPLs) from aquifers and petroleum reservoir development are examples of two-phase flow processes where NAPL and water are simultaneously present within the porous media.

The traditional approach to modelling two-phase flow systems utilizes the single phase Darcy's Law, which is extended to account for the presence of two immiscible fluids present within the porous media. In Darcy's law, fluid flux is linearly related to the pressure gradient or driving force [2]. Here the pressure gradient of the non wetting and wetting fluids is related through the Young's-Laplace capillary pressure equation (see Equation 1.0). The driving force includes capillary, viscous and gravity forces [3, 4]. Relative permeability is introduced to account for the reduced permeability of one phase with reference to the other.

Capillary pressure is introduced to account for the presence of fluid/fluid interfaces and is described by the Young's-Laplace equation:

$$P_n - P_w = P_c = \sigma_{nw/w}(2Cos\alpha/R) \qquad (1.0)$$

The capillary pressure (P_c) is given by the difference between the non-wetting (P_n) and wetting (P_w) fluid pressures. The Young's-Laplace capillary pressure equation, derived at the pore scale under static or no flow conditions, is assumed to be applicable to transient flow at the macro scale.

There is compelling experimental evidence that indicates that this may not be the case [5-9]. Air-water drainage experiments like those conducted by [5] and [10] and perchloroethylene (PCE)-water experiments conducted by [6, 11] and [12] were all conducted on different soil types and with varying saturation rates. However, the transient or dynamic effect in the P_c-S_w relationship was detected in all of the above mentioned cases, i.e. the P_c-S_w relationship measured under high desaturation rates (transient or dynamic flow conditions) lie higher than the P_c-S_w relationship measured under low desaturation rates (static or steady state flow conditions) for water drainage.

By applying the measured or optimized static P_c-S_w relationship (determined over weeks or months) to simulate transient processes on the order of minutes or hours, one assumes that any force which results in the movement of an interface is instantaneously dissipated and equilibrium is re-established in a short period of time [7]. This assumption may be violated if the system under investigation is dependant on the flow regime [3]. There exists strong experimental evidence which indicates that two phase flow systems are not

independent of the flow regime but are influenced by the saturation rate [7], the dominant driving force [13] and variable wettability of the porous media [14].

To account for the transient or dynamic effects on the capillary pressure-saturation relationship, [1] and [8] have developed similar theories to account for the observed non-uniqueness in the P_c-S_w relationship. Laws of conservation of mass, momentum and energy were used to develop microscopic flow equations for both fluid phases as well as for the interfaces which exist at the boundary between the phases. These microscopic equations were upscaled to the core or macro scale using volume averaging techniques. A constitutive relationship for capillary pressure was then developed at this scale. Here [1] introduces the concept of dynamic capillary pressure. The difference between the static and dynamic capillary pressure is said to be linearly related to the product of the saturation rate and a damping coefficient (τ). Here the Young's-Laplace P_c-S_w equation is obtained from the dynamic relationship when the desaturation rate approaches static or steady state conditions.

It is physically unrealistic to assume that equilibrium between two fluids in a multiphase flow system can be reached instantaneously at all saturations [15]. For an air-water drainage system this may only be justified at high wetting phase saturations where the permeability is near unity [3]. The presence of the damping coefficient (τ) is said to provide the necessary relaxation time which is needed for the moving fluids to reach equilibrium [16]. For scenarios where a rapid desaturation rate is induced, a dynamic

capillary pressure term may have to be implemented to simulate the transient two-phase flow process [12].

In some engineering applications, saturation rate changes may be significantly faster than that experienced under average groundwater flow rates. Examples of such engineering applications are the injection of CO_2 in deep subsurface aquifers [17], water flooding of oil reservoirs for oil recovery [16], high pressure sand filter systems, heavy rainfall/irrigation events on sands at residual saturation [18] and for the simulation and remediation of non-aqueous phase liquids [19]. It is therefore important to have the ability to capture and quantify the observed saturation rate dependency of the P_c-S_w relationship to model scenarios like those previously mentioned.

The actual physical mechanisms that result in an increased relaxation time for system equilibrium is not clearly understood [13]. Essentially, any factor that increases the time needed to achieve equilibrium increases the magnitude of τ [3]. Some of the factors that have been proposed include imposed boundary conditions [18], soil properties [20], fluid properties [21] as well as macro and microscale heterogeneities [19, 22]. However, these factors have not been extensively investigated in experimental systems. Other than [20], the other studies are comprised of only numerical modeling. Experimental work conducted by [5, 6, 10, 11] have focused on detecting the dynamic effect, however, experimental parameters such as soil properties and fluid properties have not been varied to examine the possible effects on τ, the damping coefficient.

1.0 Aims of the Thesis

The objectives of this thesis are:

- To determine if measured capillary pressures are a function of the water desaturation rate for sands of different physical properties.

- Utilize different methods to determine the magnitude of the damping coefficient, τ.

- Assess if the volume over which measurements are averaged impacts the magnitude of τ.

- Quantify the impact of sand properties (i.e. intrinsic permeability and entry pressure) on the magnitude of τ.

- Assess the validity of the proposed linear relationship between dP_c (i.e., the difference between static and dynamic capillary pressures) and dS_w/dt (i.e., the desaturation rate).

Chapter 2 - Literature Review

2.0 Introduction

Groundwater is important to the welfare of society. Approximately 50% of current potable water supplies, 40% of the demand of self-supplied industry and 20% of irrigation for agriculture comes from groundwater sources [23]. As the world's population continues to increase, so too does the demand for water. This trend has led to water scarcity in many parts of the world and the situation is further aggravated by the problem of groundwater pollution by persistent organic contaminants, originating from hazardous industrial wastes.

One group of organic contaminants of major concern is chlorinated solvents [24]. These chemicals are classified as DNAPLs or dense non-aqueous phase liquids. DNAPLs have a greater density than water and they migrate through the subsurface environment as a separate phase from water. This type of separate migration of phases constitutes multiphase flow.

2.1 Unsaturated Groundwater Flow

One important type of multiphase flow system occurs in the unsaturated zone. This is the region of the subsurface which lies between the Earth's surface and the phreatic surface [25]. In this zone, both air and water co-exist as separate phases in the void space between soil particles (see Figure 2.1). The unsaturated zone is utilized throughout the

world for the cultivation of plants, construction of buildings and for the disposal of waste [4].

Water from precipitation, irrigation or influent surface bodies must first infiltrate into the subsurface and then percolate through the unsaturated zone before replenishing the underlying aquifers. It is therefore essential that the flow of water through the unsaturated zone be understood. This enables us to quantify recharge of the underlying aquifers, to develop conservative irrigation programs and also to track the movement of dissolved contaminants such as leachate from landfills, fertilizers and pesticides from farms [4, 26].

2.2 DNAPL Subsurface Contamination

Another multiphase flow system of importance exists when aquifers are contaminated by DNAPLs. DNAPLs have been produced and utilized widely since the beginning of the 20th century [24]. In the past, disposal of DNAPLs was achieved by simply spreading them over the earth's surface [24, 27]. It was believed that due to the high volatility of these contaminants, the DNAPL would simply evaporate into the atmosphere. The importance of DNAPLs as soil and groundwater contaminants was not recognized until the 1980s [28]. By this time, the indiscriminate dumping of used DNAPLs had already resulted in widespread aquifer contamination [27].

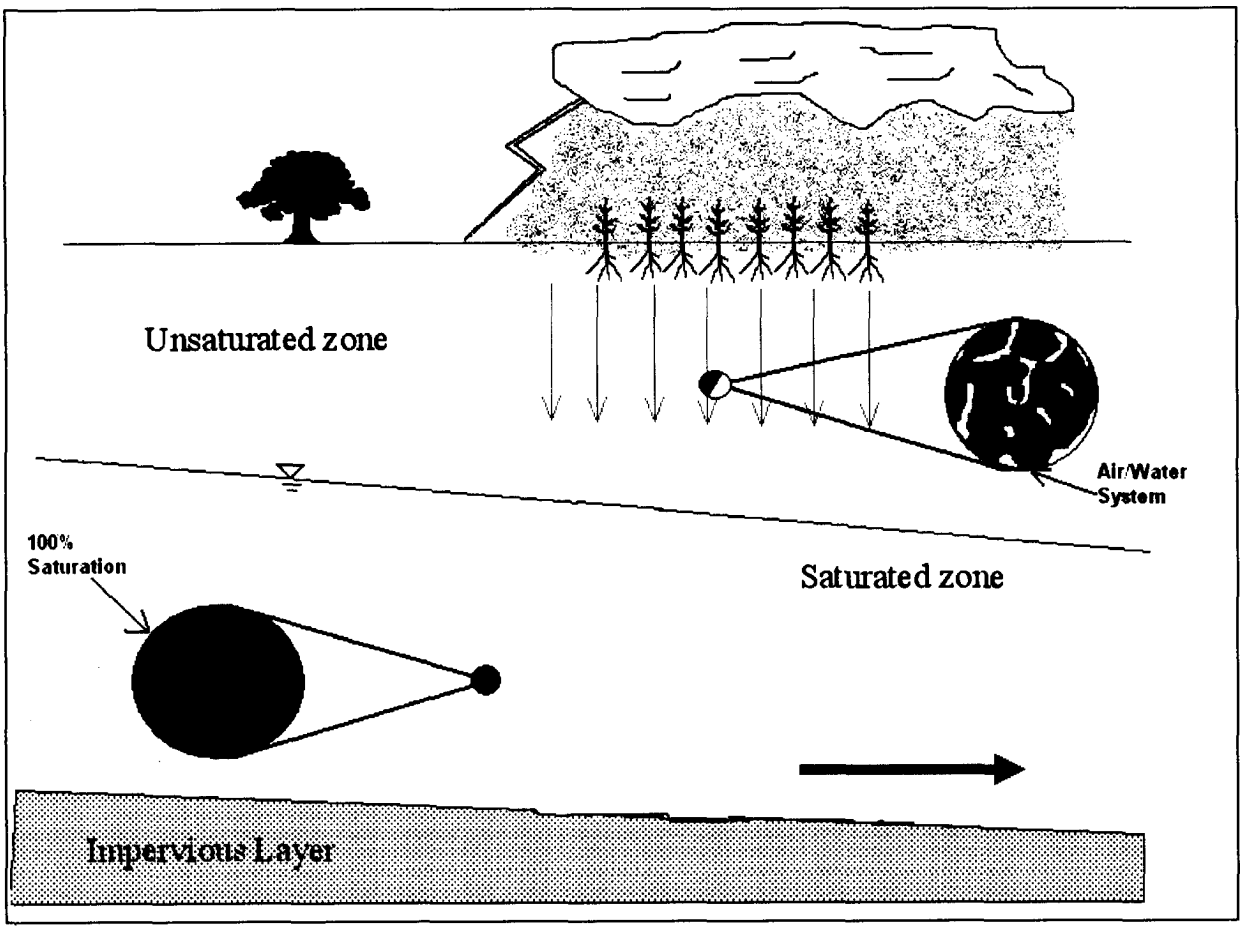

Figure 2.1. Multiphase flow scenario

DNAPLs have the ability to migrate to significant depths below the water table where they form pools of entrapped DNAPL mass [29]. Over time, these pools slowly dissolve into flowing groundwater, resulting in aqueous phase plumes. Therefore, the release of DNAPLs at the ground surface can lead to long-term contamination of groundwater both in the unsaturated and saturated zones [28].

Other sources of DNAPL contaminants have been identified as accidental spills during transport to and from storage facilities, leaks from corroded storage tanks, and malfunctioning degreasing equipment [27]. Improper landfilling practices, storage in

unlined lagoons and other surface impoundments have also contributed to DNAPL contamination [24]. Table 2.1 gives a list of common DNAPL contaminants, their main uses, and the maximum contaminant level (MCL) allowed in drinking water.

Table 2.1. Common DNAPL contaminants [27, 29, 30]

Chemical name	US EPA MCL (mg/L)	Main Usage
perchloroethylene (PCE)	0.005	Dry cleaning, metal cleaning, intermediates in processes
Trichloroethene (TCE)	0.005	Metal cleaning (>90% of UK use), dry cleaning, extractions
Dichloromethane (DCM)	0.005	Paint stripper, metal cleaning, pharmaceuticals, aerosols, acetate films
1,1,1 –Trichloroethane (TCA)	0.003	Metal/plastic cleaning, adhesives, aerosols, ink

Long term exposure of these organic chemicals has the potential to cause liver related problems and result in an increased risk of cancer in humans [30]. It is therefore important to understand the processes involved in the subsurface migration of these hazardous contaminants. Accurate computer models are needed to predict both the migration pathway and dissolution of these chemicals. Information from these models can then be used for the development and assessment of appropriate groundwater remediation technologies [27, 29].

2.3 The Challenge of Multiphase Subsurface Modeling

Two-phase flow models, including those for both DNAPL contaminant flow and unsaturated flow, are developed by utilizing model governing equations for the conservation of mass, momentum and energy [24, 31]. Both DNAPL and unsaturated flow are governed by two basic soil constitutive or material dependant relationships.

These are the capillary pressure-saturation relationship (P_c-S_w) and the relative permeability-saturation relationship (K_r-S_w) [4].

In single phase or saturated flow Darcy's Law is used to describe the conservation of momentum [26]. Darcy's Law is adapted to the modeling of two-phase flow systems by the inclusion of the P_c-S_w and K_r-S_w soil constitutive relationships [24]. Traditionally, laboratory experiments are employed to determine the P_c-S_w relationship under static or steady state conditions.

This static relationship is then used to model dynamic flow processes [12, 32]. Experimental evidence has shown that the static P_c-S_w relationship may not be unique but may be affected by the rate of change of saturation [6, 11, 12, 33, 34]. The dependence of the P_c-S_w relationship on the rate of change of saturation is referred to as dynamic or non-equilibrium effects [35].

In the following review, the importance of the soil constitutive relationships, their meanings and effects on multiphase flow systems are examined. This includes a review of recent experiments designed to detect and quantify the dynamic or transient flow effects of the P_c-S_w relationship.

2.4 Soil Constitutive Relationships

The determination of soil constitutive relationships is essential to the modeling of multiphase and unsaturated flow systems. The ability of models to predict the flow of

water and contaminants rely on the availability of accurate flow and transport properties of the porous medium, i.e., the relative permeability-saturation relationship and capillary pressure-saturation relationship [36].

2.5 Relative Permeability

For a porous medium that is at 100% saturation, the wetting fluid (i.e.; water) occupies the entire void space. In the case of two-phase flow, both wetting and non-wetting fluid phases are present simultaneously in the same void spaces. Relative permeability accounts for the influence of one fluid phase on another [37]. When the wetting phase fluid saturation decreases due to an increase of the non-wetting fluid saturation, the cross-sectional area available for flow of the wetting fluid decreases.

The wetting fluid must flow around the area of the pore space occupied by the non-wetting fluid. This results in an increase in the flow path of the wetting fluid [38]. Further decrease in wetting phase saturation would result in eventual film flow [39]. This occurs at the irreducible wetting phase saturation (S_{rw}). At S_{rw} the non-wetting phase relative permeability (k_{nw}) is less than unity. This is due to the presence of residual water within the pore spaces [39]. Figure 2.2 illustrates the dependency of relative permeability on water saturation.

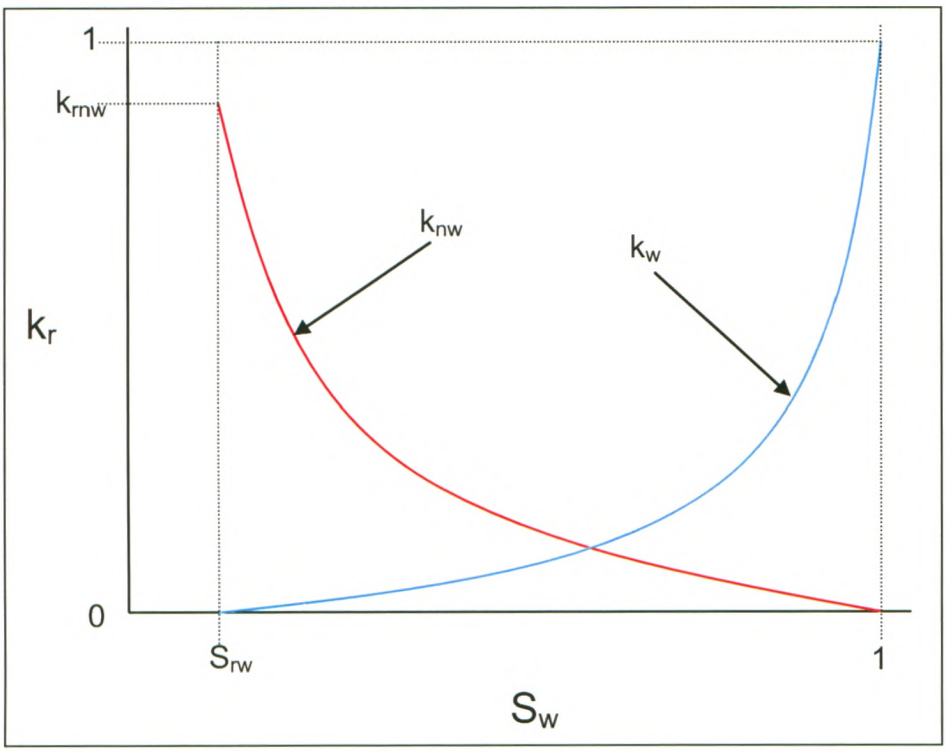

Figure 2.2. An illustration of the Relative permeability – Saturation relationship [39]

The direct measurement of the relative permeability function has proven to be both expensive and difficult to achieve [40]. Alternatively, methods have been developed where the P_c-S_w relationship is determined experimentally and this data is then used to predict the relative permeability function [36].

2.6 Capillary Pressure

When a fluid/fluid interface or meniscus is formed by the presence of two immiscible fluids in the porous media, the difference in pressure across the interface is referred to as the capillary pressure [16]. The pressure difference between phases is a direct result of the interfacial tension [4]. Molecular cohesion effects within the wetting and non-wetting phases, and adhesion effects between the wetting/non-wetting and solid phases give rise

to interfacial tension [25]. Young's equation indicates that at equilibrium, the sum of the molecular forces acting on a system in equilibrium is zero (See Figure 2.3):

$$\sigma_{nw/s} = \sigma_{w/s} + \sigma_{nw/w}(Cos\alpha) \qquad (2.1)$$

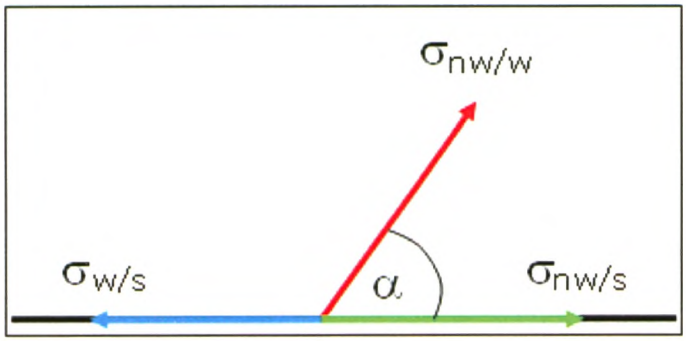

Figure 2.3. Young's Equation – air-water interfacial tension [4]

where $\sigma_{nw/s}$ and $\sigma_{w/s}$ are the molecular forces of the non-wetting fluid/solid interface and wetting fluid/solid interface respectively, $\sigma_{nw/w}$ is the molecular force experienced at the nonwetting/wetting fluid interface and α is the contact angle. A force balance for the components along the normal to the fluid/fluid interface with constant interfacial tension gives the Young's-Laplace Formula:

$$P_{nw} - P_w = P_c = \sigma_{nw/w}(2Cos\alpha/R) \qquad (2.2)$$

The capillary pressure (P_c) is said to be proportional to the interface curvature ($2\cos\alpha/R$), which in turn is related to the contact angle (α) between the meniscus and the solid surface. Here R gives the pore radius. The coefficient of proportionality is the interfacial tension ($\sigma_{nw/w}$). The Young's-Laplace capillary pressure equation was derived for a system under static or equilibrium condition [8].

2.6.1 The Static P_c-S_w Relationship

Traditional methods of determining the P_c-S_w relationship are obtained under static or equilibrium conditions [7]. Here the static P_c-S_w relationship is defined as the difference between the measured air and water pressure, for a given saturation, when the fluids are at rest. Experiments entail increasing or decreasing the pressure of the non-wetting fluid by small increments to achieve drainage or imbibition respectively. The system is allowed to equilibrate between pressure steps. The pressures of the non-wetting and wetting fluids are then measured along with the wetting phase fluid saturation. The capillary pressure at each equilibrium position is calculated using the following relationship:

$$P_c(S_w) = P_{nw} - P_w \qquad (2.3)$$

P_{nw} is the pressure of the non-wetting fluid, P_w is the pressure of the wetting fluid and S_w is the wetting fluid saturation. P_c-S_w experimental data is then fit using empirical models such as the van Genuchten [41] or Brooks and Corey [42] relationships. An illustration of the static P_c-S_w relationship is given in Figure 2.4.

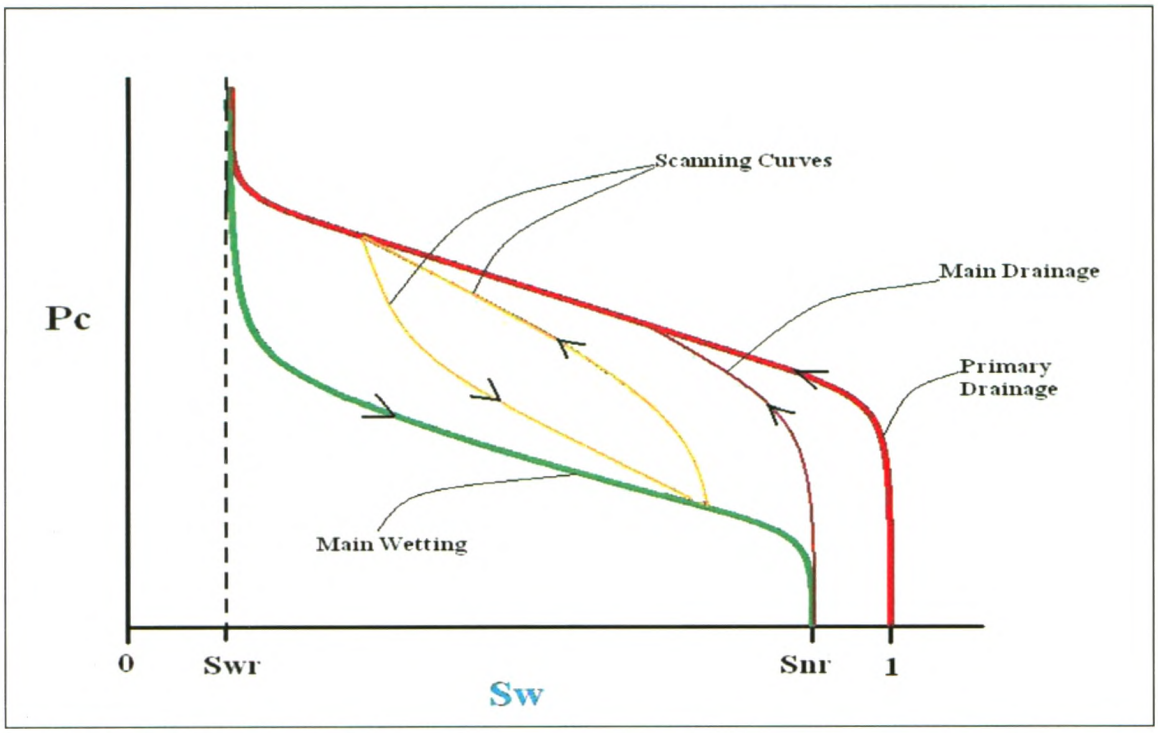

Figure 2.4. The hysteretic equilibrium P_c-S_w relationship [25]

This graph demonstrates the dependence of capillary pressure on saturation. For a particular degree of saturation, a different value of capillary pressure can be observed for drainage and imbibition, with P_c being greater under drainage. This phenomenon is known as hysteresis and has been widely documented in the literature [26, 43-45]. For a fully saturated porous medium, i.e. $S_w = 1$, increasing the capillary pressure results in a decrease in the wetting phase saturation along the primary drainage curve to a minimum value known as the residual wetting phase saturation (S_{rw}). At S_{rw}, the wetting phase may become discontinuous or be strongly attracted to the solid phase such that further decrease in saturation is not possible.

Decreasing the capillary pressure back to zero, results in the main wetting or imbibition curve. Note that the wetting phase saturation does not return to 100% or $S_w = 1$ but ends at S_{nr} (the residual air), see Figure 2.4. This is due to entrapment of the non-wetting phase during the imbibition process. The main hysteretic loop is defined as the region of the P_c-S_w graph bounded by the main drainage and main imbibition curves. Scanning curves are obtained by reversing the capillary pressure at any point within the main hysteretic loop.

2.6.2 The Dynamic P_c-S_w Relationship

Traditional experiments used to determine the static P_c-S_w relationship are time consuming and can last weeks or months [12, 46]. Recently, more rapid, dynamic experiments have been developed in which the soil constitutive relationships can be determined in a matter of hours or days [40]. However, experimental evidence of non-uniqueness in the P_c-S_w relationship determined under varying flow rates has been reported [5-12, 20, 33, 47-49]. Here the dynamic P_c-S_w relationship is defined as the difference between air and water pressure measured under non-equilibrium conditions. For studies which utilize one step outflow experimental data to obtain the P_c-S_w relationship via the inverse estimation technique, it has been shown that non-uniqueness may be due to a lack of experimental information [50]. However, for experiments which directly measure the P_c-S_w relationship, the source(s) of this non-uniqueness remains under debate.

It has been suggested that the conventional static relationship may not be adequate for the accurate description of dynamic multiphase flow systems [1, 16]. Under dynamic flow, the macroscopic capillary pressure may not only be a function of saturation as shown in Equation 2.3, but may also depend on the rate of change of saturation [19].

Since the traditional static P_c-S_w relationship was based entirely on experimental observation it was necessary to derive the P_c-S_w relationship from first principles in order to account for non equilibrium behavior. To address this issue, researchers have developed similar theories to account for this observed non-equilibrium effect based on thermodynamic and volume averaging techniques [16, 31].

Utilizing a pore scale approach, [8] demonstrated the importance of including fluid/fluid interfaces for the correct description of the multiphase flow system. A physical cause of dynamic or non-equilibrium effects was proposed as a process called Haines Jumps. Here, if the capillary pressure of a system that is at rest (i.e.; possesses a stationary fluid/fluid interface) is rapidly increased to a high value, the fluid/fluid interface becomes unstable and jumps to a new position where it once again comes to rest. During the movement of the dynamic interface, free energy is dissipated and the energy of the interface returns to its static value at a new position [12]. Here the capillary pressure of the moving interface will be higher than that of a static interface for a given saturation [7].

[31, 51] identified parameters that are traditionally neglected in the models that govern multiphase flow (e.g.: interfaces and contact lines). In their study they expressed capillary pressure in terms of the change in free energy of the phases and interfaces as a result of a change in saturation. Here, capillary pressure was determined to be equal to the difference of the phase pressures only at equilibrium and a first order non-equilibrium expression was derived to account for the dynamic condition:

$$P_c^{dynamic} = P_c^{static} - \tau\left(\delta S_w / \delta t\right) \qquad (2.4)$$

where $P_c^{dynamic}$ is the dynamic capillary pressure, P_c^{static} is the static capillary pressure, τ is the damping coefficient ($ML^{-1}T^{-1}$) and $\delta S_w/\delta t$ is the saturation rate. Equation 2.4 states that the dynamic capillary pressure must be greater than the static capillary pressure during drainage while the opposite is true for the imbibition process.

This is in agreement with experimental observations made by [12, 33] using variations of the inverse modeling technique to fit the P_c-S_w relationship to experimental data and by [5, 6, 8, 10, 11, 44] using methods developed to directly measure the P_c-S_w relationship in-situ. However, researchers such as [47, 48] caution that a lack of reproducibility of transient experiments may also lead to non-unique results.

2.7 Experimental Evidence of Dynamic Effects in P_c-S_w

2.7.1 The Direct Measurement Method

To quantify the extent to which dynamic or transient flow affects the P_c-S_w relationship, [8] devised a procedure to calculate the dynamic effect coefficient from the direct measurement of the static P_c-S_w relationship, the dynamic P_c-S_w relationship and the experimental saturation rate. A series of three imbibition experiments were conducted using limestone and sandstone core samples initially saturated with oil.

A pair of hydrophobic and hydrophilic pressure sensors measured the non-wetting and wetting phase pressures respectively at four levels along the length of the vertically positioned core samples. This enabled the calculation of the capillary pressure using Equation 2.4. Saturation was measured using an ultrasonic method at the same time and level as the pressure sensors. (no info given on exactly how fluids were injected)

Imbibition experiments were conducted by injecting water at 1 cc/hr, 5 cc/hr and 15 cc/hr at the lower end of the cores. The relatively slow flow rate experiment of 1 cc/hr represented the static P_c-S_w relationship, while the faster flow rates of 5 cc/hr and 15 cc/hr represented the dynamic P_c-S_w relationship. The time derivative of saturation was calculated from experimental data for each given flow rate. Equation 2.4 can be arranged to give:

$$\tau = \frac{(P_c^{static} - P_c^{dynamic})}{\delta S_w / \delta t} \qquad (2.5)$$

By substituting $P_c^{dynamic}$, P_c^{static} and $\delta S_w/\delta t$ into Equation 2.5, values of τ were calculated for the dynamic experiments. Results from these experiments indicated that τ, the damping coefficient, was inversely proportional to flow rate. τ was also shown to vary with saturation, although the exact functional relationship was not determined.

Utilizing both quasi-static and dynamic drainage of an air-water system, [20] investigated the influence of dynamic effects of the P_c-S_w relationship for homogeneous quartz sand. Experiments were conducted using both a coarse (K_s = 2.07 to 2.17 X 10^{-2} cm.s^{-1}) and a fine sand (K_s = 1.42 X 10^{-2} cm.s^{-1}). Water pressure was measured at different locations along the length of the column. Water saturation was measured using a gamma ray absorption technique, while air pressure was measured at one location in the column. Both quasi-static and dynamic experiments were conducted. Here, [20] defines dynamic effects as the difference between the measured dynamic and quasi-static capillary pressures for a given saturation.

A linear relationship was found between the difference in dynamic and quasi-static capillary pressure and the rate of change of saturation for drainage of both fine and coarse sands. Here, the slope of this linear relationship gives the magnitude of τ. Using data from both dynamic and static experiments, [20] developed the following empirical relationship to determine the value of τ from fluid and porous media properties:

$$\tau \propto \frac{\phi\mu}{k\lambda}\left(\frac{P_d}{\rho g}\right)^2 \qquad (2.6)$$

In this relationship, τ was shown to be dependent on porosity (ϕ), intrinsic permeability (k), the Brooks and Corey parameters λ and P_d , wetting fluid viscosity (μ) and wetting fluid density (ρ). τ was shown to be larger for the fine sand (2.4×10^5 Pa.s) in comparison to the coarse sand (7.0×10^4 to 9.5×10^4 Pa.s). Here τ was calculated from static and dynamic drainage P_c-S_w measurements of 3 different locations in the column for the coarse sand and from measurements at one location in a shorter column for the fine sand.

Similar methods for the estimating the damping coefficient was employed by [6] for a PCE/water system and by [10] for an unsaturated flow (air/water) system. In the dynamic experiments conducted by [6], no membranes were placed at the outflow or inflow boundaries. It was hypothesized that the hydrophobic and hydrophilic membranes commonly used in transient experiments, may significantly affect the distribution of fluids inside the soil sample. However, the static P_c-S_w relationship used to calculate the dynamic effect coefficient in this study was taken from an experiment which utilized these membranes.

Tensiometric measurements of both wetting and non-wetting phases were made by [6] while [10] measured the pore pressure of the water phase and assumed that the air phase remained at atmospheric pressure throughout the experiment. This assumption is commonly made in unsaturated flow experiments [9, 49] and has been confirmed by [20, 52]. The saturation and P_c measured at the same level and time in the column, along with the saturation rate was used to calculate the damping coefficient for transient

experiments. [6] reported a maximum value of τ to be 1 x 10^7 $kg.m^{-1}.s^{-1}$ for the PCE/water system while [10] reported a maximum value of 1 x 10^6 $kg.m^{-1}.s^{-1}$ for the air/water system.

Using a relatively small pressure cell, [44] investigated the saturation rate dependency of sand and silt for the air/water fluid pair. Silt was shown to possess higher τ values (1.6 X 10^4 $kg.m^{-1}.s^{-1}$ at S_{eff} = 0.8) than sand (1.1 X 10^3 $kg.m^{-1}.s^{-1}$ at S_{eff} = 0.8). This was attributed to a faster response to changes in capillary pressure expected for porous media with higher conductivity (i.e. the sand). Here τ was determined by linear regression of dP_c (the difference between static and dynamic capillary pressures) and dS_w/dt for a given wetting phase saturation. In this study τ was shown to increase as a power function with decreasing effective water saturation.

Experimental evidence indicates that τ may vary with saturation [6, 8, 10, 11, 44]. However, the exact functional relationship has not yet been developed. To address this issue, [11], conducted both static and dynamic outflow experiments using a PCE/water system. Similar to [8], wetting and non-wetting phases measured inside the soil sample were used to calculate static and dynamic capillary pressure relationships.

Failure of a static capillary model to predict the results of the dynamic experiments lead to the development of a two-phase dynamic flow model in which the difference in phase pressures i.e. the capillary pressure, depended on the rate of change of saturation. The static capillary pressure model was shown to under predict the value of the experimental

saturation. Various functional relationships between τ and saturation were tested using the dynamic model and it was reported that a reasonable fit to experimental data was achieved using Gaussian and error functions to relate τ to saturation [11]. A comparison of the τ values determined from experimental data is presented in Table 2.2.

Table 2.2. Summary of τ determined from experimental data

Study	Fluids	Porous Media	τ ($kg.m^{-1}.s^{-1}$)
Stauffer (1978)	Air/water	Fine sand	2.4×10^5
		Coarse sand	7.0×10^4
Kalaydjian (1992)[a]	Oil/water	Sand stone	2.0×10^6
Topp et al. (1967)[a]	Air/water	Sand	2.0×10^7
Chen (2006)	Air/water	Sand	1.1×10^3
		Silt	1.6×10^4
Bottero (2006)	PCE/water	Sand	1.0×10^7
O'Carroll (2005)	PCE/water	Sand	1.0×10^6
Berentsen (2006)	PCE/water	Sand	1.0×10^6

[a] τ values taken from [7]

The dependency of τ and wetting phase saturation has been directly determined by [6, 8, 10, 11]. Here [6] found τ to increase as the wetting phase saturation decreased. By using different functions to fit to experimental data, [11] found the relationship between τ and saturation to be best represented by an error function or a Gaussian relationship.

2.7.2 The Inverse Modeling Method

The inverse modeling approach has been shown capable of estimating the soil hydraulic properties from transient experimental data [35, 40]. Thus more rapid experimental

techniques, such as the multi-step outflow and one step outflow have evolved from longer static experiments of the past. Another advantage this technique offers is the ability to simultaneously estimate the capillary pressure and relative permeability functions from one experiment [53].

The following is a brief summary of the inverse modeling technique. For a detailed discussion of the inverse technique, refer to [40, 46]. The first step in the inverse modeling technique is to conduct a transient flow experiment with predetermined boundary conditions. During the experiment, flow variables such as cumulative flow and phase pressures are measured [12].

Next a numerical flow model is employed to simulate the transient flow regime of the experiment by using initial estimates of the soil hydraulic function. For the modeling of unsaturated flow, Richard's Equation has been used in the numerical model [9, 49]. However, the applicability of Richard's Equation is under debate and a few researchers have questioned its use to model unsaturated flow [54]. Alternatively, the use of two-phase flow model governing equations can be substituted for Richard's Equation [53].

Typically the P_c-S_w and K_r-S_w soil hydraulic functions are represented by coupling various constitutive models such as the van Genuchten/Burdien or Brooks and Corey/Mualem equations [36]. Once the flow regime has been calculated, an optimization algorithm is employed to estimate the fit parameters of the soil hydraulic

functions by minimizing the difference between experimental and simulated flow variables through an iterative solution of the governing flow equations [12].

The inverse method is now widely applied to determine the soil hydraulic characteristics of various porous media both from laboratory and field data [40]. This technique has been adapted to investigate dynamic effects or the saturation rate dependence of the P_c-S_w relationship. According to the dynamic P_c-S_w relationship developed by [31], the inverse simulation of transient experiments should yield different soil parameters if experiments are conducted at different saturation rates. To test this hypothesis, experiments have been conducted using air-water systems [9, 33, 49] and PCE-water systems [12].

To investigate the saturation rate dependency of the soil hydraulic functions, [33], conducted drainage experiments on initially saturated soil columns. One step outflow, multi-step outflow and quasi-static syringe pump experiments were performed on initially saturated columns packed with either a course textured or fine textured soil. The matric potential versus time and the cumulative outflow versus time were recorded during the experiments and the data used to estimate the unsaturated hydraulic properties of each soil type under varying flow rates. No flow rate dependence was observed for the fine textured soil type. However, high flow rate one step outflow experiments conducted with the course textured soil resulted in larger retention and residual water content in comparison to the low flow rate multi-step outflow and quasi-static experiments.

Inverse modeling of a two-phase PCE-Water system was carried out by [12] using data from two multi-step outflow experiments conducted using different experimental boundary conditions i.e. varying flow rates. Comparison of model results and experimental data show a significant difference between simulated and experimental outflow data. The inclusion of a constant dynamic capillary pressure term in the NAPL governing equation of the flow simulator led to no real improvement in the model fit. However, when τ was made to vary linearly with saturation, a significant improvement between simulated and experimental outflow data was achieved and quantified by a 30% and 18% decrease in the RMSE of cumulative outflow data. The maximum reported values of τ were 1.06×10^{6} and 5.64×10^{7} $kg \cdot m^{-1} \cdot s^{-1}$.

Combining both the direct measurement method and inverse method to simultaneously predict the retention characteristic of an undisturbed sandy forest soil, [9] demonstrated that these experiments were not affected by varying the rate of change of saturation. Four cycles of continuous drainage and imbibition were conducted on the same soil column, with the speed of each cycle increased by a factor of four.

Inverse simulation of the experiments was achieved using Richard's Equation in the flow model and the van Genuchten/Mualem parameterization for the hydraulic properties. Simulated results indicate that the retention characteristic was not affected by varying the experimental flow rate. This is contradictory to the findings of [12] and [33]. In situ measurements of water pressure and water content taken at the same depth and time were

used to plot the retention curve. Comparison of the in situ and inverse method shows that similar retention curves can be achieved by using either method.

By using the soil hydraulic parameters obtained from the inverse modeling of multi-step outflow experiments (low flow rate) to model the outflow regime of two-step experiments (fast flow rate), [49] arrived at a similar conclusion to [9]. Inversion of the Richards Equation along with a k-modal form of the van Genuchten equation was used to obtain the hydraulic properties of the soil. Results show a good fit between simulated and experimental outflow data for the multi-step outflow experiments. These soil hydraulic parameters were then used to forward model the two-step experiment. Since both the cumulative outflow and the tensiometer data of the two-step experiments were reproduced with high accuracy, the author concluded that dynamic effects were not experienced in this study. However, it should be noted that no attempt was made to directly measure the P_c-S_w relationship to confirm the optimized P_c-S_w relationship.

Based on a review of literature dating back to 1967, [7] used data from experiments believed to be affected by dynamic effects to calculate values of τ. These values ranged form 3×10^4 to 5×10^7 $kg \cdot m^{-1} \cdot s^{-1}$. The physical nature of the phenomenon which causes dynamic or non-equilibrium effects is not clear at this point. Various researchers offer differing reasons, which may result in the saturation rate dependency of the P_c-S_w relationship.

[33] proposed water entrapment, pore water blockage (membrane effects), air entrapment and air-entry value effect as possible processes which may affect the flow in pressure cells commonly used to conduct laboratory experiments of multiphase flow systems. [7], also adds to this list, the dynamic contact angle effect. [22] used simulations to demonstrate that as the intensity of heterogeneities increase, the value of τ increases for a given saturation, however actual experiments conducted by [49], using heterogeneous sand columns showed no dynamic effects.

2.8 Conclusions

To date, [20] has been the only researcher to produce an empirical relationship between τ and soil properties. Stauffer's empirical relationship has yet to be confirmed [7]. If Stauffer's relationship holds, then τ can be rapidly estimated from measured soil properties such as the permeability, porosity and entry pressure. Modeling studies conducted by [2, 19, 55] suggests that τ scales with the square of the system's length. If this is a reality, then τ may become arbitrarily large for systems at the field scale. However, this dependency of τ on domain length has not been investigated through experimental work.

The validity of the proposed linear δP_c v.s. $\delta S_w/\delta t$ relationship has been tested in experimental studies presented in [7] and in modeling studies by [19, 55]. This relationship was found to be linear for high saturation rates. However, as the saturation

rate diminishes, the relationship becomes non-linear, suggesting that a non-linear relationship may be needed to account for dynamic effects over the entire saturation rate range encountered in these studies. The proposed linear relationship should be investigated in experimental work.

Finally, the influence of hysteresis (wetting and drainage cycles) on the behavior of τ needs to be established to fully understand how dynamic effects may influence multiphase flow in the natural environment.

Chapter 3 - Methods and Materials

3.0 Introduction

The following is a description of the methods and materials used to investigate the flow rate dependency of the P_c-S_w relationship. A fully automated outflow set up was designed for the direct measurement of the P_c-S_w relationship during both static and dynamic air-water primary drainage experiments. All experiments were conducted at a temperature of 22°C (± 2°C).

3.1 Solid, Non-Wetting and Wetting Phases

The solid phase used in all experiments was either a 50/50 (by weight) mixture of F32 and F50 or F70 Ottawa sand (Opta Minerals Inc., Brantford, Ontario). The F32-F50 sand mixture has a mean grain size of 0.042 cm and a uniformity index of 2.3. The F70 sand has a mean grain size of 0.018 cm and a uniformity index of 1.6. The grain size distribution of both sands is given in Figure 3.1.

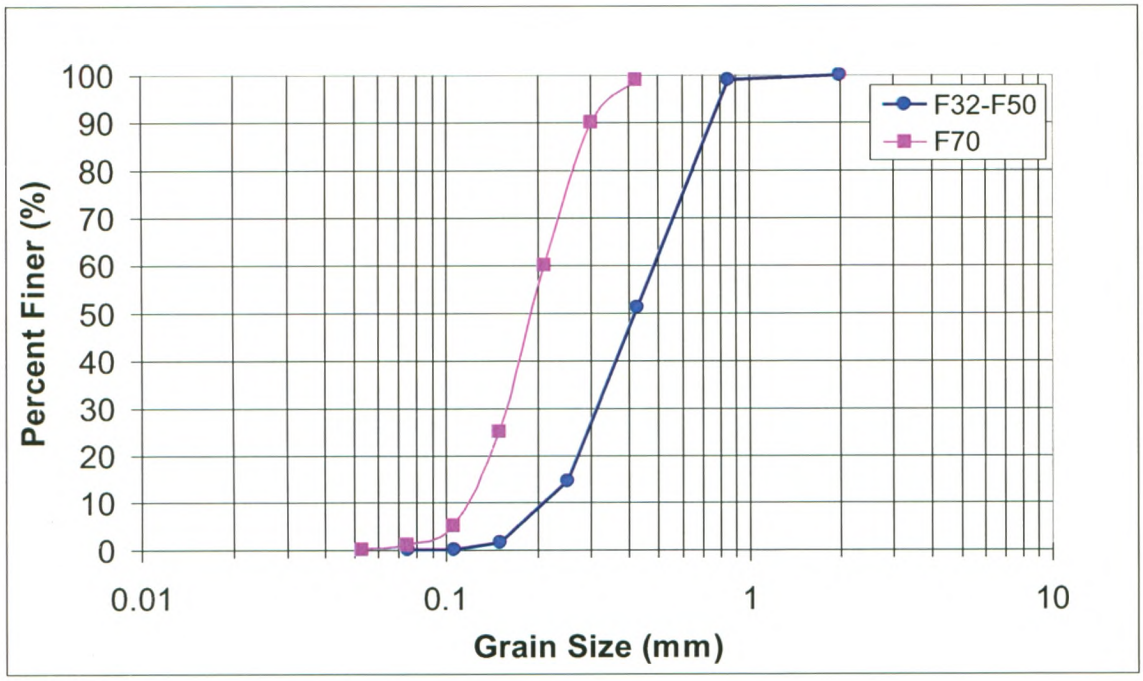

Figure 3.1. Grain size distribution of F32-F50 and F70 Ottawa sand.

In the unsaturated flow investigations, the non-wetting fluid (i.e.; air) was supplied via the lab air/suction system. De-ionized water was used as the aqueous phase in all experiments. Table 3.1 summarizes the physical properties of fluids used in the subsequent study.

Table 3.1. Physical properties of fluids at 20°C

	Air	*Water*
Density ($kg.m^{-3}$)	1.2[b]	999[a]
Viscosity ($N.s.m^{-2}$)	1.81×10^{-5} [b]	1.12×10^{-3} [a]
	Air-water	
Interfacial Tension ($N.m^{-1}$)	0.0681[b]	

[a] [12]
[b] [53]

3.2 1-D Pressure Cell

All experiments were conducted in a custom built aluminum pressure cell, consisting of a cylindrical soil chamber and end caps. The soil chamber (see Figure 3.2) is 20 cm in length with an internal diameter of 10 cm.

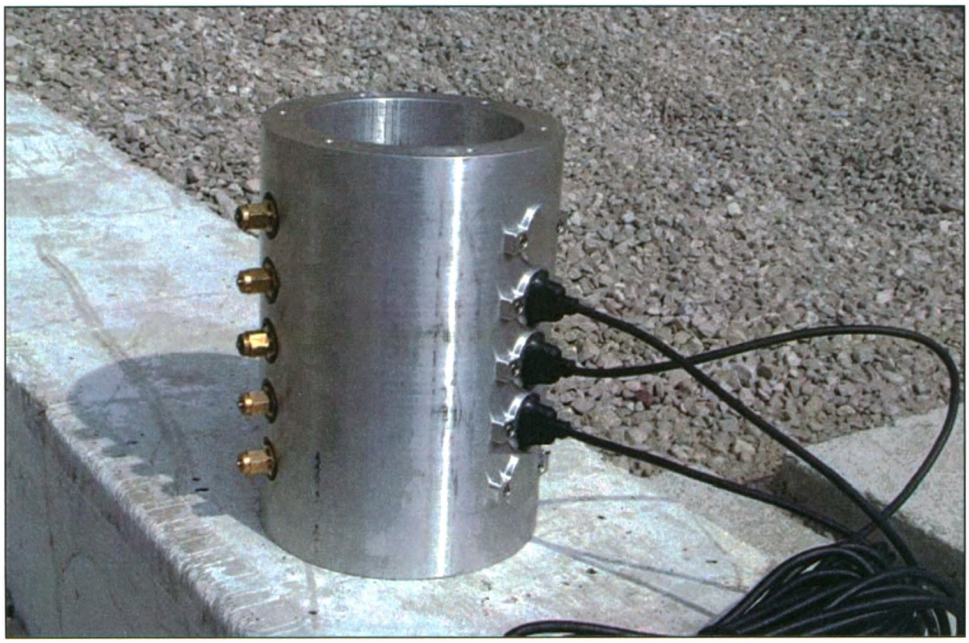

Figure 3.2. The soil chamber, fitted with ports for P_c-S_w measurement instruments

Ports along the length of the column allow for installation of up to 5 sets of P_c-S_w measurement instruments. Each set (see Figure 3.4) consists of one non-wetting phase tensiometer, one wetting phase tensiometer and one EC-5 soil moisture probe (Decagon Devices, WA, USA). End caps were fitted with Viton O-rings to allow for an air tight seal once they were fastened to the soil chamber.

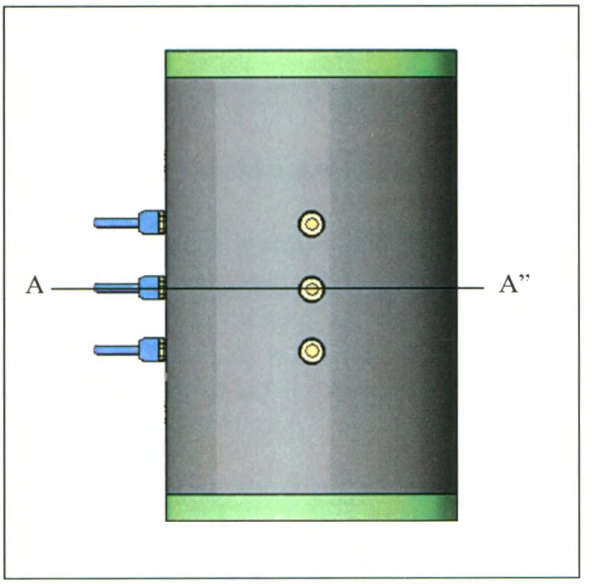

Figure 3.3. Side view of soil chamber

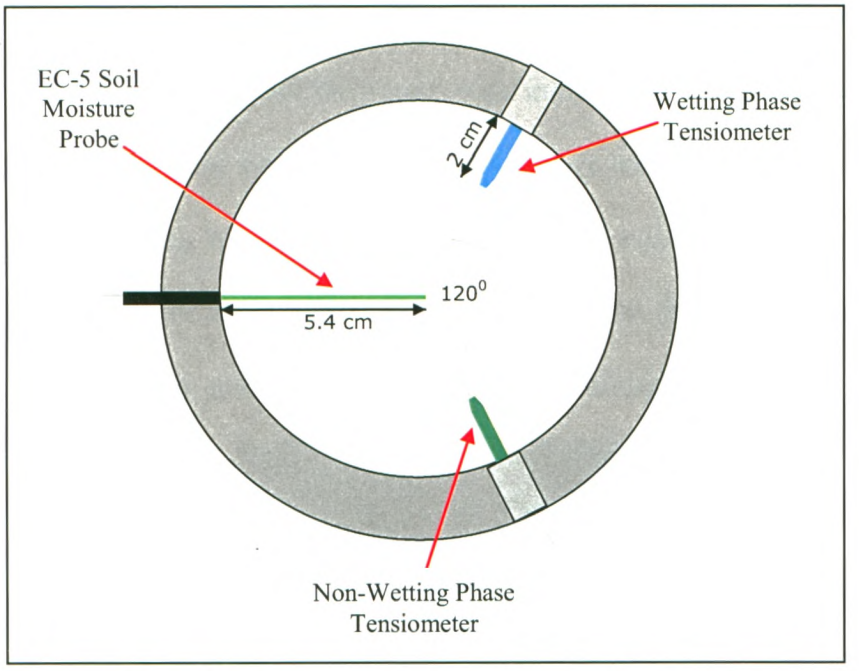

Figure 3.4. Cross-sectional view of soil chamber (A-A")

3.3 P_c-S_w Measurement Instruments

For one dimensional flow, direct measurement of the P_c-S_w relationship involves measuring the wetting fluid phase pressure, the non-wetting fluid phase pressure and the

wetting fluid saturation at the same time and level in the soil chamber (assuming sand is homogeneous throughout the level at which measurements are taken). See Figure 3.3 for the side view and Figure 3.4 for the cross-sectional view of the soil chamber illustrating the position of the P_c-S_w measurement instruments. In some experiments in this study it was assumed that the air phase had an infinite mobility and the upper boundary air phase pressure was used to approximate air phase pressure throughout the column [56].

3.3.1 Wetting Phase Tensiometer (WPT)

Wetting phase tensiometers (see Figure 3.5) were constructed by attaching ceramic porous cups (Soil Moisture Corp., Santa Barbara, CA. USA), to Swagelok fittings (0.25 inch pipe thread). In order to insert the porous cups into the Swagelok fittings, a hole (ID = 0.6cm) was drilled into the fittings and an O-ring grove was made on the inner wall of the hole. A Viton O-ring was then placed in the grove which allowed for a snug fit between the fitting and the ceramic cup. Finally, liquid Viton (Pelseal Technologies, PA. USA) was used to seal any space remaining between the fittings and the porous cups.

Figure 3.5. Ceramic porous cup attached to Swaglok fittings.

3.3.2 Non-Wetting Phase Tensiometer

To construct non-wetting phase tensiometers (NWPT), the ceramic cups were treated using either Octedecytrichlorosaline, Chlorotrimethysilane or Mythyltrichlorosilane with the latter treatment being the most effective.

Ceramic cups were treated with a 2% solution of Octedecytrichlorosaline (OTS) (Fisher Scientific, Ottawa, Ontario) in ethanol [57]. The ceramic cups and OTS solution were introduced into a screw lid container. The container was covered and placed into a shaker for 2 hours. The container was then uncovered and placed into a vacuum chamber for a period of 12 hours, after which the porous cups were then removed and excess OTS solution was allowed to drain. Finally, the cups were rinsed with pure ethanol. The treated cups were air dried for 24 hours before being attached to the customized Swaglok fittings.

Alternatively, NWPT were made by treating the ceramic cups with Chlorotrimethysilane (Fisher Scientific, Ottawa, Ontario) for 2 hours, followed by rinsing twice with toluene and twice with methanol [58]. The ceramic cups were then air dried over night before being attached to the customized Swaglok fittings. Prior to use in outflow experiments, the NWPT's were placed in a vacuum chamber for 5 hours.

Alternatively, NWPT were made by treating the ceramic cups with a 15% solution by volume of Mythyltrichlorosilane (100%) (Sigma-Aldrich Co.) in toluene (100%) [59], for 24 hours, followed by rinsing thoroughly with methanol (100%). The ceramic cups were

then air dried over night before being attached to the customized Swaglok fittings. Prior to use in outflow experiments, the NWPT's were placed in a vacuum chamber for 5 hours. This was done to ensure that the pores of the ceramic cups were completely saturated with the non-wetting fluid (air) at the beginning of each experiment.

3.4 FP2000 Pressure Transducer

Both wetting and non-wetting tensiometers were connected to FP2000 pressure transducers (Honeywell, Columbus, OH. USA). The FP2000 pressure transducers were configured to measure gage pressure between ±350 cm water with an accuracy of 0.10% - 0.25%. Data acquisition from these transducers was achieved by connecting them to a CR7 data logger (Campbell Scientific, Logan, Utah). When a 5V excitation is applied, the sensor's output voltage is linearly related to the gage pressure.

3.4.1 Pressure Transducer Calibration Procedure

The calibration of the transducers involves connecting them to a manometer and taking readings at known water heights or heads. Raw mV readings were plotted against these known water level heads. A linear equation was then fit to the calibration data. Calibrations were conducted prior to both hydraulic conductivity and outflow experiments. This ensured minimal drift (< 2 mm) in readings over the experimental time period.

3.5 EC-5 Soil Moisture Probe

Wetting phase saturation was determined by EC-5 soil moisture sensors (Decagon Devices, WA. USA). The EC-5 probe uses the capacitance technique to measure the dielectric permittivity of the surrounding medium [60].

3.5.1 EC-5 Calibration Procedure

A 2 point calibration procedure developed by [61], was used to calibrate the EC-5 probes so that moisture content in the near dry and near saturated ranges are accurately predicted. In this procedure, raw EC-5 readings are taken at 0% saturation (i.e.; dry sand) and at 100% saturation (i.e.; after saturating the column). Raw EC-5 readings (mV) were recorded by the Campbell Scientific data logger. These readings were first converted to ADC (Analogue to Digital Converter numbers) using the following equation:

$$ADC = mV * 1.6384 \qquad (3.1)$$

Saturation is then given by:

$$S_w = \frac{(ADC^{2.5} - ADC_{dry}^{2.5})}{(ADC_{sat}^{2.5} - ADC_{dry}^{2.5})} \qquad (3.2)$$

Where ADC is the experimental readings (taken during an outflow experiment) and converted using Equation 3.1, ADC_{dry} is the reading taken at 0% saturation (dry soil) and ADC_{sat} is the reading taken at 100% saturation. This procedure has been shown to have an error of ± 0.005 cm^3cm^{-3} for dry sand and $\pm 0.028 cm^3cm^{-3}$ for saturated sand when the calibration procedure is applied to multiple instruments [61]. However, it was reported

that the instrument error decreases with sensor specific calibration. Therefore sensor specific calibrations were conducted for each EC-5 sensor used in the following study.

A comparison study between the 2 point calibration [61] and a linear calibration procedure [62] is given in Appendix C. The 2 point calibration procedure has been shown to significantly improve the accuracy of the saturation predictions and is capable of capturing saturation over the full range of saturation values i.e. 0 to 100%. Therefore the 2 point calibration procedure was chosen to determine the saturation from EC-5 experimental data for all experiments in the following study.

3.6 Dry Packing and Saturation Procedure

Once the tensiometers and EC-5 probes were calibrated and positioned along the length of the soil chamber, a stainless steel mesh (0.015 by 0.015 cm pore size) was placed at the lower end of the chamber and the end cap was attached. Sand was poured into the cell in 2 cm lifts. After each lift was in place, the pressure cell was vibrated to allow the sand to settle.

Layering was minimized by using a small spatula to slightly disturb the surface layers of the sand before the addition of subsequent lifts. After dry packing, a stainless steel mesh was positioned at the upper end of the soil chamber and an end cap was attached. The weight of the packed sand (M_s) was determined. Next the porosity (ϕ) was calculated by:

$$\phi = 1 - [(M_s / \rho_s) / V_T] \qquad (3.3)$$

where ρ_s is the particle density (assumed to be 2.65 g/cm^3) and V_T is the total volume of the soil chamber (1571 cm^3). Once the porosity of the packing was within an acceptable range (i.e. 0.3 to 0.33) then the pressure cell was then flushed with CO_2 for 20 minutes. After flushing with CO_2, the column was slowly saturated with de-ionized water at a rate of 1 mL/minute for at least 24 hours.

3.7 Saturated Hydraulic Conductivity Measurements

Hydraulic conductivity for the sand and membranes was quantified using the constant head method as illustrated in [63]. Figure 3.6 shows the experimental set up used to measure the hydraulic conductivity. The column inlet is connected to a large manometer (ID = 7cm). Pressure in the headspace above the manometer is regulated via a pressure regulator to increase inlet boundary water pressure above hydrostatic conditions.

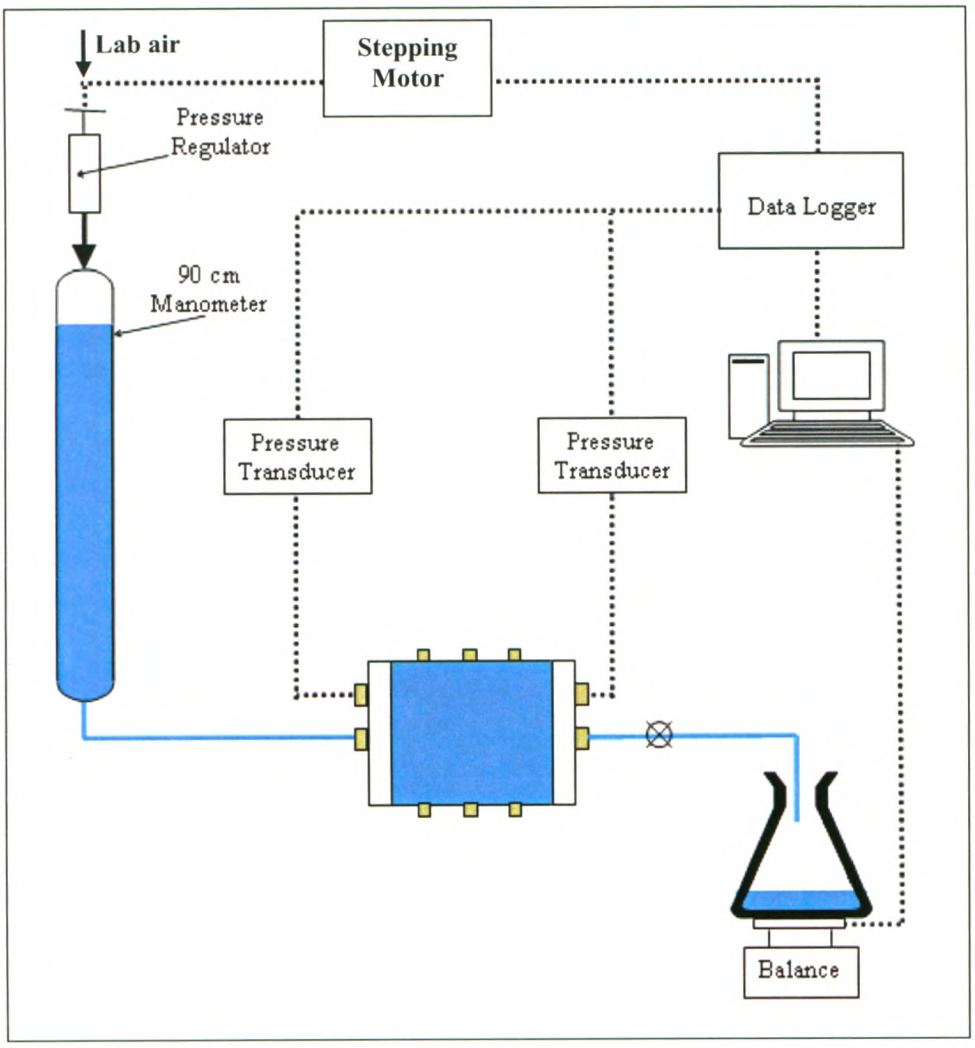

Figure 3.6. Hydraulic conductivity experimental setup

Water flows from the manometer through the horizontally oriented pressure cell and outflow was measured at 30 second intervals using a balance (Adventure Pro., Ohaus NJ. USA) connected to a computer. The pressure heads at both the inflow and outflow boundaries were also measured every 30 seconds using the pressure transducers. During the hydraulic conductivity experiment, the water pressure at the inflow boundary was automatically lowered by decreasing the air pressure above the water phase via a stepping motor attached to a pressure regulator (ever 4 minutes).

For one-dimensional flow, Darcy's law can be arranged to give:

$$K = \frac{QL}{A(\Delta H)} \qquad (3.4)$$

Where K is the saturated hydraulic conductivity, Q is the flow rate, L is the length of the soil chamber, A is the cross-sectional area and ΔH is the difference in pressure measured at the inflow and outflow boundaries. Results from a representative hydraulic conductivity experiment are presented in Appendix D.

After measuring the hydraulic conductivity of the packed column, the bottom end cap of the pressure cell was removed and a pre-saturated hydrophilic membrane (Nylaflo 0.2μm pore size, Pall Corporation, Ann Arbor Michigan) was placed at the lower end of the pressure cell. Care was taken to ensure that no air bubbles were trapped under the membrane as this may result in pore water blockage during the outflow experiments [33]. The hydraulic conductivity procedure was then repeated and the K of both sand and membrane was obtained. Hydraulic conductivity of the membrane is given by the following equation:

$$K_{mem} = \frac{L_{mem}}{\left(\frac{L_T}{K_T} - \frac{L_{sand}}{K_{sand}}\right)} \qquad (3.5)$$

where K_{mem} is the hydraulic conductivity of the nylon membrane, K_{sand} is the hydraulic conductivity of the sand, K_T is the hydraulic conductivity of the combination of sand and

membrane, L_{mem} is the thickness of the membrane and L_T is the length of the sand and membrane.

3.8 Static and Dynamic Outflow Experiments

To determine the effect of flow rate on the measured P_c-S_w relationship, both static and dynamic primary drainage experiments were conducted using an automated laboratory apparatus developed to investigate one-dimensional, two-phase flow in porous media. The experimental set up is illustrated in Figure 3.7. Here the pressure cell was positioned vertically on a stand.

In experiments conducted with F32-F50 sand, a nylon membrane was emplaced at the lower boundary while a stainless steel mesh was used to hold the sand in place at the upper boundary. Three sets of P_c-S_w instruments were located at three levels along the length of the column as shown in Figure 3.7. Each set of P_c-S_w instruments consists of one non-wetting phase tensiometer, one wetting phase tensiometer and one EC-5 soil moisture probe.

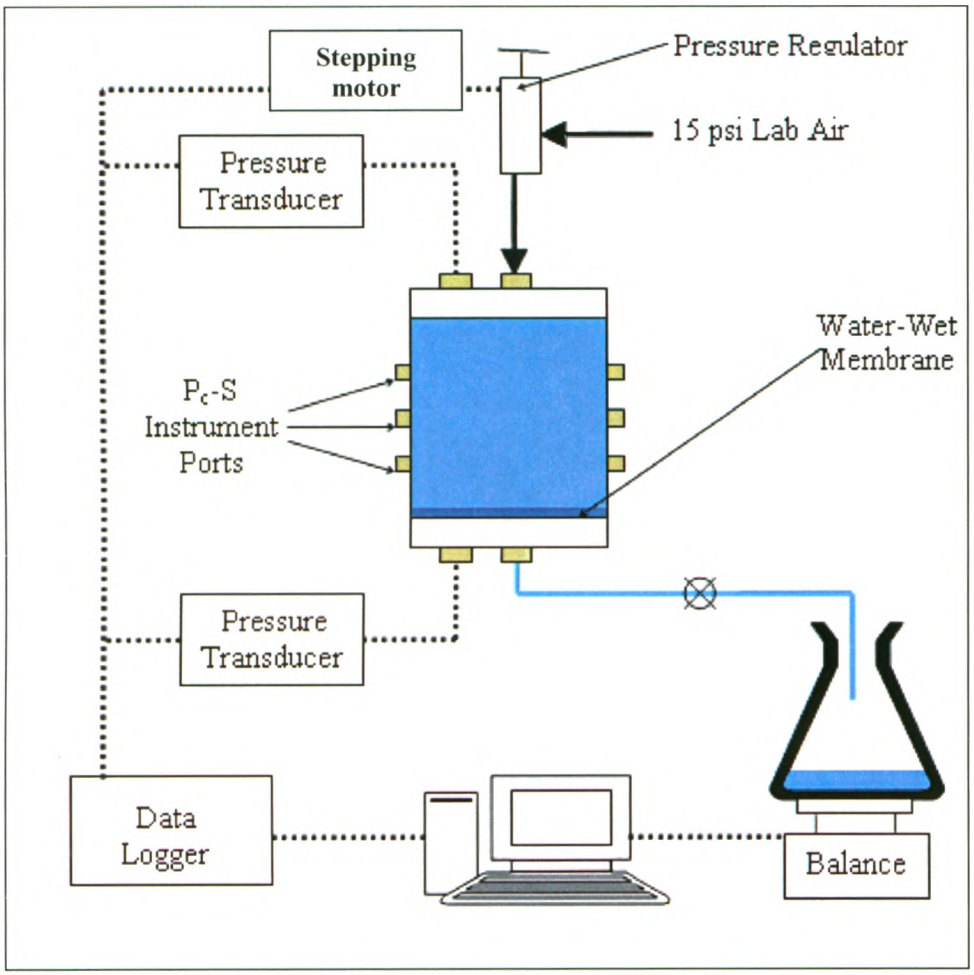

Figure 3.7. Outflow experimental setup

Outflow was induced by increasing the air boundary pressure above atmospheric at the top of the column. Water was allowed to drain out of the cell from the bottom boundary to a constant head reservoir. All experiments were started with the system in hydrostatic equilibrium at 100% saturation.

Static experiments were conducted by increasing the air phase pressure in small increments (2-3cm water) and allowing the system to equilibrate (i.e. an outflow rate of < 0.2 g/hr). Once equilibrium was achieved, this process was repeated until a residual water

saturation was achieved. Dynamic experiments were conducted by increasing the upper boundary air pressure to either 135 or 214 cm water in one step. This large initial step ensures a rapid rate of saturation change.

Chapter 4 - Results

4.0 Introduction

Results from the primary drainage experiments conducted on packed cores of F32-F50 and F70 sands at varying boundary conditions are presented in this section. For the F32-F50 sand, drainage was induced under three desaturation rate regimes. Two experiments were conducted under static or slow desaturation rates (See Figure 4.1 for example). Five experiments were conducted at an intermediate desaturation rate induced by maintaining a constant upper boundary air pressure of 135 cm H_2O (See Figure 4.2 for an example) and three experiments were conducted at a fast desaturation rate induced by imposing a constant upper boundary air pressure of 214 cm H_2O (See Figure 4.3 for an example).

For the F70 sand, two static and three dynamic experiments were conducted, similar to those for the F32-F50 sand. The major difference being that no membranes were used in the F70 experiments. Here F70 dynamic experiments were induced by applying an initial upper boundary air pressure of 135cm water. The measured parameters i.e. cumulative outflow, air and water pressures and water saturation are provided in Appendix A for all experiments.

A comparison of the column properties is provided in Table 4.1. Variations in the measured porosity and permeability between experiments were consistent with other studies e.g. [14] as shown by the normalized 95% confidence intervals of the mean measured parameter (see Table 4.1).

Table 4.1. Summary of unsaturated experimental results

Experiment Type	Porosity (ϕ)	$k_{sand}(m^2)$	$k_{mem}(m^2)$	Total Pore Vol. (cm^3)	Cumulative Outflow (g)
F32-F50 Static 1	0.32	$6.32X10^{-11}$	$1.15X10^{-15}$	499.3	361.0[c]
F32-F50 Static2	0.32	$6.06X10^{-11}$	$1.09X10^{-15}$	504.1	446.0
F32-F50 Dynamic1[a]	0.32	-	-	502.2	467.0
F32-F50 Dynamic2[a]	0.32	$5.26X10^{-11}$	$1.07X10^{-15}$	504.5	461.7
F32-F50 Dynamic3[a]	0.32	$2.67X10^{-11}$	$8.76X10^{-16}$	498.2	453.4
F32-F50 Dynamic4[a]	0.30	$5.71X10^{-11}$	$1.09X10^{-15}$	471.0	433.6
F32-F50 Dynamic5[a]	0.32	$5.61X10^{-11}$	$1.50X10^{-15}$	504.1	469.6
F32-F50 Dynamic6[b]	0.31	-	-	492.1	467.3
F32-F50 Dynamic7[b]	0.31	-	-	491.0	444.5
F32-F50 Dynamic8[b]	0.33	-	-	512.0	443.2
Mean	0.32	$5.27X10^{-11}$	$1.13X10^{-15}$	490.1	454.0
Normalized 95% C.I.	1.6	6.2	14.5	1.4	1.9
F70 Static 1	0.32	-	n/a	506.5	390.2
F70 Static 2	0.32	-	n/a	509.5	379.9
F70 Dynamic 1[a]	0.32	-	n/a	498.3	365.9
F70 Dynamic 2[a]	0.32	-	n/a	508.5	376.7
F70 Dynamic 3[a]	0.32	-	n/a	504.9	368.3
Mean	0.32	-	n/a	505.5	376.2
Normalized 95% C.I.	0.7	-	n/a	0.8	2.7

[a] Experiments conducted with upper boundary air pressure increased to 135cm H_2O in one step
[b] Experiments conducted with upper boundary air pressure increased to 214cm H_2O in one step
[c] Experiment stopped before S_{rw} achieved (inflow at equilibrium of final pressure step). This reading was not used to compute the mean cumulative outflow.
[d] $Normalized95\%C.I. = \frac{95\%C.I.}{Mean} \times 100$

4.1 Static Drainage Experiments

Upper boundary air pressure, lower boundary water pressure, tensiometric water pressure at 3 levels, S_w at 3 levels and cumulative outflow were measured for the static experiments and plotted in Figure 4.1. Cumulative outflow was induced by increasing the upper boundary air pressure above atmospheric pressure in approximately 2 cm H_2O pressure increments. After each pressure step, sufficient time was allowed for equilibrium to be achieved between the air and water phases within the sample. Equilibrium was

assumed to be achieved when an outflow rate of < 0.2g/hr was reached. The time needed to achieve this hydraulic equilibrium varied with saturation.

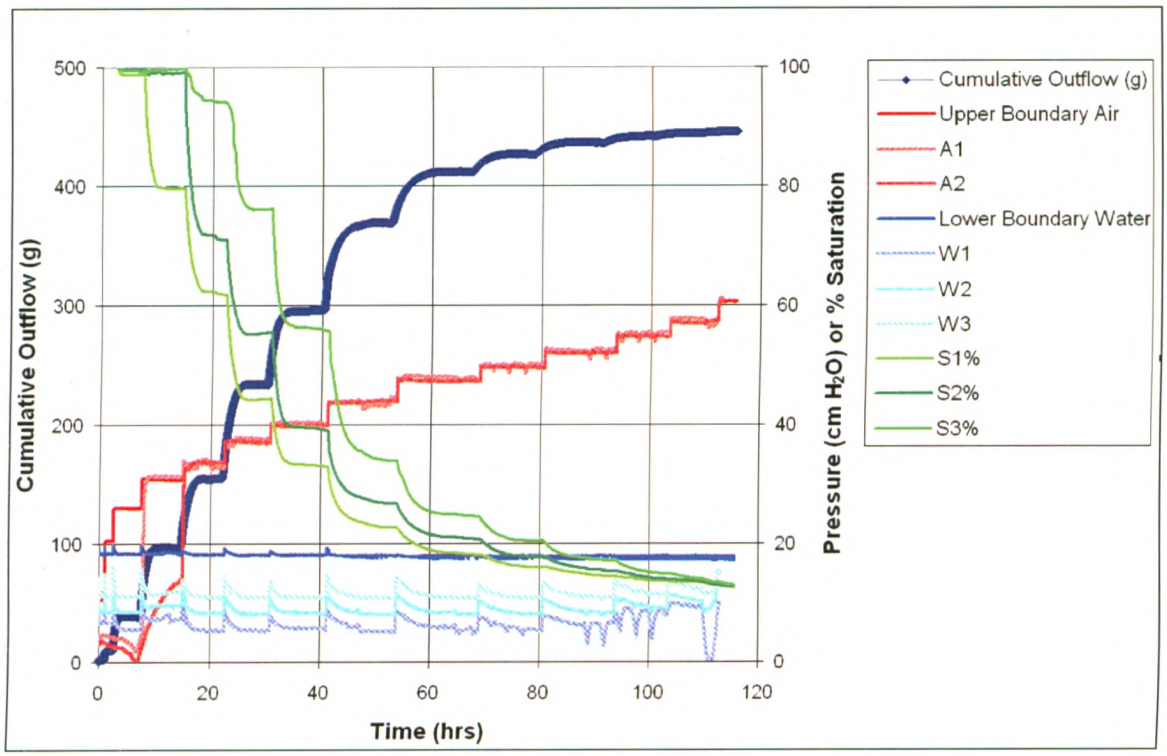

Figure 4.1. Measured experimental parameters at levels 1, 2 and 3 for F32-F50 Static Experiment 2: cumulative outflow, tensiometric air pressures (A1, A2 and A3), tensiometric water pressures (W1, W2 and W3) and saturations (S1, S2 and S3) vs. time

The outflow rate was highest at high saturations and hydraulic equilibrium was quickly achieved. At lower saturations, the outflow rate decreased resulting in a longer time to equilibrium. The observed lower flow rate was a result of a reduced relative wetting phase permeability at lower saturations. The evolution of saturation with time for all static experiments revealed that drainage occurred sequentially starting at level 1 followed by level 2 and then level 3. (e.g. Figure 4.1)

During static experiments water pressure remained near hydrostatic pressure at measured various levels in the column. Small increases in water pressure were recorded immediately following an increase in air pressure. The increase in water pressure dissipated as equilibrium was approached. F32-F50 Static experiment 1 was stopped at $S_w \sim 0.25$ (measured at the midpoint of the column) due to inflow occurring at equilibrium after the last pressure step. The other static experiment (F32-F50 Static experiment 2) was conducted until a residual water saturation (S_{rw}) was achieved, i.e. $S_{rw} \sim 0.13$ (measured at the midpoint of the column).

Tensiometric air pressure was only measured in F32-F50 static experiment 2. Air pressure results recorded at level 3 was not reported due to water infiltration into the ceramic cup connected to this tensiometer. At level 1 and 2, the tensiometric air pressures were in good agreement with the upper boundary air pressure at the onset of desaturation.

4.2 Dynamic Drainage Experiments

The measured parameters for F32-F50 dynamic experiments 1 to 5 are presented in Figures A.2 to Figure A.6 respectively (see Appendix A). In these experiments, drainage was initiated by increasing the upper boundary air pressure to 135cm water at the start of the experiment and then held constant throughout the F32-F50 drainage experiments (see for e.g. Figure 4.2).

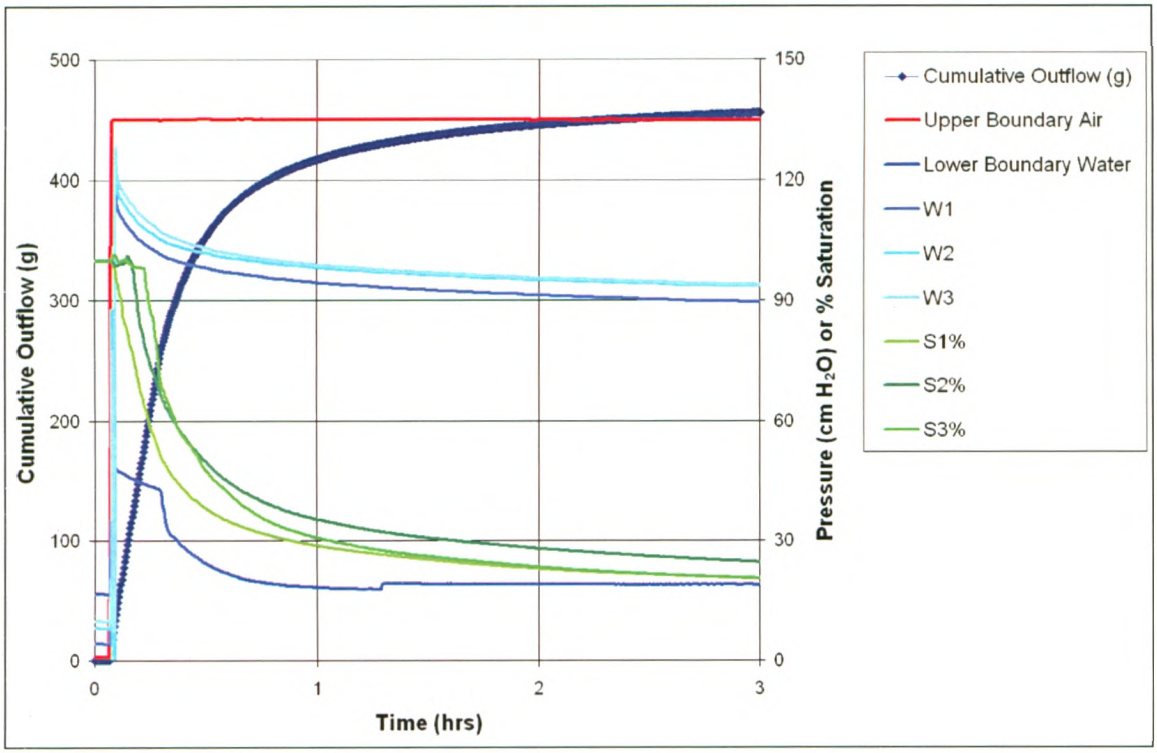

Figure 4.2. Measured experimental parameter at levels 1, 2 and 3 for F32-F50 Dynamic Experiment 5 (Pair=135 cm): outflow, tensiometric water pressures (W1, W2 and W3) and saturations (S1, S2 and S3) vs. time

The average maximum desaturation rate measured during these experiments was determined to be 1.4×10^{-03} s^{-1} (see Table 4.2) which was 2.4 times faster than that measured in the F32-F50 static experiments.

Table 4.2. A comparison of the measured desaturation rate (dS_w/dt) and residual saturations (S_{rw}) for dynamic drainage experiments

Experiment Name	Instrument Level	S_{rw}	Mean S_{rw}	Max dS_w/dt (s^{-1}) [a]	Mean max $\delta S_w/\delta t$
F32-F50 Dynamic 1	3	0.21	0.27	0.0017	0.0014
F32-F50 Dynamic 2	3	0.27		0.0016	
F32-F50 Dynamic 3	3	0.38		0.0012	
F32-F50 Dynamic 4	1	0.3		0.0009	
F32-F50 Dynamic 5	2	0.24		0.0014	
	3	0.2		0.0015	
F32-F50 Dynamic 6	2	0.26	0.22	0.0027	0.0024
F32-F50 Dynamic 7	1	0.18		0.0020	
	2	0.18		0.0019	
	3	0.23		0.0019	
F32-F50 Dynamic 8	2	0.21		0.0024	
	3	0.24		0.0033	
F70 Dynamic 1	1	0.23	0.28	0.0033	0.0021
	2	0.26		0.0017	
	3	0.29		0.0015	
F70 Dynamic 2	1	0.26		0.0024	
	2	0.3		0.0012	
	3	0.31		0.0015	
F70 Dynamic 3	1	0.25		0.0027	
	2	0.29		0.0021	
	3	0.34		0.0026	

[a] The max dS_w/dt rate is defined as the highest desaturation rate determined from experimental EC-5 readings.

To investigate the impact of pressure step size and desaturation rate on the measured P_c-S_w relationship, F32-F50 dynamic experiments 6, 7 and 8 were conducted with a constant upper boundary air pressure of 214cm H_2O. A representative plot of the measured parameters is shown in Figure 4.3. A mean maximum desaturation rate of $2.4x10^{-03}$ s^{-1} (see Table 4.3) was observed. This was approximately 4.2 times larger than the mean maximum desaturation rate determined for the F32-F50 static experiments.

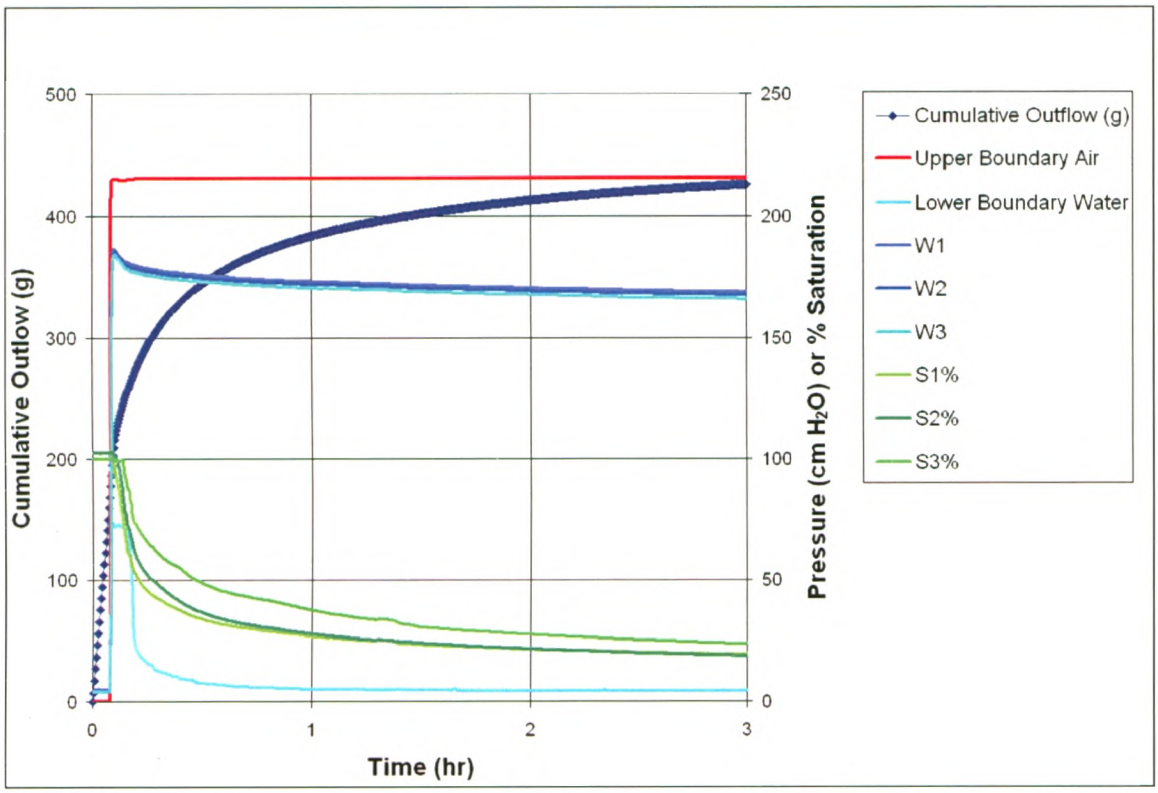

Figure 4.3. Measured experimental parameters at levels 1, 2 and 3 for F70 Dynamic Experiment 7: outflow, tensiometric water pressures (W1, W2 and W3) and saturations (S1, S2 and S3) vs. time

Since hydrophilic membranes were used in all F32-F50 experiments, air pressure within the column was assumed to be equal to the measured air pressure at the upper boundary. Here capillary pressure was calculated as the difference between the upper boundary air pressure and the tensiometric water pressure. This assumption was verified by conducting F32-F50 dynamic drainage experiment 9 (Pair=135cm) which is reported in Figure A.10, Appendix A. In this experiment, in situ air pressure was measured with non-wetting tensiometers while desaturation was measured using the EC-5 probes. Air pressure and saturation measurements on all three levels indicated that the measured in situ air pressure was equal to the applied upper boundary air pressure at the onset of desaturation.

In the F70 dynamic experiments 1 to 3, the upper boundary air pressure was initially set to 135 cm water (See for e.g. Figure 4.4).

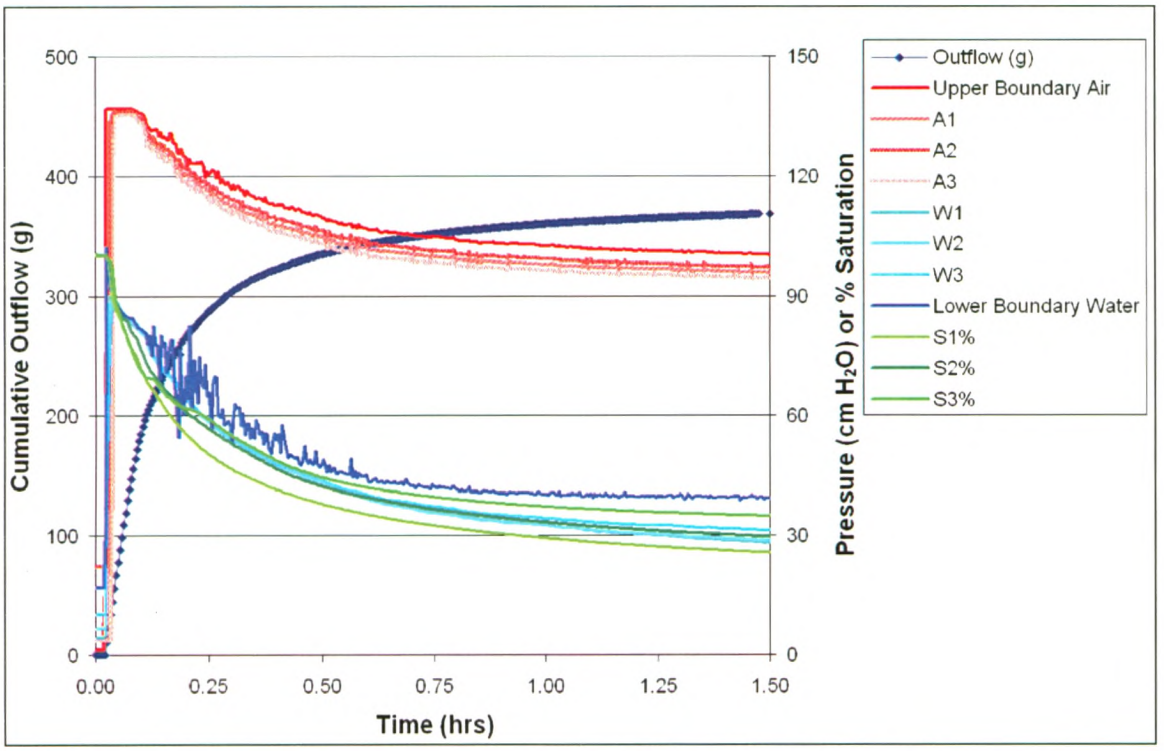

Figure 4.4. Measured experimental parameters at levels 1, 2 and 3 for F70 Dynamic Experiment 3: outflow, tensiometric air pressures (A1, A2 and A3), tensiometric water pressures (W1, W2 and W3) and saturations (S1, S2 and S3) vs. time

Since no hydrophilic membranes were used in the F70 sand experiments, the upper boundary pressure was shown to decrease as air began to exit the column. For F70 Dynamic experiments 2 and 3, the tensiometeric air and water pressure measurements were used to calculate the capillary pressure as the upper boundary air pressure could no longer be assumed constant over the entire saturation range. In order to determine if the difference between the measured dynamic and static capillary pressure was due to a delay in the wetting phase porous cup/tensiometer setup, a comparison between the response time of the lower boundary pressure reading and the response time of the tensiometer at level 3 was conducted for a F70 Dynamic experiment. The pressure measurement at the

lower boundary was shown to respond almost instantaneously while the tensiometer at level 3 was shown to have a small response time of approximately 30 sec. This small initial response time is not thought to have affected the determination of the dynamic capillary pressure since the wetting phase tensiometers respond before desaturation takes place at any given level in the column.

In F70 Dynamic experiment 1, the non-wetting tensiometers failed, therefore the capillary pressure was calculated as the difference between the upper boundary air pressure and tensiometeric water pressures. Here in situ air pressure can be assumed to be equal to the upper boundary air pressure once air has not exited the column. In this experiment air begun to exit the column at the time when the water saturation was 52%, 65% and 66% at level 1, level 2 and level 3 respectively. These saturations were used as the lower limit for the reported τ values in this experiment.

The average maximum desaturation rate in the F70 Dynamic experiments was $2.1x10^{-03}$ s^{-1} (see Table 4.2). Although the F70 sand had a lower permeability ($1.5X10^{-11}$ m^2), a faster desaturation rate was recorded in comparison to the F32-F50 sand for experiments with identical initial conditions. This may have been due to the hydrophilic membranes used in the F32-F50 experiments. The permeability of the F32-F50 sand column was reduced to $1.7X10^{-12}$ m^2 when a hydrophobic membrane was placed at the lower end of the column.

Water saturations at levels 1 and 2 were not reported for F32-F50 dynamic experiments 1 to 3 and for levels 2 and 3 for F32-F50 dynamic experiment 4 since the EC-5 probes at these levels were oriented horizontally in the soil column. The horizontally oriented EC-5 probes yielded unrealistically high water saturations, which were likely due to water pooling on the flat end of the probes.

Following the start of these experiments, tensiometric water pressures immediately increased from hydrostatic to a maximum value depending on the applied air pressure. Unlike the static experiments, the in situ water pressure did not return to hydrostatic conditions but reached an equilibrium value of approximately 80 cm, 170 cm and 35 cm at residual saturation for F32-F50 Dynamic (Pair=135cm), F32-F50 Dynamic (Pair=214cm) and F70 Dynamic (Pair=135cm) experiments respectively. This increase in the equilibrium water pressure was attributed to the applied boundary conditions (see for example [56]. As residual saturation is approached, wetting phase relative permeability decreases [39] resulting in film flow, eventually leading to a discontinuous wetting phase [4]. Here the high, constant air pressure acting on the slowly flowing films and disconnected portions of the wetting phase (both within the pores and around the tensiometers), prevent the tensiometric water pressure from attaining hydrostatic equilibrium.

In F32-F50 dynamic experiment 5, 6 and 8, the EC-5 probes were shown to detect a change in saturation before wetting phase tensiometers reached a maximum. This may have occurred because the EC-5 probes were vertically larger than the tensiometers.

Since both instruments were centered at each level, this meant that the EC-5 probes extended approximately 1 cm above the tensiometers. This may have resulted in the EC-5 detecting a change in saturation before the tensiometers responded especially at the high desaturation rates measured at level 1. In these cases data from these levels were omitted from any further analysis as this would suggest water desaturation prior to an increase in capillary pressure. During dynamic experiment 6, air bubbles were trapped in the line connecting the wetting phase tensiometer at level 3 to the pressure transducer. This resulted in erroneous water pressure readings at this level. Therefore data from this level was omitted from further analysis.

In general, experiments conducted with identical boundary conditions were shown to be reproducible with the static P_c-S_w experiments yielding the highest reproducibility. For example at $S_w = 0.5$, the normalized 95% C.I. on capillary pressure for F32-F50 static experiments, F32-F50 dynamic experiments (P_{air} = 135cm) and F32-F50 dynamic experiments (P_{air} = 214cm) was 0.01%, 4.6% and 3.4% respectively. A comparison of P_c-S_w curves measured at three levels within the same column for a static experiment (Figure 4.5) and a dynamic experiment (Figure 4.6) show that measurements made on all three levels were reproducible, i.e. having similar P_d and S_{rw}. This is an indication that a homogeneous packing was achieved within the column.

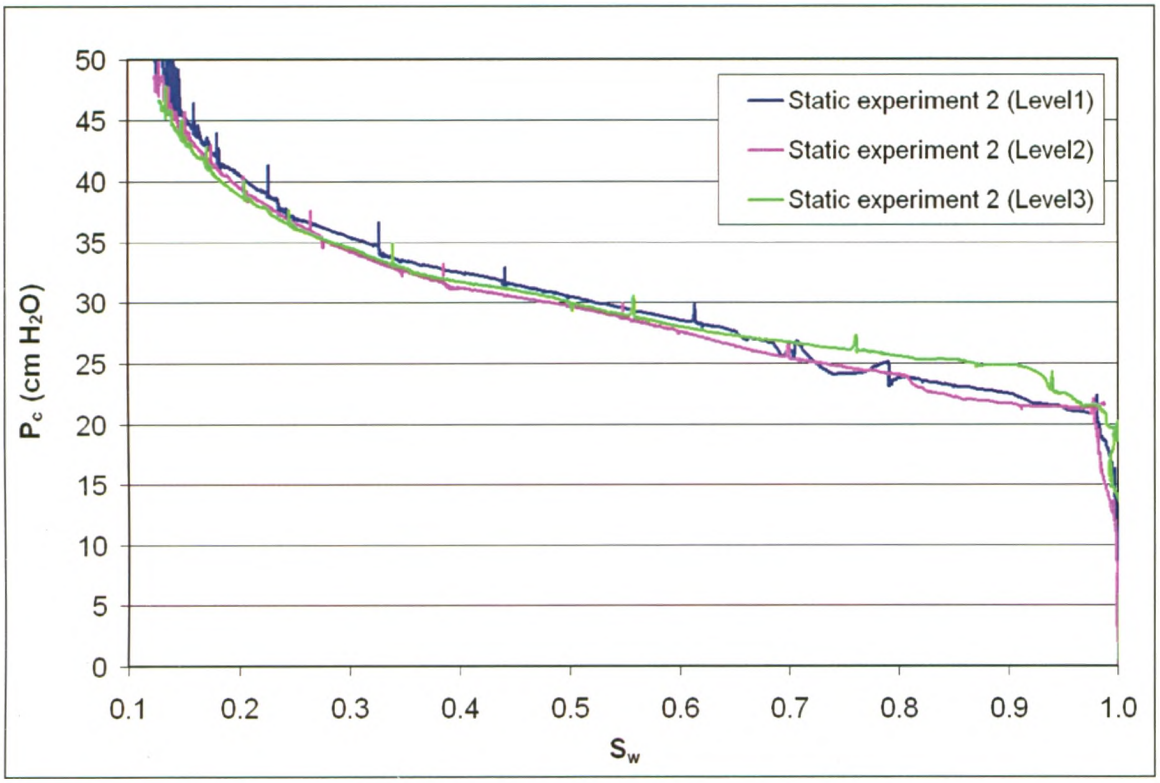

Figure 4.5. Comparison of P_c-S_w Curves measured at three different levels for F32-50 Static Experiment 2.

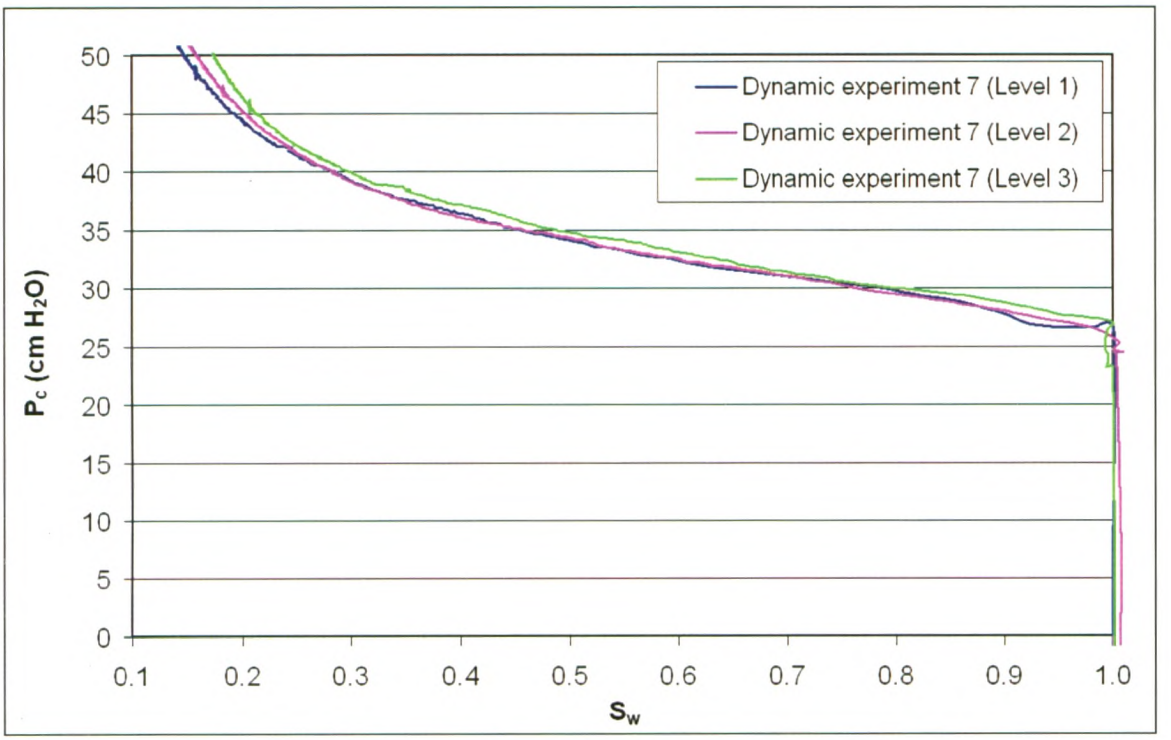

Figure 4.6. Comparison of Pc-S_w curves for Dynamic Experiment 7 (Pair=214cm water)

A comparison of the normalized effective cumulative outflow is given in Figure 4.7, Figure 4.8 and Figure 4.9 for F32-F50 dynamic experiments conducted at P_{air} = 135cm, F32-F50 dynamic experiments conducted at P_{air} = 214cm and for F70 dynamic experiments conducted with an initial upper boundary air pressure of 135cm, respectively. The outflow data was normalized in order to facilitate a direct comparison between experiments conducted with different column packings (i.e. variable total pore volumes). Here the normalized effective cumulative outflow is given by Equation 4.1

$$Norm.Q_c^{eff} = \left(\frac{Norm.Q_c - Norm.Q_c^{residual}}{1 - Norm.Q_c^{residual}} \right) \qquad (4.1)$$

where $Norm.Q_c = \frac{Q_c}{P.V.}$. $Norm.Q_c^{eff}$ is the normalized effective cumulative outflow, $Norm.Q_c^{residual}$ is the normalized residual cumulative outflow, $Norm.Q_c$ is the normalized cumulative outflow, Q_c is the cumulative outflow and $P.V.$ is the pore volume.

These comparisons shows that outflow induced under identical boundary conditions was reproducible over the first 10 minutes and 30 minutes for F32-F50 dynamic experiments (Pair=135cm) (see Figure 4.7) and F32-F50 dynamic experiments (Pair=215cm) (see Figure 4.8) respectively. The outflow of the F70 dynamic experiments was highly reproducible over the first 60 minutes (see Figure 4.9). After the first 10 minutes, the outflow measured during F32-F50 dynamic experiment 4 was shown to be lower in comparison to the outflow of the other F32-F50 dynamic experiments conducted at the same boundary conditions (see Figure 4.7). The F32-F50 dynamic experiment 4 packing had the lowest measured porosity (0.30) and lowest cumulative outflow (433.6g). The measured maximum desaturation rate was also shown to be the lowest recorded at level 1 (0.009). During this experiment, there was a small leak originating from the EC-5 probe port at level 1. These experimental variations may have contributed to the observed lower cumulative outflow as this experiment progressed. Due to the above states reasons, F32-F50 dynamic experiment 4 was not included in any further analysis.

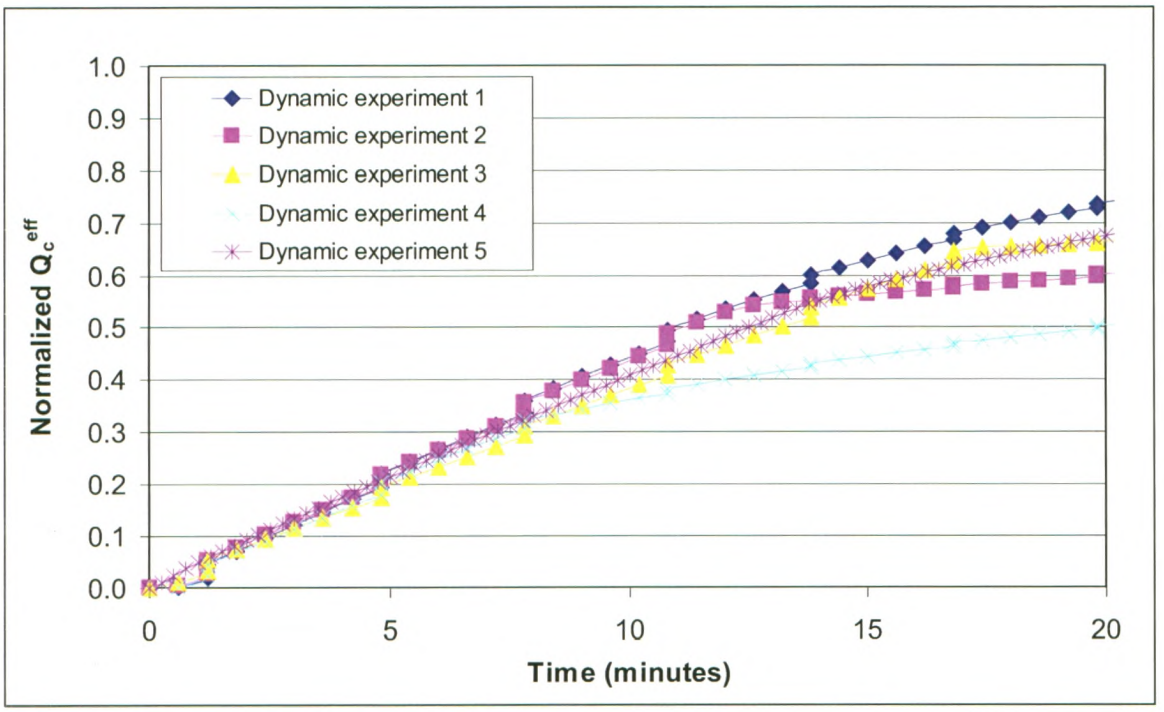

Figure 4.7. A comparison of the normalized effective cumulative outflow vs. time for dynamic experiments conducted at constant upper boundary air pressure of 135 cm water

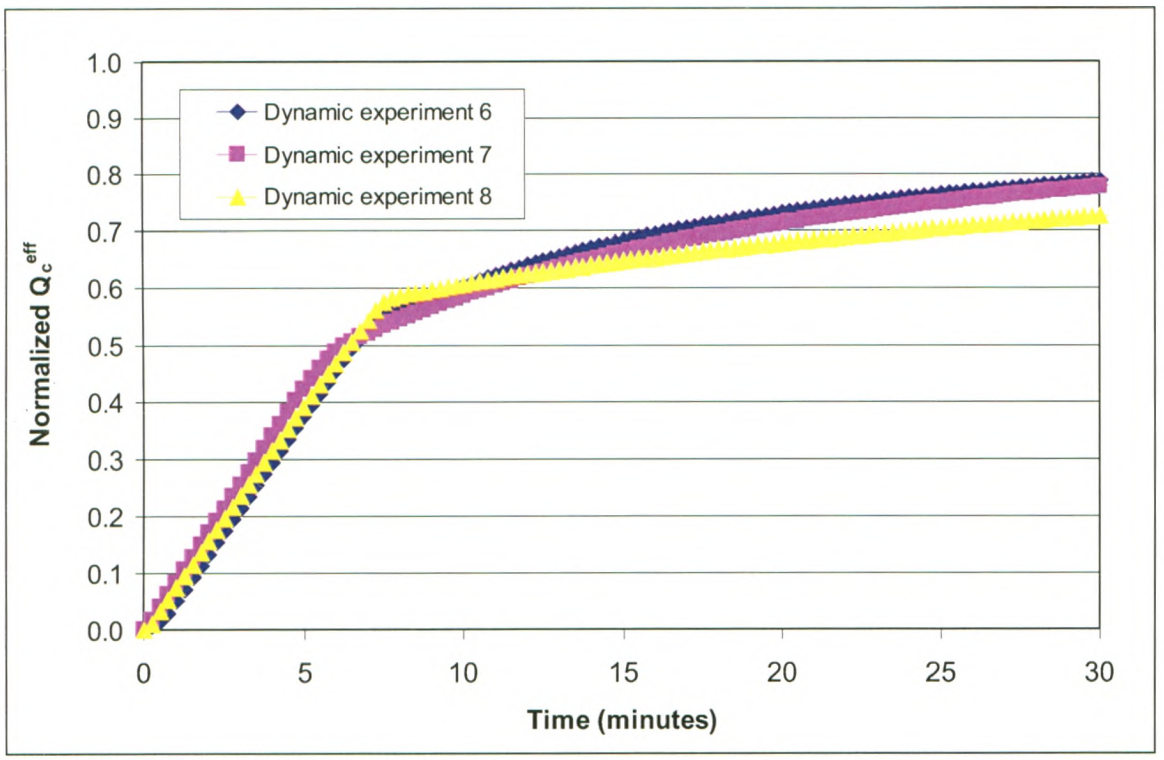

Figure 4.8. A comparison of the normalized effective cumulative outflow vs. time for dynamic experiments conducted at a constant upper boundary air pressure of 214 cm water

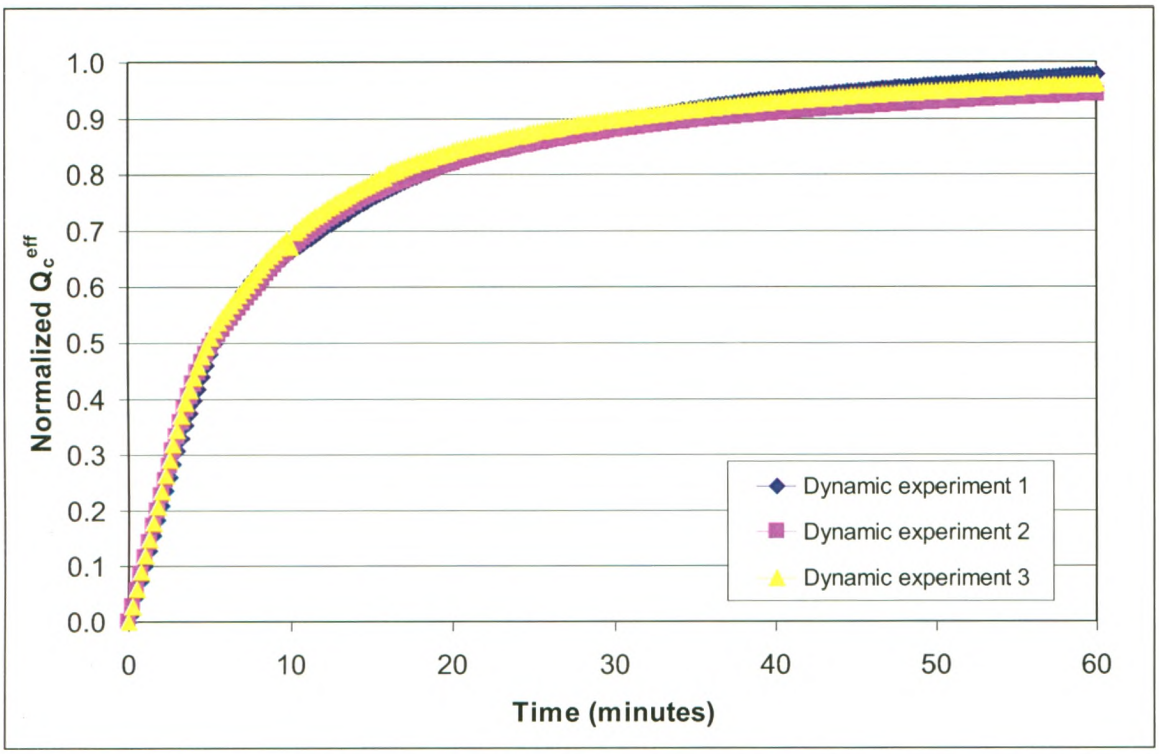

Figure 4.9. A comparison of the normalized effective cumulative outflow vs. time for F70 dynamic experiments conducted at an initial upper boundary air pressure of 135 cm water.

4.3 Statistical Analysis of Measured Static and Dynamic P_c-S_w Curves

In order to make a comparison between P_c-S_w curves measured under varying boundary conditions, the saturation data was divided into 0.005 intervals for static experiments and 0.01 intervals for dynamic experiments. For static experiments at least 3 independent points used to calculate the mean. For dynamic experiments at least 2 independent data points were used for S_w greater than 0.7 and at least 4 independent data points for S_w less than 0.7. For each saturation interval, the mean P_c and the 95% confidence interval about the mean were computed for each experiment type i.e. static, dynamic (P_{air}=135cm) and dynamic (P_{air}=214cm). The 95% confidence intervals were used to compare mean P_c-S_w curves for experiments conducted under varying boundary conditions. Figure 4.10 and Figure 4.11 show this comparison for the F32-F50 and F70 drainage experiments

respectively. As the maximum experimental desaturation rate increased, capillary pressure, measured at a given water saturation increased.

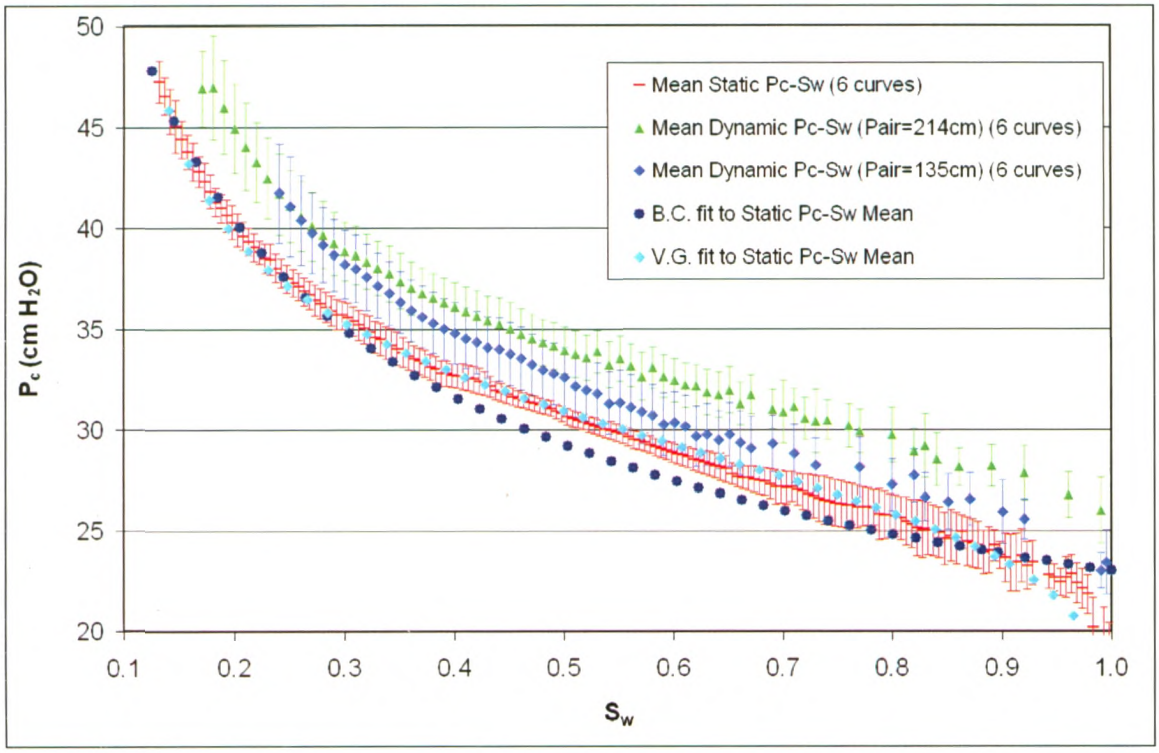

Figure 4.10. Comparison of the F32-F50 mean static, F32-F50 mean dynamic (upper boundary = 135cm water) and F32-F50 mean dynamic (upper boundary air pressure = 215cm water) measured capillary pressure-saturation curves. Error bars indicate the 95% confidence intervals about the mean.

The mean entry pressure (P_d) increased with the desaturation rate. For the F32-F50 sand, a mean P_d of 18.1 cm (C.I. = 1.6), 23.0 cm (C.I. = 0.89) and 26.0 cm (C.I. = 3.1) was recorded for experiments conducted at the slowest (static), intermediate (Pair=135cm) and fastest (Pair=214cm) desaturation rates respectively. A comparison of experiments conducted under the fastest (P_{air}=214cm) and the slowest (static) desaturation rates, reveal that there was a statistical difference between the measured P_c-S_w curves as shown in Figure 4.10. For the F70 sand, a clearly defined P_d for the mean static experiments was

not observed. However a statistical difference between the static mean and dynamic mean P_c-S_w curves was detected as shown in Figure 4.11.

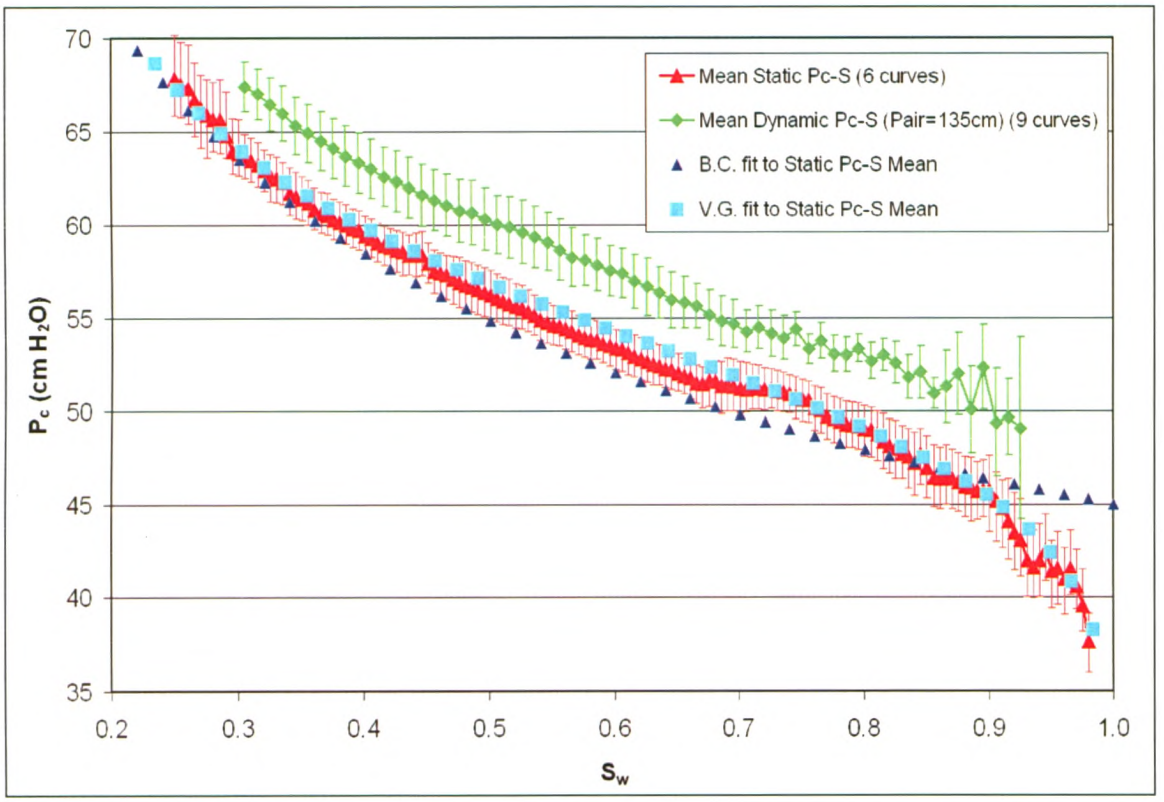

Figure 4.11. Statistical analysis of drainage experiments conducted on F70 sand. Static and dynamic (initial upper boundary air pressure = 135 cm water) primary drainage capillary pressure-saturation curves show 95% confidence intervals of the mean static and dynamic curves.

4.4 Direct Quantification of τ: Method 1

The damping coefficient (τ) has been calculated for all dynamic experiments based on the linear relationship proposed by [1] (see Equation 4.2).

$$P_c^{dynamic} = P_c^{static} - \tau\left(\delta S_w / \delta t\right) \qquad (4.2)$$

Here, P_c^{static} (the static P_c-S_w relationship) was determined by fitting van Genuchten P_c-S_w function (see equation 4.3) parameters to the mean static P_c-S_w curve .α, n, and S_{rw} were determined to be $3.47X10^{-02}$ cm^{-1}, 8.9 and 0.11 respectively.

$$P_c = \left[S_w^{eff\,(-1/m-1)^{1/n}} \right] \Big/ \alpha \qquad (4.3)$$

where S_w^{eff} is the effective water saturation and is given by $S_w^{eff} = (S_w - S_{rw}) \Big/ (1 - S_{rw})$.

The van Genuchten function was selected over the Brook and Corey function [42], (see Figure 4.3) due to its ability to give a better match to the mean static curves as shown in Figure 4.10 and Figure 4.11.

$$P_c = P_d S_w^{eff\,-1/\lambda} \qquad (4.4)$$

where P_d is the air entry pressure and λ is the Brooks and Corey parameter.

$P_c^{dynamic}$ (the measured dynamic P_c-S_w relationship) was determined for experiments conducted at P_{air} = 135 cm and P_{air} = 214 cm. The difference between $P_c^{dynamic}$ and P_c^{static} was referred to as dP_c. A representive plot of dP_c vs. saturation is provided in Figure 4.12. dP_c was shown at first to decrease with decreasing saturation until $S_w \sim 0.8$, after which dP_c was approximately constant between $S_w = 0.8$ and $S_w = 0.6$. This general trend was also observed for the mean dP_c vs S_w as shown in Figure 4.13.

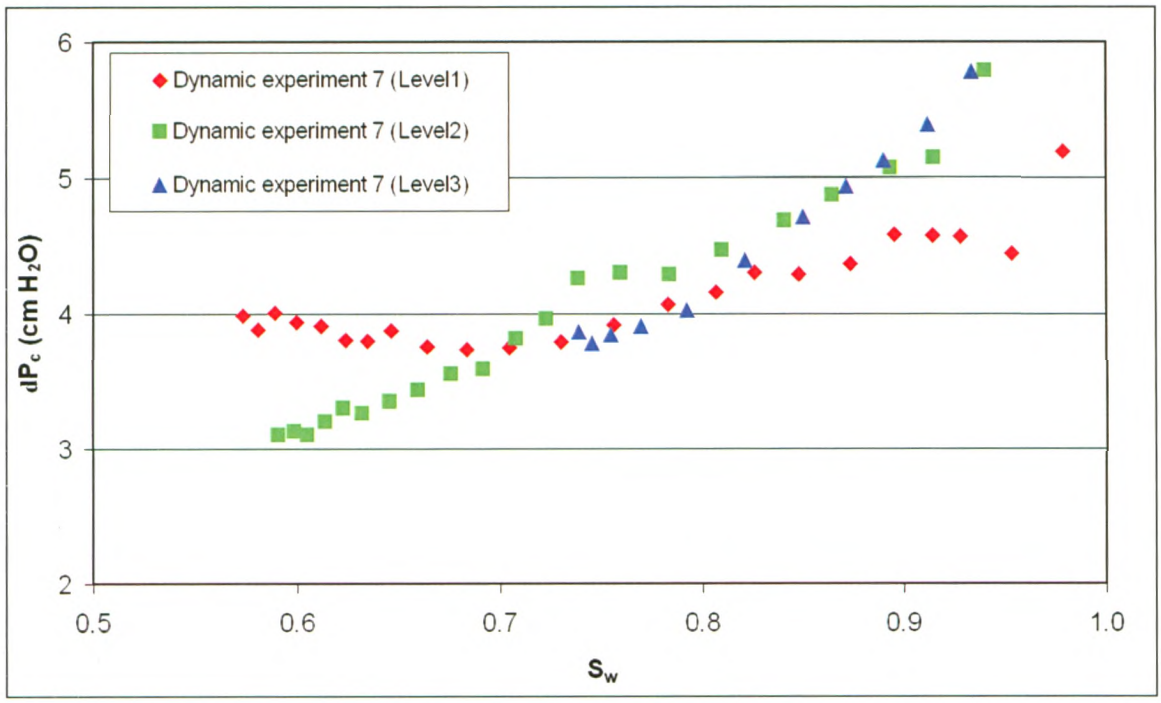

Figure 4.12. Comparison of dP_c vs. saturation measured at three different levels during F32-F50 Dynamic experiment 7.

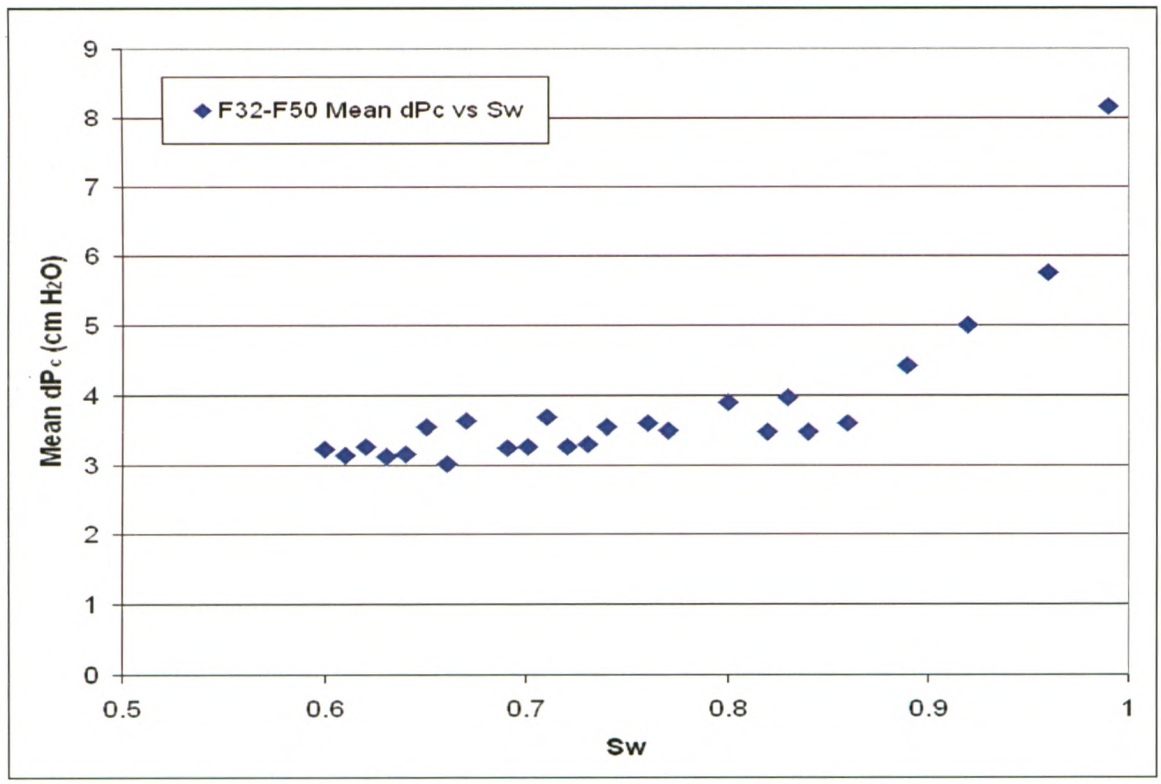

Figure 4.13. Comparison of the mean F32-F50 (P_{air} = 214 cm) dP_c vs. saturation .

dS_w/dt (the desaturation rate) was determined for each individual dynamic drainage experiment. A 7 point moving polynomial smoothing routine [64] was used to calculate the desaturation rate over 105 second time intervals. dS_w/dt was calculated once the difference between two consecutive saturation readings was larger than the experimental detection limit of the EC-5 moisture probes. The EC-5 detection limit or the instrument error was quantified by taking at least 100 readings at 5 different saturations when the column was under equilibrium conditions. For each saturation, the mean EC-5 readings was then used to calculate the detection limit based on the 95% confidence intervals. If the difference between EC-5 readings fall within the instrument error (based on the 95% C.I.), then the data is not included in any further analysis. For F32-F50 dynamic experiment 7 (Pair=214cm), the EC-5 detection limit was determined to occur at S_w= 0.57, 0.59 and 0.74 for the EC-5 probes at level 1, level 2 and level 3 respectively.

A representative plot of dS_w/dt vs. time is presented in Figure 4.14.

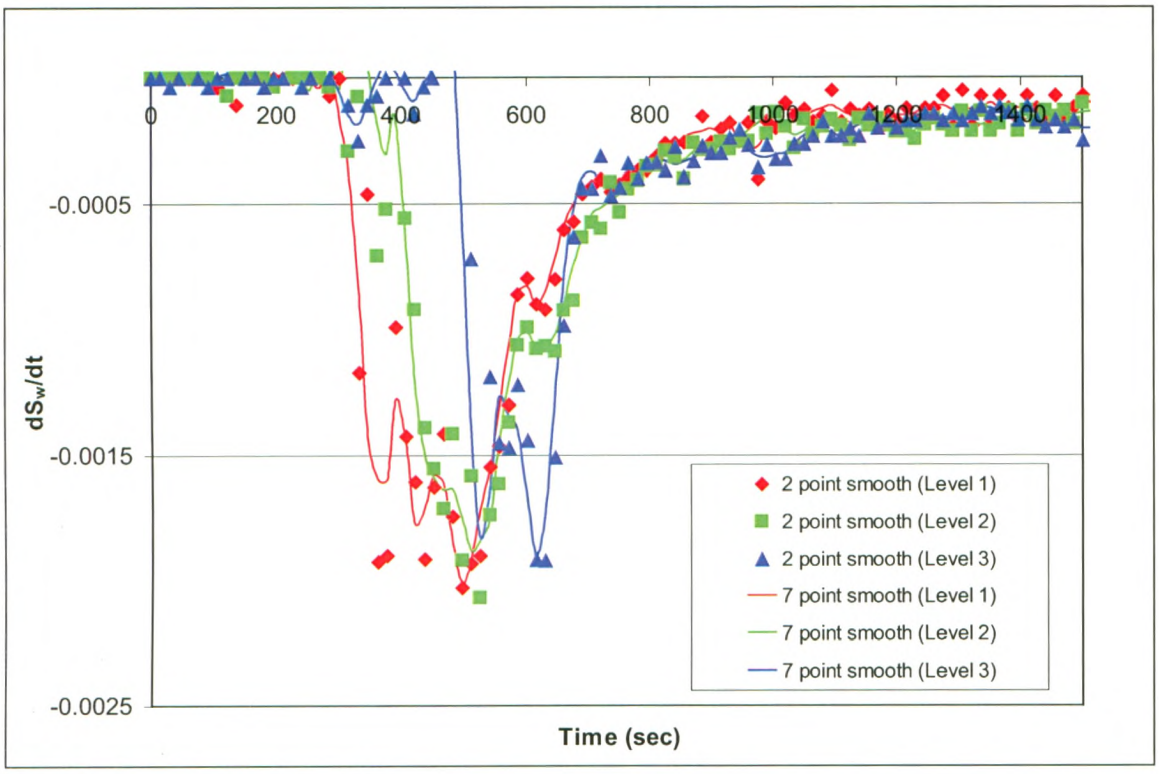

Figure 4.14. Comparison of dS_w/dt vs. time measured at three different levels during Dynamic Experiment 7. Data points represent dS_w/dt calculated from consecutive saturation readings taken 15 seconds apart (2 point smooth). Solid lines represents dS_w/dt calculated from the 7 point moving polynomial smoothing routine [64].

This graph reveals that desaturation occurred sequentially from level 1 to level 3. Similar behavior was observed in the other non-equilibrium experiments. Here, dS_w/dt vs time curves calculated from the 7 point moving polynomial smoothing routine was selected for further analysis because this smoothing routine eliminates more instrument noise in comparison to the dS_w/dt vs time curves calculated from consecutive saturation readings. For a comparison of the mean maximum desaturation rate of each type of drainage experiment see Table 4.2. Figure 4.15 shows that the maximum desaturation rate for F32-F50 Dynamic experiment 7 was achieved between S=0.9 and S=0.7 for all three levels. As saturation decreases, the desaturation rate approaches zero. This may be attributed to the decreasing relative permeability of the sand at lower saturations and also to the fact

that the system becomes closer to equilibrium with decreasing water saturation, which in turn decreases the driving force.

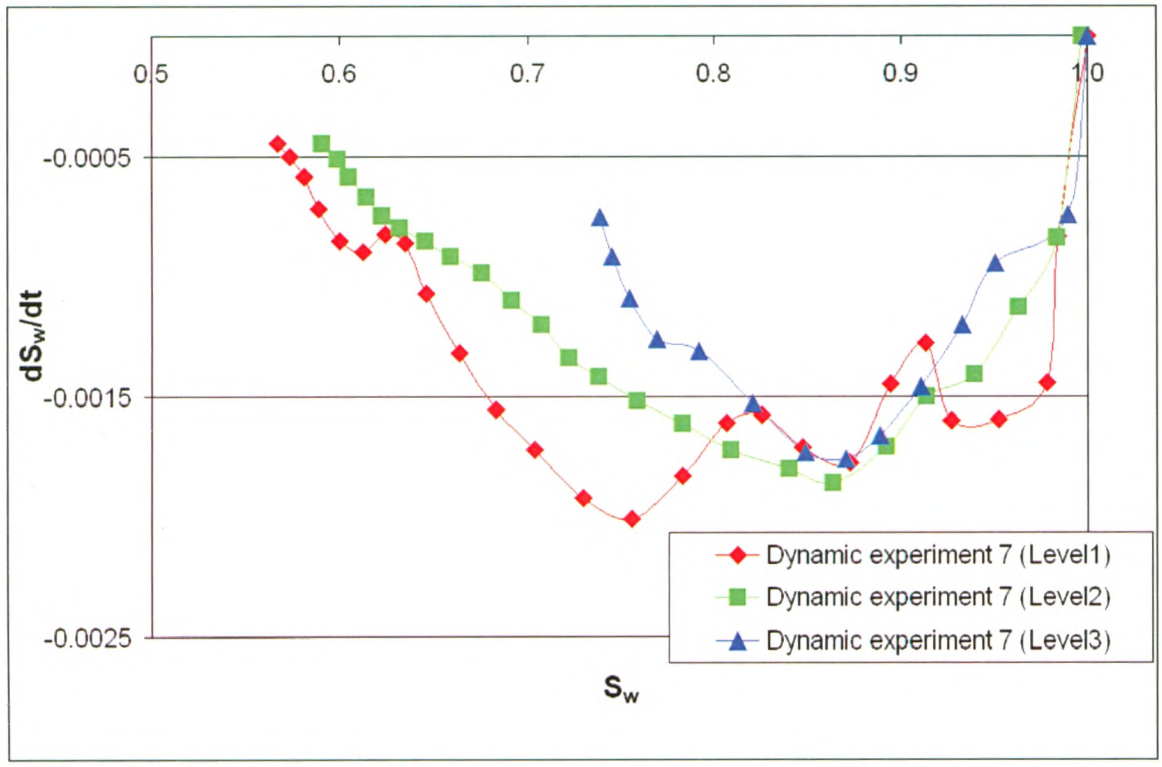

Figure 4.15. Comparison of dS_w/dt vs. saturation measured at three different levels during Dynamic Experiment 7

Using the measured $P_c^{dynamic}$, P_c^{static} and dS_w/dt, τ was calculated for all dynamic experiments by applying the following equation:

$$P^{Dynamic} - P^{Static} = -\tau\left(\frac{\delta S_w}{\delta t}\right) \qquad (4.5)$$

Figure 4.16 show plots of the mean τ vs. saturation curves for F32-F50 and F70 experiments conducted at P_{air}= 135 cm water and for F32-F50 experiments conducted at P_{air}= 214 cm water respectively. The data was binned into 0.3 saturation intervals and the mean τ value over each saturation interval was determined. Error bars indicate the 95% confidence intervals of the mean curves. Here, τ was quantified once the difference between two consecutive saturation readings was greater than the detection limit of the EC-5 probe.

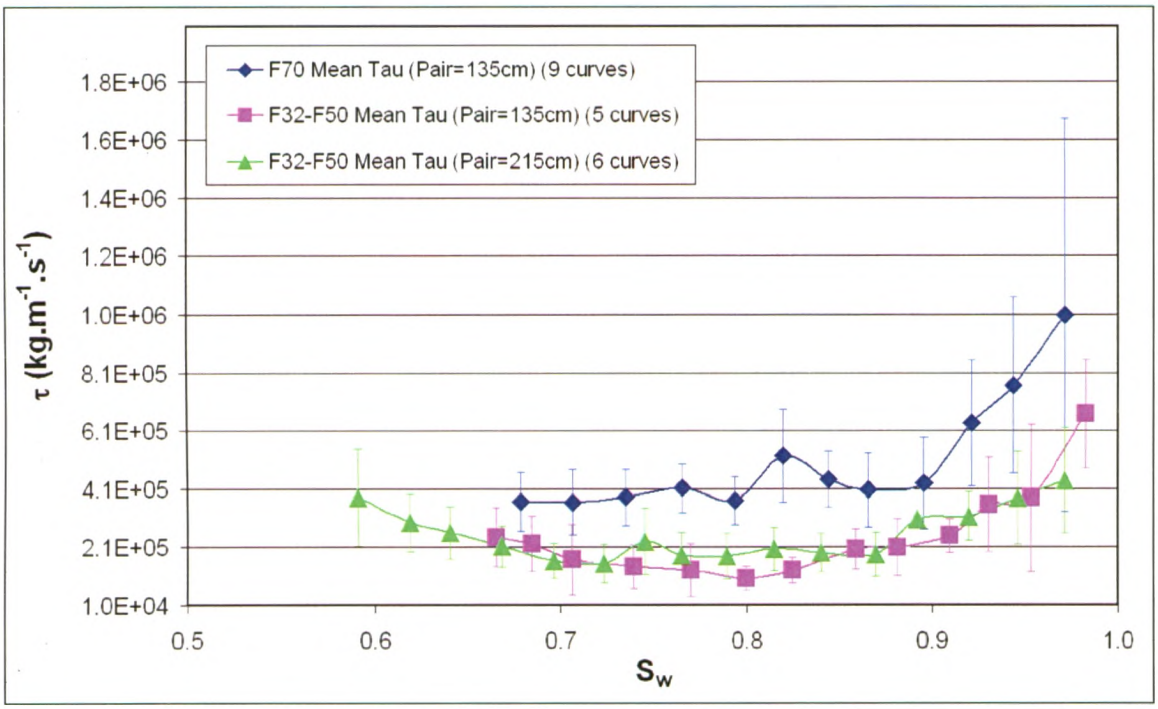

Figure 4.16. Comparison of the dynamic effect coefficient (τ) vs. wetting phase saturation (S_w) for mean F70 and F32-F50 dynamic experiments (Upper boundary air pressure of 135 cm) and mean F32-F50 dynamic experiments (Upper boundary air pressure = 214cm).

The magnitude of τ was generally largest at high water saturations. τ decreases with decreasing water saturation for higher saturations and then increases as saturation

decreases. For the F70 sand τ varies between $1.0X10^{6}$ to $3.7X10^{5}$ $kg.m^{-1}.s^{-1}$ while for the F32-F50 sand, τ varies between $6.7X10^{5}$ and $1.0X10^{5}$ $kg.m^{-1}.s^{-1}$. There was no significant difference between the F32-F50 mean τ vs S_w curves measured at a desaturation rate of $1.4X10^{-03}$ s^{-1} and $2.4X10^{-03}$ s^{-1}. For the F70 sand, the magnitude of τ was shown to be generally higher than that determined for the F32-F50 sand type. A significant difference between the F32-F50 and F70 mean curves was observed between water saturations of S_w= 0.85 and S_w= 0.75. The mean F32-F50 curve shows that τ increases below S_w = 0.7. Here the EC-5 probe detection limit allows for the quantification of τ at slightly lower saturations.

4.5 Upscaling Pressures and Saturations

When considering the simulation of a two-phase flow system at the core scale (5-10cm) or the field scale (>100cm), it is common practice to utilize averaged parameters to arrive at the capillary pressure-saturation relationship [19]. To achieve this objective, saturations and fluid pressures must be related to some averaging volume [2]. Here we upscale from point measurements of fluid pressures and saturations to the core scale to investigate whether volume averaging has any effect on the magnitude of τ. Point measurements were upscaled to lengths of 6 cm or 9 cm using a volume averaging technique [19].

Pressures and saturations were averaged over a 6 cm length from measurements made at level 2 and 3 for F32-F50 dynamic experiments 5 (P_{air}= 135 cm) and F32-F50 dynamic experiment 8 (Pair=214cm). Measurements at all three levels were used to average over

9cm for F32-50 dynamic experiment 7 (P_{air}= 214 cm) and F70 dynamic experiments 1, 2 and 3 (Pair= 135 cm). The averaging technique was not applied to the other F32-F50 dynamic experiments in this study because data from multiple levels were not available.

To calculate the average pressures using the experimental data, the column domain was subdivided into sections. Each section was centered over one of the levels which pressure and saturation measurements were taken. Here each section or sub division was referred to as a sub volume.

The average capillary pressure $< P_c >$ was given by:

$$< P_c >= P^{upperboundryair} - < P_w > \qquad (4.6)$$

To calculate the average water pressures $< p_w >$, the following relationship is used:

$$< P_w^V >= \frac{\sum_i^m P_{wi} V_{wi}}{\sum_i^m V_{wi}} \qquad (4.7)$$

where.

$$V_{wi} = S_{\alpha i} \phi_i A.x \qquad (4.8)$$

and $< P_w^V >$ is the volume weighted wetting phase pressure. m is the number of sub volumes, P_{wi} is the phase pressures measured at the midpoint of the sub volume, V_{wi} is the volume occupied by the wetting phase over a given sub volume, S_{wi} is the saturation

measured by the EC-5 probes at the midpoint of the sub volume, ϕ is the porosity, A is the area of the sub volume and x is the length of the sub volume taken to be 3cm.

To calculate the average wetting phase saturations i.e. $< S_w >$, the following relationship was used:

$$< S_w >= \frac{\sum_{i}^{m} V_{(sub)i} S_{wi}}{\sum_{i}^{m} V_{(sub)i}} \qquad (4.9)$$

where V_{sub} is the sub volume and S_{wi} is the EC-5 reading at the midpoint of the sub volume. The averaged pressures and saturations were then used to calculate τ using 5.1.

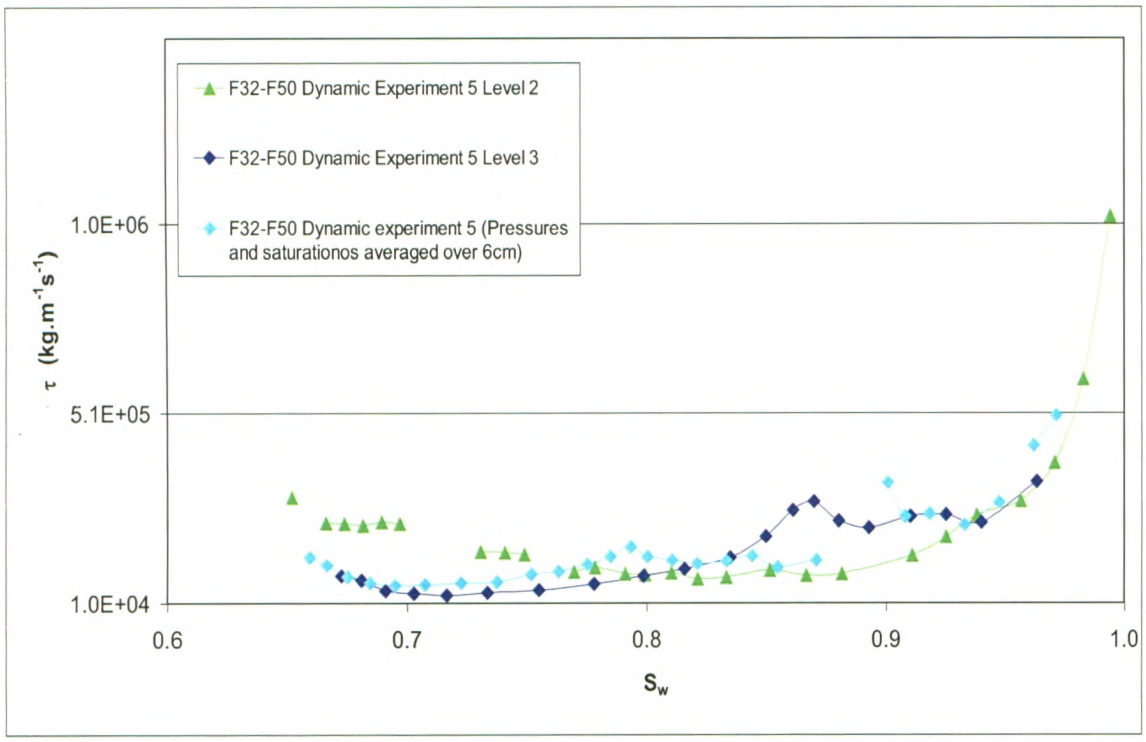

Figure 4.17. A comparison of τ vs S_w determined from either point measurements or from averaged pressures and saturations for F32-F50 Dynamic experiment 5.

Figure 4.18 to Figure 4.22 gives a comparison of τ vs S_w determined from point measurements and from volume averaged saturations and pressures for F32-F50 Dynamic experiment 5, 7 and 8 and F70 Dynamic experiments 1, 2 and 3 respectively. This comparison reveals that τ vs. S_w determined from volume averaged saturations and pressures was a good match to τ vs. S_w determined from point measured saturations and pressures. This trend was seen in all the experiments used for this analysis.

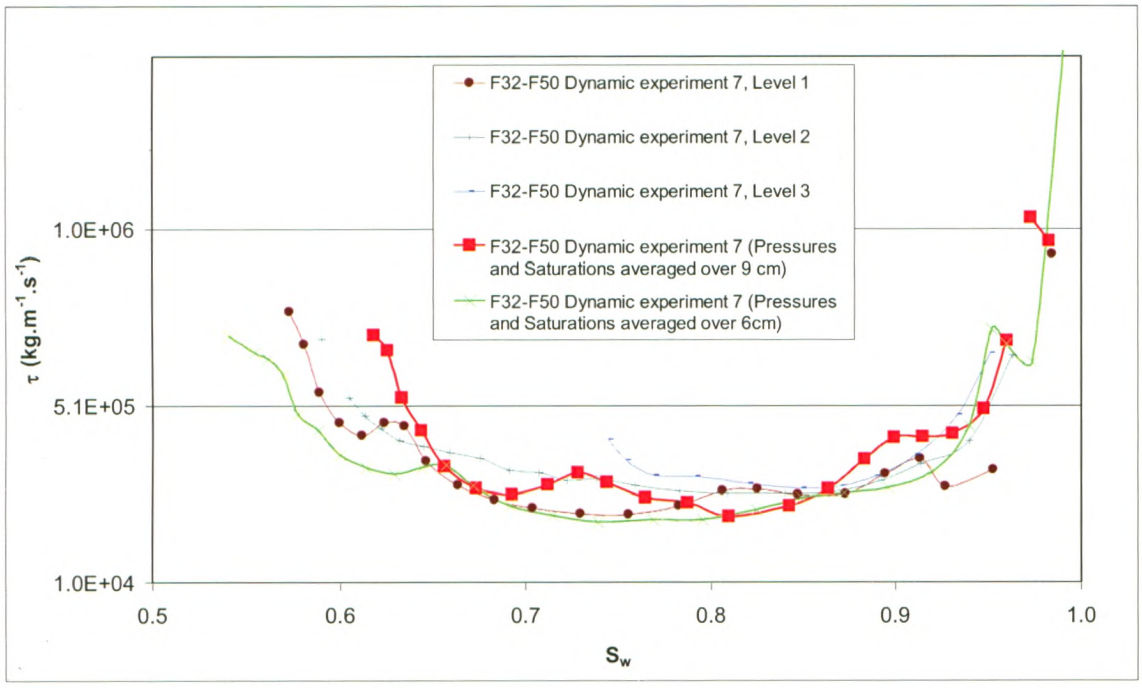

Figure 4.18. A comparison of τ vs S_w determined from either point measurements or from averaged pressures and saturations for F32-F50 Dynamic experiment 7.

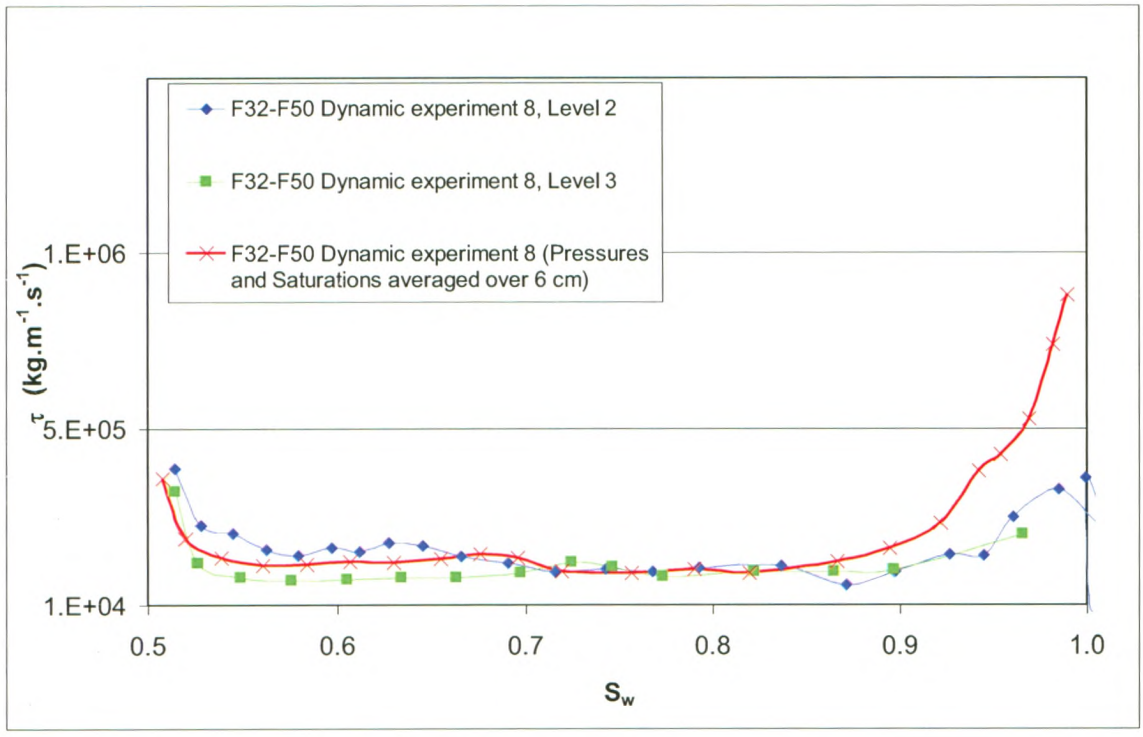

Figure 4.19. A comparison of τ vs S_w determined from either point measurements or from averaged pressures and saturations for F32-F50 Dynamic experiment 8.

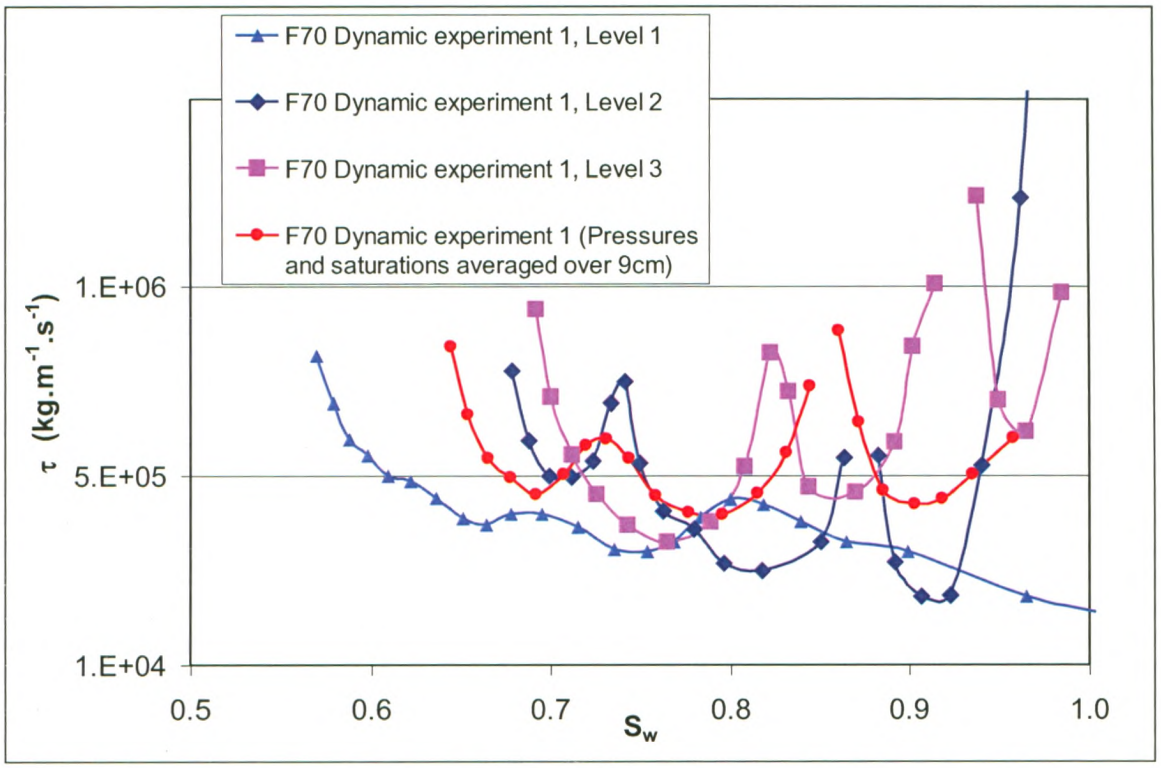

Figure 4.20. A comparison of τ vs S_w determined from either point measurements or from averaged pressures and saturations for F70 Dynamic experiment 1.

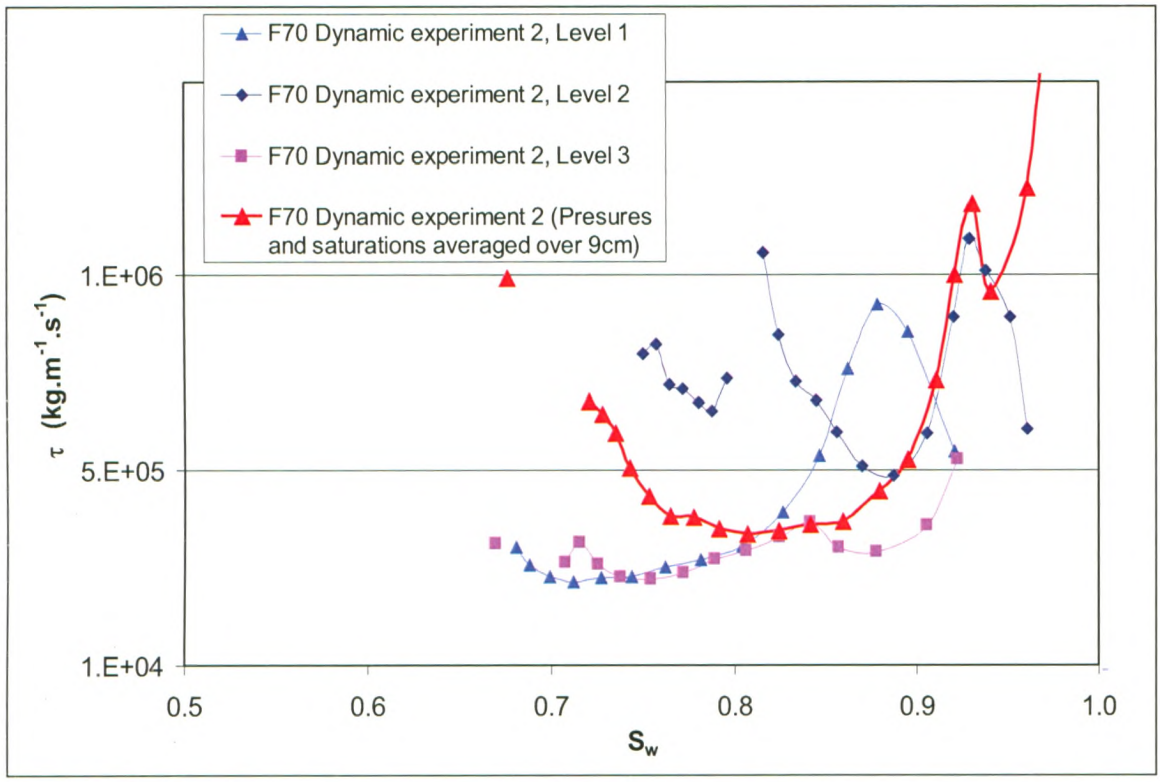

Figure 4.21. A comparison of τ vs S_w determined from either point measurements or from averaged pressures and saturations for F70 Dynamic experiment 2.

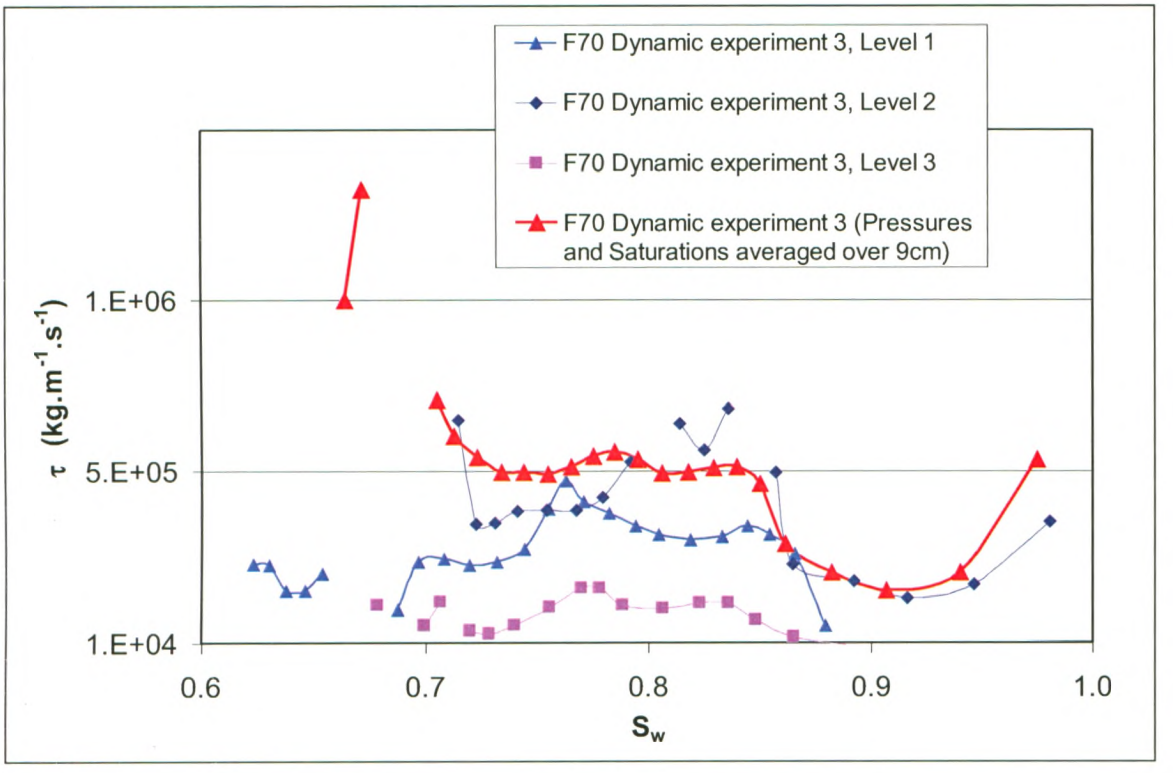

Figure 4.22. A comparison of τ vs S_w determined from either point measurements or from averaged pressures and saturations for F70 Dynamic experiment 3.

4.6 Direct Quantification of τ: Method 2

According to the extended P_c-S_w relationship proposed by [1], for a given water saturation, a plot of the experimentally determined dP_c vs. dS_w/dt should yield a linear relationship. Here, the slope of this line gives τ. This method was used to calculate τ for all experiments where capillary pressure and water saturation were measured at multiple levels. Since the dP_c measured at various levels within the same experiment was more reproducible than dP_c between experiments, this analysis was restricted to the measurements taken at the various levels within an individual experiment. Since τ may vary with water saturation, the slope of dP_c and dS_w/dt was quantified over a number of

small saturation ranges (typically 2 to 3% saturation ranges were used) for the same experiment. Here, saturation ranges were chosen so that there were at least 3 data points of dP_c v.s. dS_w/dt (see Appendix B, Figures B.1 to B.6). The fit parameters, slope, intercept and R^2 from the linear equations are provided in Appendix B, Tables B.1, B.2 and B.3.

τ calculated using method 2 was generally smaller, and in some cases lay outside the lower 95 % confidence interval of the mean τ quantified using method 1. See Figure 4.23, Figure 4.24 and Figure 4.25 for a comparison of τ quantified using both methods. For method 2, τ values were reported once the R^2 value of the linear fit was greater than 0.69 (See Tables B.1, B.2 and B.3, Appendix B). Here all linear fits had non-zero intercepts. Generally, for both methods, τ decreases with decreasing water saturation at high water saturations.

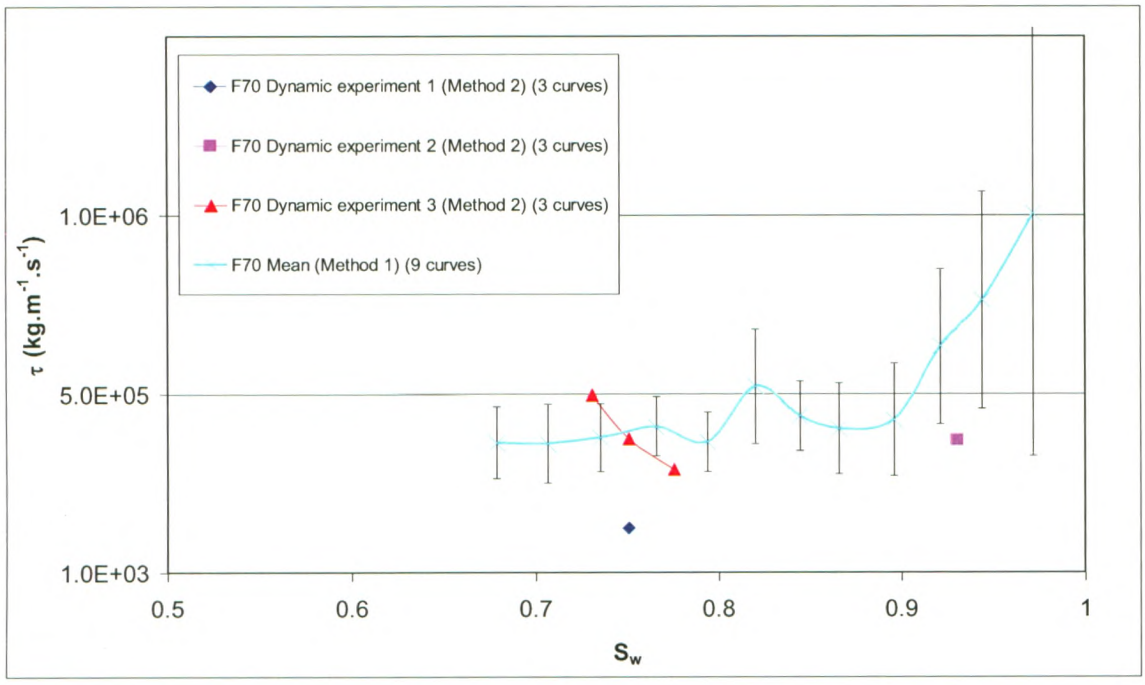

Figure 4.23: A comparison of τ vs. S_w between Direct Measurement Method 1 and Direct measurement Method 2 for F70 Dynamic experiments 1, 2 and 3.

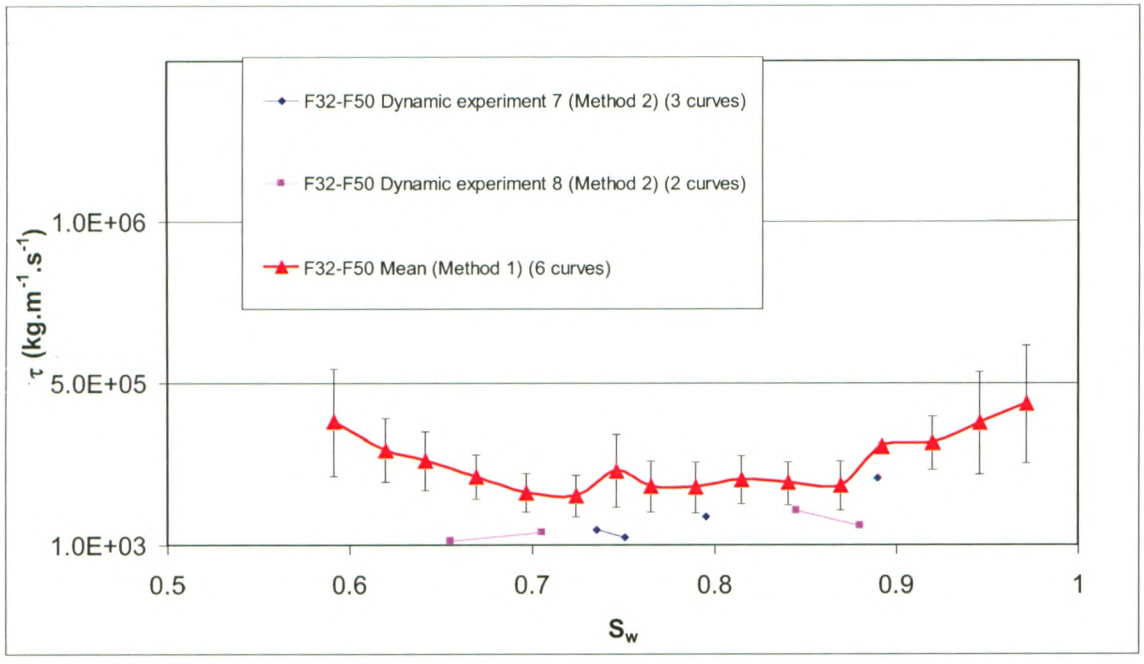

Figure 4.24: A comparison of τ vs. S_w between Direct Measurement Method 1 and Direct Measurement Method 2 for F32-F50 Dynamic experiments 7 and 8.

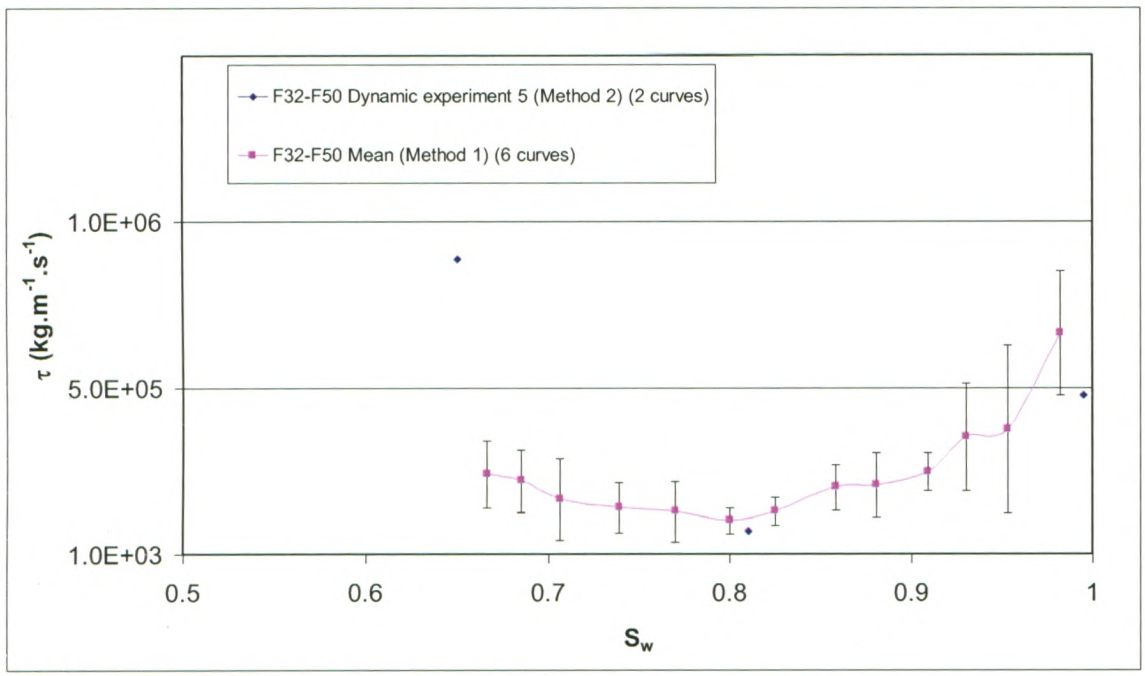

Figure 4.25: A comparison of τ vs. S_w between Direct Measurement Method 1 and Direct Measurement Method 2 for F32-F50 Dynamic experiment 5.

Chapter 5 - Discussion

5.0 Introduction

Primary drainage experiments conducted on packed columns of F32-F50 and F70 sand showed that the measured capillary pressure-saturation relationship was not unique but a function of the water desaturation rate.

5.1 Desaturation Rate Effects on the Measured P_c-S_w Relationship

Measured P_c-S_w relationships generally indicated that as the water desaturation rate increased, primary drainage capillary pressure increased at a given saturation. There was a statistical difference between the curves measured under static conditions and curves measured at the fastest desaturation rates (see Figure 4.10 and Figure 4.11). This trend has also been observed in air-water experiments conducted by [5, 10, 20, 33, 44, 65], and PCE-water experiments conducted by [6, 11].

The apparent dependency of the P_c-S_w relationship on the desaturation rate/boundary condition has been attributed to various physical processes which may account for the observed dynamic or non-equilibrium effects. [7], [33] and [20] suggest pore water blockage and water entrapment, [18] and [33], suggest dynamic contact angle effects, while [35] and [33], suggest air-phase continuity to be phenomena which may contribute to the observed dynamic P_c-S_w. These processes are now examined in relation to the results of this study.

Although it is known that measured dynamic contact angle differ from the static contact angle [66], this change is said not to be large enough under drainage of an air-water system to result in significant changes of the capillary pressure [7]. To investigate whether the dynamic contact angle could account for the relatively small difference between static and dynamic P_c, the Laplace equation was used to calculate the ratio of dynamic P_c to static P_c. At the entry pressure, the dynamic P_c was 1.1 and 1.13 times larger for the F70 and F32-F50 sand respectively. If we assume that the contact angle, measured under dynamic conditions through the water phase, is 0^o, Laplace's equation suggests that the contact angle under equilibrium would be between 25^o and 28^o. This contact angle range is in the range reported in the literature for quartz sand [18, 67]. As a result dynamic contact may be one reason for observed differences in capillary pressure measured under static and dynamic conditions.

For the F32-F50 drainage experiments, hydrophilic membranes were emplaced at the lower boundary. Dynamic drainage experiments result in a large capillary pressure gradient near the membrane [56]. According to [33], high P_c gradients can result in drainage first occurring at the outflow end of the column. This reduces the conductivity within this zone which impedes drainage of the upper layers in the column. If this occurred, higher water saturations would be observed in dynamic drainage experiments for a given capillary pressure. However, all drainage experiments reported in this study showed that desaturation occurred sequentially from level 1 to level 3.

This was an indication that drainage began in the upper regions of the column while the lower regions remained fully saturated for the F32-F50 sand. In the F70 drainage experiments no membranes were used however dynamic effects in the measured P_c-S_w relationships were detected. Therefore it was concluded that membrane effects were minimal and likely did not significantly contribute to the resulting dynamic effects.

One of the main assumptions made in both unsaturated zone experiments and modeling is that the air phase pressure within the porous media does not deviate from atmospheric pressure during the drainage process [26]. This may not be the case for experiments which induce drainage of a column by applying a high suction to the lower boundary. For this type of drainage experiment, air is allowed to enter through the top of the column via small openings. If these openings are not large enough to facilitate the movement of air into the column air pressure within the sample may deviate from atmospheric pressure [9].

This issue can be avoided if drainage is induced by injecting air into the column at the upper boundary [56]. In the current study this method was chosen to induce drainage. It was assumed that the in situ air pressure was equal to the applied air pressure at the upper boundary. Since air pressure was the driving force for drainage, any movement of water must have resulted from air replacing the water within the pore spaces. Air is known to have a viscosity which is approximately two orders of magnitude lower than water [68]. Therefore any pressure increase of the air phase is commonly assumed to be instantaneously transferred to all regions where the air phase is present within the sample

[53, 56]. This assumption has been verified with an additional F32-F50 dynamic experiment (Pair=135cm) in which the in situ air phase pressure was shown to be equal to the applied upper boundary air pressure once desaturation has occurred (See Figure A.10, Appendix A).

During dynamic drainage, water may become entrapped in smaller pores as the entry pressure of the larger surrounding pores is exceeded [7]. The resulting drainage of the larger pores isolates and water trapped within the smaller pores [33]. This phenomenon may explain why, during dynamic experiments, the saturation is higher at a given capillary pressure than for static experiments. To determine if water entrapment was the cause of discrepancies between static and dynamic capillary pressures, a comparison of the cumulative water outflow of the F32-F50 static and dynamic experiments (P_{air} = 214cm) were compared at the moment the air-water front arrived at a depth of 7cm (See

Table 5.1). At this time, the cumulative outflow gives the quantity of water removed from the region of the column between the upper boundary and level 1. This comparison suggests that for experiments conducted at the fastest desaturation rate, the normalized cumulative outflow was not significantly different from the static experiments. Since water entrapment would result in the dynamic drainage experiments having a lower cumulative outflow than the static experiments, water entrapment was not a major contributing factor to the observed dynamic effects.

Table 5.1. Comparison of the cumulative outflow at the time desaturation first occurs at Level 1.

Experiment Name	$Norm.Q_c^{eff}$ [a]	Time air-water front arrives at level1 (hrs)
F32-F50 Static experiment 1	0.07	1.79
F32-F50 Static experiment 2	0.06	3.17
F32-F50 Dynamic experiment 6	0.07	0.12
F32-F50 Dynamic experiment 7	0.08	0.10
F32-F50 Dynamic experiment 8	0.07	0.13

[a] Normalized effective cumulative outflow as defined in Equation 4.1

In the extended P_c-S_w relationship proposed by [31], τ acts as a capillary damping coefficient. This means that τ relaxes the time needed for the static and dynamic capillary pressures to become equivalent. For a system with small τ values, the free energy added to the system dissipates quickly and equivalence between the static P_c and dynamic P_c is re-established quickly [16]. The ability of a porous medium to dissipate energy and hence re-establish equivalence between static and dynamic P_c has been related to both the permeability of the medium [20, 22], and the applied boundary conditions [18].

For homogeneous sands, it is thought that the applied boundary conditions will determine the length of time needed to establish equivalence between dynamic and static capillary pressure. Higher applied air pressure results in more energy being added to the system hence a longer time is needed to achieve this equivalence [1]. For the dynamic experiments conducted in this study P_c increases rapidly following an increase in the air phase boundary pressure. A rapid P_c increase may not allow sufficient time for equivalence between dynamic and static capillary pressure [16]. Therefore larger dynamic capillary pressures should be observed at a given saturation, for higher applied P_{air} according to theories proposed by both [1] and [16]. A larger dynamic capillary

pressure was observed for the large applied air pressure experiments. However, for F32-F50 experiments conducted at an applied air pressure of 135 cm and 214 cm, the τ v.s. S_w curves were in agreement. Since τ is given by dP_c divide by dS_w/dt, the value of τ may not increase significantly for the relatively small change in dP_c resulting from the pressure step sizes chosen for this study. Here, the larger applied air pressure step also induces a higher desaturation rate.

Both modeling and experimental studies aimed at the quantification of dynamic effects in two phase flow systems have shown that τ may not be constant but may depend on saturation [6, 12, 55]. In this study τ varied with saturation, decreasing between S_w=1 and S_w=0.9 and then increasing with decreasing water saturations (see Figure 4.16). This type of non-monotonic behavior was also detected in dynamic simulations conducted by [55]. According to the extended P_c-S_w relationship [1], τ is directly proportional to the dP_c and inversely proportional to dS_w/dt. Here the minimum value of τ occurs over the saturation range where the desaturation rate was the largest. This result was in agreement with the extended P_c-S_w relationship.

In 2002, [7] reviewed the literature and quantified τ for a number of published air-water experimental studies. Average values of τ were determined to range from $3x10^{+04}$ $kg.m^{-1}.s^{-1}$ to $5x10^{+07}$ $kg.m^{-1}.s^{-1}$. For a PCE-water system, [6] reported τ values on the order of 10^{+05} to 10^{+07} $kg.m^{-1}.s^{-1}$ depending on the saturation. Using an inverse method to fit experimental outflow [12] proposed a linear relationship between τ and S_w, with a maximum τ on the order of 10^{+07} $kg.m^{-1}.s^{-1}$ for a PCE-water system. [8] determined τ to

be on average $2x10^{+06}$ $kg.m^{-1}.s^{-1}$ for an oil/water system. [10] made direct measurement of both static and dynamic P_c-S_w relationships for the same sand and determined τ to be approximately $1x10^{+06}$ $kg.m^{-1}.s^{-1}$ for the Air/Water system. In this study, τ was determined to vary between 10^{+04} to 10^{+06} $kg.m^{-1}.s^{-1}$. With respect to the magnitude of τ, measured values compare well to those presented by [6-8, 10, 12, 18, 24]

5.2 Desaturation Rate Effects on τ

To examine the effects of desaturation rate on τ, dynamic experiments were conducted at two desaturation rates for the F32-F50 sand. The mean τ vs S_w graphs are compared for experiments conducted at a mean maximum desaturation rate of $1.4X10^{-03}$ s^{-1} (Pair=135cm) and $2.4X10^{-03}$ s^{-1} (Pair=214cm). This comparison reveals that there was no significant difference between the magnitude of τ determined from experiments with differing desaturation rate regimes. Based on simulations conducted on heterogeneous sands, [19] showed that for three different desaturation regimes, there was no pronounced difference between the τ vs S_w relationship for $S_w > 0.7$. However, for lower saturations, τ was shown to increase as the applied pressure step size increased.

5.3 Upcaling Effects on τ

In this study, τ was determined directly from point measurements (Direct quantification method 1) or by upscaling to either 6 cm or 9 cm lengths. This was done to see if τ was dependant on domain size as has been reported in the literature [2, 13, 19, 55]. A volume averaging technique commonly utilized to upscale pressures and saturations was employed to achieve this goal [18].

The effect of domain size on the magnitude of τ has been investigated by [19]. A two-phase flow simulator utilizing the same averaging techniques employed in the current study was used to simulate non-equilibrium experiments at varying length scales. τ was determined to scale with length squared. This conclusion was also arrived at by [55] and by [2] in modeling and theoretical studies. [19] reported that as the domain size increases, the difference between the averaged dynamic and static P_c increased while the saturation rate (determined from the averaged saturations) was shown to decrease. This resulted in a higher magnitude of τ for larger domain sizes.

A comparison of the averaged and measured dP_c vs. S_w for F32-F50 dynamic experiment 7 and 8 was provided in Appendix B, Figures B.7 and B.9 respectively. A comparison of dS_w/dt vs. S_w for F32-F50 dynamic experiment 7 and 8 was provided in Appendix B, Figures B.8 and B.10 respectively. These comparisons showed that averaged parameters were good representations of point measured parameters. Therefore it was concluded that upscaling did not have a significant effect on the magnitude of τ for this experimental system i.e., homogeneous sand, air-water fluids, boundary conditions and scale. In the study conducted by [19], a PCE-water fluid pair was used with a heterogeneous domain ranging from 3 to 100m in length. These differences may have resulted in the higher magnitude of τ calculated for larger domain sizes.

5.4 *Porous Media Property Effects on τ*

The F70 sand contained predominantly finer material than the F32-F50 sand (see Table 5.2 for a comparison of the mean grain sizes). The time relaxation coefficient, τ was shown to be lower for the coarser sand (F32-F50) in comparison to the finer sand (F70) (see Figure 4.16).

Table 5.2. A comparison of the magnitude of τ and soil properties for dynamic or transient experiments.

Sand Type	τ ($kg.m^{-1}.s^{-1}$) (for S_w=0.82)	k (m^2)	P^d (cm)	λ	Mean Grain Size (cm)
F32-F50	$1.2X10^5$	$5.3X10^{-11}$	22.5	2.7	0.042
F70	$5.2X10^5$	$1.47X10^{-11}$	47.0	3.9	0.018

In 1978, Stauffer developed an empirical relationship to determine the value of τ from fluid and porous media properties. In this relationship, τ was shown to be dependent on soil properties such as porosity (ϕ), intrinsic permeability (k) and the Brooks and Corey parameters λ and P_d and fluid properties such as viscosity (μ) and density (ρ):

$$\tau \propto \frac{\phi\mu}{k\lambda}\left(\frac{P_d}{\rho g}\right)^2 \qquad 5.1$$

This relationship suggests that τ is proportional to P_d and inversely proportional to the intrinsic permeability of the porous media. Applying the soil parameters in Table 5.2 for both sand types, Stauffer's equation suggests that τ calculated for the F70 sand would be 11 times greater than for the F32-F50 sand. The maximum and minimum difference between the directly measured τ for both sands occurred at $S_w \sim 0.82$ and $S_w \sim 0.67$ respectively (see Figure 4.16). Here the F70 sand was 4 times larger at $S_w \sim 0.82$ and 1.6 times larger at $S_w \sim 0.67$.

Since τ, calculated either by direct measurement or using Stauffer's equation has the same unit ($kg.m^{-1}.s^{-1}$), it was concluded that Stauffer's equation was able to only qualitatively predict the behavior of τ between the sand types used in this study. [19] used a two-phase flow simulator to investigate any dependencies of τ on soil properties. In this modeling study τ was not incorporated directly into the multiphase flow simulator but calculated from the difference between dynamic and static capillary pressure and the saturation rate obtained from simulations using the extended capillary pressure relationship. They concluded that the magnitude of τ increases with decreasing intrinsic permeability. This result was in qualitative agreement with Stauffer's equation and also the results of the current study.

5.5 The Experimentally Determined dP_c vs. dS_w/dt Relationship

In the extended P_c-S_w relationship proposed by [1], dP_c (the difference between dynamic and static capillary pressures) is said to be linearly related to dS_w/dt. Here τ is given by the slope of this linear relationship. τ calculated from linear fits to experimentally determined dP_c vs dS_w/dt (i.e. direct quantification method 2) gives a reasonable match to the mean τ values calculated using direct quantification method 1. At some saturations, lower τ values were predicted by direct quantification method 2. The reason for the lower τ values is not clear since the same experimental data set was used in both methods.

[1] suggest that the proposed linear equation passes through the origin as indicated by the absence of an intercept. Therefore, as the desaturation rate tends to zero, the static P_c-S_w relationship is obtained. This was not the case in this work as the linear fits to experimentally determined dP_c and dS_w/dt all possessed non-zero intercepts. Intercepts were obtained from 3.75 cm to -1.12 cm, for the F32-F50 sand and from 3.56 cm to -2.65 cm, for the F70 sand. The maximum intercept for the F70 and F32-F50 sand was 7.5% and 16.0% of the static entry pressures of each respective sand type. The presence of an intercept indicates that the linear relationship may not be justified near the origin i.e., as the desaturation rate tends to zero, the relationship between dP_c and dS_w/dt becomes non-linear. The degree of this non linear behaviour was thought to be small as indicated by relatively small intercepts.

A similar conclusion was arrived at by [19] after conducting simulations using the extended P_c-S_w relationship to investigate transient flow in both homogeneous and heterogeneous media. Here linear plots of dP_c vs dS_w/dt were shown to possess negative intercepts. These intercepts were shown to be inversely proportional to S_w while the gradient i.e. τ, was shown to have a non-linear dependence on saturation. In the current study, there was no clear trend between the intercept and S_w, however, τ was shown to have a non linear dependence on S_w at lower saturation rates. In simulations conducted with a bundle-of-tubes model for calculating dynamic effects, [55] also showed that the linear relationship between dP_c and dS_w/dt possessed a non-zero intercept .

The extended P_c-S_w relationship also indicates that at saturations near unity, τ should be minimal because equilibrium is achieved quickly as permeability is high [69]. Contrary to

this, τ was shown to decrease in magnitude between S_w=1 and S_w~0.9. This behaviour has also been observed in experimental work by [10] and in simulations by [55]. An examination of a representative plot of dS_w/dt vs. S_w (see Figure 4.15) reveals that the maximum desaturation rate is not achieved at S_w=1 but at a saturation range between 0.9 and 0.75. This saturation range coincides to the region where τ possessed its lowest value.

Chapter 6 - Summary and Conclusions

6.0 Conclusions

This thesis presents experimental evidence of the saturation rate dependency of the P_c-S_w relationship for two-phase flow in permeable media. An extended P_c-S_w relationship proposed by [1] was employed to quantify the extent to which the measured dynamic P_c-S_w relationship deviates from the equilibrium P_c-S_w. In this extended relationship, the saturation rate is said to be linearly related to the difference between the dynamic and static capillary pressure for a given water saturation. Here τ, the damping coefficient is introduced as the factor of proportionality. Analysis of both static and dynamic P_c-S_w relationships using the extended relationship was conducted and the following conclusions were drawn:

1. Capillary pressure measured under dynamic conditions was shown to be larger than capillary pressure measured under static conditions. Therefore it can be said that the measured P_c is a function of the saturation rate. This effect becomes important for two-phase flow scenarios where rapid saturation rates are encountered. The dynamic contact angle was identified as the most likely pore scale process which may have resulted in the measured difference between dynamic and static capillary pressure relationships.

2. The coefficient τ was quantified for two sands of varying properties. Here τ was shown to possess a lower magnitude for the sand with a lower intrinsic

permeability. This result is in agreement with Stauffer's equation although the equation is not able to accurately predict the magnitude of τ, it is in qualitative agreement with the results of this study. The maximum value of τ (10^6 $kg.m^{-1}.s^{-1}$) was observed for the finer textured sand. Since large τ values on the order of 10^7 $kg.m^{-1}.s^{-1}$ were shown to have significant effects on simulations [7] we expect that the extended relationship should be used for homogeneous sands which possess large τ values, i.e. sands with low intrinsic permeability and high entry pressures.

3. The coefficient τ was shown to be independent of domain size up to a domain length of 9 cm. Here point measurements of pressures and saturations were used along with a volume averaging technique commonly utilized in continuum scale models to calculate τ. There was no significant difference observed between τ calculated from point measurements of pressures and saturations and τ calculated from volume averaged pressures and saturations. This result is not in agreement with simulations conducted by [19] and by [55]. In both these studies, τ was shown to scale with the square of the system's length. Therefore for large averaging lengths, τ becomes extremely large. This implies that the magnitude of τ has no limit and thus a REV may not be defined [18]. This type of scaling was not observed for the experimental conditions of the current study.

4. The linearity of the proposed extended relationship was examined. It was shown that this relationship becomes non linear for low saturation rates. This implies that a non-linear relationship may be needed to describe the relationship between dP_c and

dS_w/dt over the entire saturation rate range encountered in this study. The degree of non-linearity was determined to be small, as indicated by the magnitude of the offsets in relation to entry pressure.

6.1 Future Work

To date, there exist many experimental works which were aimed at detecting dynamic effects on the core scale. The magnitude of the damping coefficient τ is said to depend on both soil and fluid properties. The dependency of τ on fluid properties has only been investigated using numerical models. There is a need to experimentally investigate this dependency for different fluid pairs using the same porous media.

Since the subsurface is comprised of layers of soil, each possessing different hydraulic properties, there is a need to conduct experiments designed to examine the effects of a layered or heterogeneous domain on τ. The development of a 3-D model which incorporates dynamic effects, would give us the capability to characterize field sites by accurately predicting the transient distribution of fluids within the subsurface. This type of model can then be used to assess situations where dynamic effects may be of importance when evaluating two-phase flow processes at the field scale.

The transient effects of two-phase flow in porous media is an ongoing area of research. The physical pore scale processes which result in these transient effects are not yet well understood. These processes have been shown to influence the measured P_c-S_w relationship at the core scale. However, an understanding of transient two-phase flow

processes on larger scales is needed to address issues relating to contaminant hydrology, agronomy and petroleum reservoir engineering. This study has contributed to the understanding of transient effects at the core scale and has given some experimental insight into a volume averaging technique used to upscale parameters to achieve simulations on larger scales.

Bibliography

1. Hassanizadeh, S.M. and W.G. Gray, *Thermodynamic basis of capillary-pressure in porous-media.* Water Resources Research, 1993. **29**(10): p. 3389-3405.

2. Nordbotten, J.M., et al., *On the definition of macroscale pressure for multiphase flow in porous media.* Water Resources Research, 2008. **44**(6).

3. Juanes, R., *Nonequilibrium effects in models of three-phase flow in porous media.* Advances in Water Resources, 2008. **31**(4): p. 661-673.

4. Bear, J. and A. Verruijt, *Modeling Groundwater Flow and Pollution.* 1987: Reidel Publ.

5. Topp, G.C., A. Klute, and D.B. Peters, *Comparison of water content-pressure head data obtained by equilibrium steady-state and unsteady-state methods.* Soil Science Society of America Proceedings, *1967.* **31**(3): p. 312-314.

6. Bottero, S., et al., *Experimental Study of Dynamic Capillary Pressure Effects in Two-Phase Flow in Porous Media* CMWRXVI, 2006.

7. Hassanizadeh, S.M., M.A. Celia, and D.H. K, *Dynamic Effect in the Capillary Pressure-Saturation Relationship and its Impacts on Unsaturated Flow.* Vadose Zone Journal, 2002. **1**: p. 38-57.

8. Kalaydjian, F., *Dynamic Capillary Pressure Curve for Water/Oil Displacement in Porous Media, Theory vs. Experiment*, in *SPE Conference*. 1992 b: Washington, DC. p. 491-50.

9. Schultze, B., et al. *Dynamic Nonequilibrium During Unsaturated Water Flow*. in *Proc. Int. Workshop on Characterization and Management of the Hydraulic Properties of Unsaturated Porous Media*. 1997.

10. Sakaki, T., D.M. O'Carroll, and T.H. Illangasekare, *Dynamic effects in field soil water retention curves: Direct labratory quantification of dynamic coefficient for drainage and wetting cycles*, in *Water Resources Research*. 2008.

11. Berentsen, C., et al., *Modelling of Two-phase Flow in Porous Media Including Non-Equilibrium Capillary Pressure Effects*, in *CMWRXVI*. 2006.

12. O'Carroll, D.M., T.J. Phelan, and L.M. Abriola, *Exploring dynamic effects in capillary pressure in multistep outflow experiments.* Water Resources Research, 2005. **41**(11).

13. Manthey, S., et al., *Dimensional Analysis of Two-Phase Flow Including a Rate-Dependent Capillary Pressure-Saturation Relationship.* Advances in Water Resources, 2008.

14. O'Carroll, D.M., et al., *Prediction of two-phase capillary pressure-saturation relationships in fractional wettability systems.* Journal of Contaminant Hydrology, 2005. **77**(4): p. 247-270.

15. Hassanizadeh, S.M. and W.G. Gray, *Toward an improved description of the physics of 2-phase flow.* Advances in Water Resources, 1993. **16**(1): p. 53-67.

16. Kalaydjian, F., *A Macroscopic Description of Multiphase flow in Porous Media Involving Space-Time Evolution of Fluid-Fluid Interfaces.* Transport in Porous Media, 1992 a. **2**: p. 491-506.

17. Celia, M.A., et al., *Geological storage as a carbon mitigation option.* Geochimica Et Cosmochimica Acta, 2007. **71**(15): p. A153-A153.

18. Manthey, S., *Two-phase Flow Processes with Dynamic Effects in Porous Media - Parameter estimation and Simulation*, in *Institute of Hydraulic Engineering.* 2006, University of Stuttgart: Stuttgart. p. 139.

19. Manthey, S., S.M. Hassanizadeh, and R. Helmig, *Macro-scale dynamic effects in homogeneous and heterogeneous porous media.* Transport in Porous Media, 2005. **58**(1-2): p. 121-145.

20. Stauffer, F. *Time Dependence of the Relations between Capillary Pressure, Water Content and Conductivity During Drainage of Porous Media.* in *IAHR Symp. on Scale Effects in Porous Media.* 1978. Thessaloniki, Greece.

21. Das, D.B., R. Gauldie, and M. Mirzaei, *Dynamic effects for two-phase flow in porous media: Fluid property effects.* Aiche Journal, 2007. **53**(10): p. 2505-2520.

22. Mirzaei, M. and D.B. Das, *Dynamic effects in capillary pressure-saturations relationships for two-phase flow in 3D porous media: Implications of micro-heterogeneities.* Chemical Engineering Science, 2007. **62**(7): p. 1927-1947.

23. UNESCO. *Statistics on global groundwater usage* 2007 http://portal.unesco.org/science/en/ev.php-URL_ID=6480&URL_DO=DO_TOPIC&URL_SECTION=201.html.

24. Abriola, L.M., *Modeling Multiphase migration of organic-chemicals in groundwater systems - a review and assesment.* Environmental Health Perspectives, 1989. **83**: p. 117-143.

25. Helmig, R., *Multiphase Flow and Transport Processes in the Subsurface: a Contribution to the Modeling of Hydrosystems.* 1997, Berlin, Germany: Springer, c1997.

26. Pinder, G.F. and M.A. Celia, *Suburfac Hydrology*. 2006: John Wiley & Sonss, Inc. Hoboken, New Jersey.

27. Rivett, M.O., D.N. Lerner, and J.W. Lloyd, *Chlorinated solvents in UK aquifers.* Journal of the Institution of Water and Environmental Management, 1990. **4**(3): p. 242-250.

28. Kueper, B.H., et al., *An Illustrated Handbook of DNAPL Transport and Fate in the Subsurface*. 2003: Environment Agency.

29. Soga, K., J.W.E. Page, and T.H. Illangasekare, *A review of NAPL source zone remediation efficiency and the mass flux approach.* Journal of Hazardous Materials, 2004. **110**(1-3): p. 13-27.

30. USEPA. *Non-Aqueous Phase Liquids (NAPLS) and Groundwater*. 2007 http://www.epa.gov/superfund/health/conmedia/gwdocs/non_aqu.htm.

31. Hassanizadeh, S.M. and W.G. Gray, *Mechanics and thermodynamics of multiphase flow in porous-media including interphase boundaries.* Advances in Water Resources, 1990. **13**(4): p. 169-186.

32. Kool, J.B. and J.C. Parker, *Analysis of the inverse problem fro transient unsaturated flow.* Water Resources Research, 1988. **24**(6): p. 817-830.

33. Wildenschild, D., J.W. Hopmans, and J. Simunek, *Flow rate dependence of soil hydraulic characteristics.* Soil Science Society of America Journal, 2001. **65**(1): p. 35-48.

34. Oung, O., S.M. Hassanizadeh, and A. Bezuijen, *Two-phase flow experiments in a geocentrifuge and the significance of dynamic capillary pressure effect.* Journal of Porous Media, 2005. **8**(3): p. 247-257.

35. Durner, W., B. Schultze, and T. Zurmuhl. *State-of-the-Art in Inverse Modeling of Inflow/Outflow Experiments*. in *Proc. Int. Workshop on Characterization and Management of the Soil Hydraulic Properties of Unsaturated Porous Media* 1997.

36. van Genuchten, M.T., F.J. Leij, and S.R. Yates, *The RETC Code for Quantifying the Hydraulic Functions of Unsaturated Soils*, U.S.D.o. Agriculture, Editor. 1991, U.S. EPA: California 92501.

37. Gerhard, J.I. and B.H. Kueper, *Influence of constitutive model parameters on the predicted migration of DNAPL in heterogeneous porous media.* Water Resources Research, 2003. **39**(10).

38. Helmig, R., *Multiphase Flow and Transport Processes in the Subsurface: a Contribution to the Modeling of Hydrosystems*. 1957, Berlin, Germany: Springer, c1997.

39. Gerhard, J.I. and B.H. Kueper, *Relative permeability characteristics necessary for simulating DNAPL infiltration, redistribution, and immobilization in saturated porous media.* Water Resources Research, 2003. **39**(8).

40. Hopmans, J.W. and J. Simunek, *Review of Inverse Estimation of Soil Hydraulic Properties.* 1997: p. 643-659.

41. van Genuchten, M.T., *Closed-form equation for predicting the hydraulic conductivity of unsaturated soils.* Soil Science Society of America Journal, 1980. **44**: p. 892-898.

42. Brooks, R.H. and A.T. Corey, *Hydraulic properties of porous media.* Hydrol. pap. 3 , Colo. State Univ., Fort Collins., 1964.

43. Beliaev, A.Y. and S.M. Hassanizadeh, *A theoretical model of hysteresis and dynamic effects in the capillary relation for two-phase flow in porous media.* Transport in Porous Media, 2001. **43**(3): p. 487-510.

44. Chen, L.X., G.A. Miller, and T.C.G. Kibbey, *Rapid pseudo-static measurement of hysteretic capillary pressure-saturation relationships in unconsolidated porous media.* Geotechnical Testing Journal, 2007. **30**(6): p. 474-483.

45. Gerhard, J.I. and B.H. Kueper, *Capillary pressure characteristics necessary for simulating DNAPL infiltration, redistribution, and immobilization in saturated porous media.* Water Resources Research, 2003. **39**(8).

46. Kool, J.B., J.C. Parker, and M.T. Vangenuchten, *Parameter-estimation for unsaturated flow and transport models- a review.* Journal of Hydrology, 1987. **91**(3-4): p. 255-293.

47. Hollenbeck, K.J. and K.H. Jensen, *Experimental evidence of randomness and nonuniqueness in unsaturated outflow experiments designed for hydraulic parameter estimation.* Water Resources Research, 1998. **34**(4): p. 595-602.

48. Mortensen, A.P., et al., *Visualization of microscale phase displacement processes in retention and outflow experiments: Nonuniqueness of unsaturated flow properties.* Water Resources Research, 2001. **37**(6): p. 1627-1640.

49. Vogel, H.J., A. Samouelian, and O. Ippisch, *Multi-step and two-step experiments in heterogeneous porous media to evaluate the relevance of dynamic effects.* Advances in Water Resources, 2008. **31**(1): p. 181-188.

50. Kool, J.B., J.C. Parker, and M.T. Van Genuchten, *Determining soil hydraulic properties from one-step ouflow experiments by parameter estimation: 1. Theory and numerical studies.* Soil Science Society of America Journal, 1985. **49**: p. 1348-1354.

51. Gray, W.G. and S.M. Hassanizadeh, *Macroscale continuum mechanics for multiphase porous-media flow including phases, interfaces, common lines and common points.* Advances in Water Resources, 1998. **21**(4): p. 261-281.

52. Vachaud, G.M., M. Vauclin, and M. Wakil, *A study of the uniquenes of the soil moisture caracteristic during desorbtion by vertical drainage.* Soil Science Society of America Journal, 1972. **36**: p. 531-532.

53. Chen, J., J.W. Hopmans, and M.E. Grismer, *Parameter estimation of two-fluid capillary pressure-saturation and permeability functions.* Advances in Water Resources, 1999. **22**(5): p. 479-493.

54. Hopmans, J.W., et al., *Simultaneous determination of water transmission and retention properties. Inverse Methods. IN: Methods of Soil Analysis. Part 4. Physical Methods.* 2002: Soil Society of America Book Series No. 5.

55. Dahle, H.K., M.A. Celia, and S.M. Hassanizadeh, *Bundle-of-tubes model for calculating dynamic effects in the capillary-pressure-saturation relationship.* Transport in Porous Media, 2005. **58**(1-2): p. 5-22.

56. Hopmans, J.W., et al., *Parameter Estimation of Two-Fluid Capillary Pressure-Saturation and Permeability Functions*, U.S.E.P. Agency, Editor. 1996, EPA: Cincinnati, OH 45268.

57. Anderson, W.G., *Wettability literature survey: Part 4. Effects of wettability on capillary pressure.* . Journal of Petroleum Technology, 1987. **39**: p. 1283-1300.

58. Lenhard, R.J. and J.C. Parker, *Experimental validation of the theory of extending 2-phase satration-pressure relations to 3-fluid phase systems for monotonic drainage paths.* Water Resources Research, 1988. **24**(3): p. 373-380.

59. Sah, A., et al., *Hydrophobic modification of alumina membranes with organochlorosilanes.* Journal of Membrane Science, 2004(243): p. 125-132.

60. Czarnomski, N., et al., *Precision and accuracy of three alternative instruments for measuring soil water content in two forest soils of the Pacific Northwest.* Canadian Journal of Forest Research-Revue Canadienne De Recherche Forestiere, 2005. **35**(8): p. 1867-1876.

61. Sakaki, T., et al., *Empirical two-point alpha-mixing model for calibrating ECH2O EC-5 soil moisture sensors in sands.* Water Resources Research, 2008.

62. Decagon Devices Inc., *ECH20 oil moiture sensor. Operator's manual for models EC-20, EC-10 and EC-5, Version 5, Decagon Devices Inc., Pullman, W.A.* 2006.

63. Klute, A. and C. Dirksen, *Hydraulic Conductivity and Diffusivity: Laboratory Methods.* American Society of Agronomy, 1986: p. 687-734

64. Golay, M.J.E., *Smoothing of data by least-squares procedures and by filtering.* Ieee Transactions on Computers, 1972. **C 21**(3): p. 299-&.

65. Smiles, D., G. Vachaud, and M. Vauclin, *Application of diffusion equation to water flows in unsaturated soils - influence of flow dynamics on value of psi (theta) during drainage.* Comptes Rendus Hebdomadaires Des Seances De L Academie Des Sciences Serie A, 1971. **272**(5): p. 401-&

66. Friedman, S.P., *Dynamic contact angle explanation of flow rate-dependent saturation-pressure relationships during transient liquid flow in unsaturated porous media.* Journal of Adhesion Science and Technology, 1999. **13**(12): p. 1495-1518.

67. Lord, D.L., A.H. Demond, and K.F. Hayes, *Effects of Organic Base Chemistry on Interfacial Tension, Wettability, and Capillary Pressure in Multiphase Subsurface Waste Systems.* Transport in Porous Media, 2000. **38**: p. 79-92.

68. Lide, D.R., *CRC Handbook of Chemistry and Physics: A Ready-reference Book of Chemical and Physical Data*. 2004: CRC Press, 2004.

69. Manthey, S., et al., *Dynamic capillary pressure effects in two-phase flow through heterogeneous porous media*. 2004.

Appendix A: Measured Drainage Parameters

This section contains the results of primary drainage experiments conducted under both static and dynamic flow conditions for two sand types (F32-F50 and F70). For each experiment, the directly measured parameters i.e. cumulative outflow, air pressure, water pressure and water saturation vs. time was provided in the following figures.

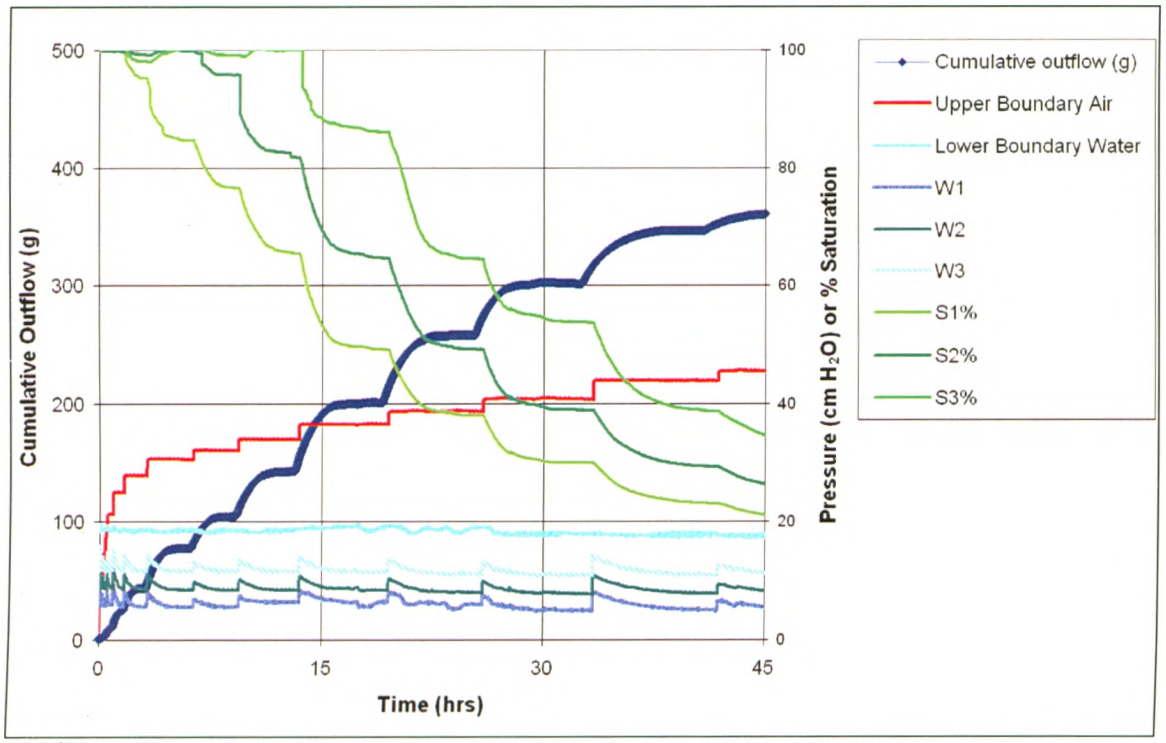

Figure A.1. Measured experimental parameters for F32-F50 Static Experiment 1: cumulative outflow, upper boundary air, water pressures (W1, W2 and W3) and saturations (S1, S2 and S3) vs. time

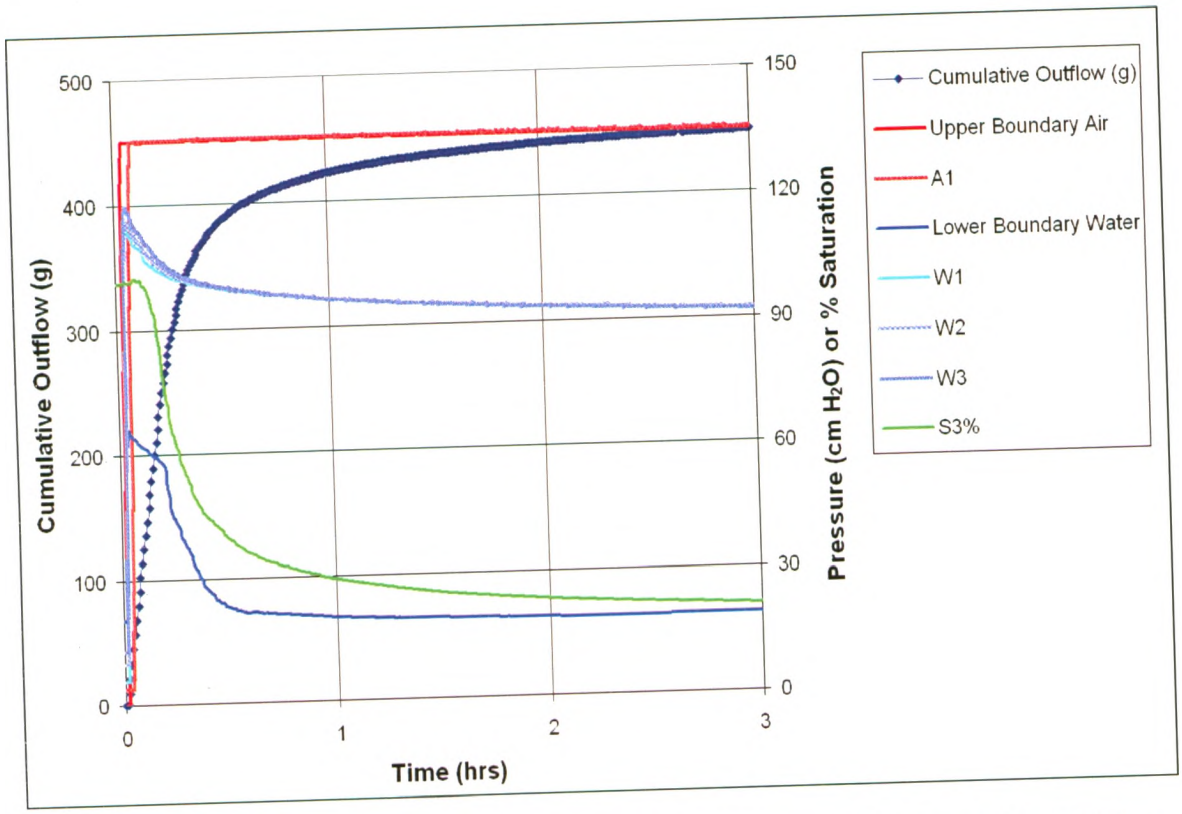

Figure A.2. Measured experimental parameters for F32-F50 Dynamic Experiment 1: cumulative outflow, air pressures (A1 and A2), water pressures (W1, W2 and W3) and saturation (S3) vs. time

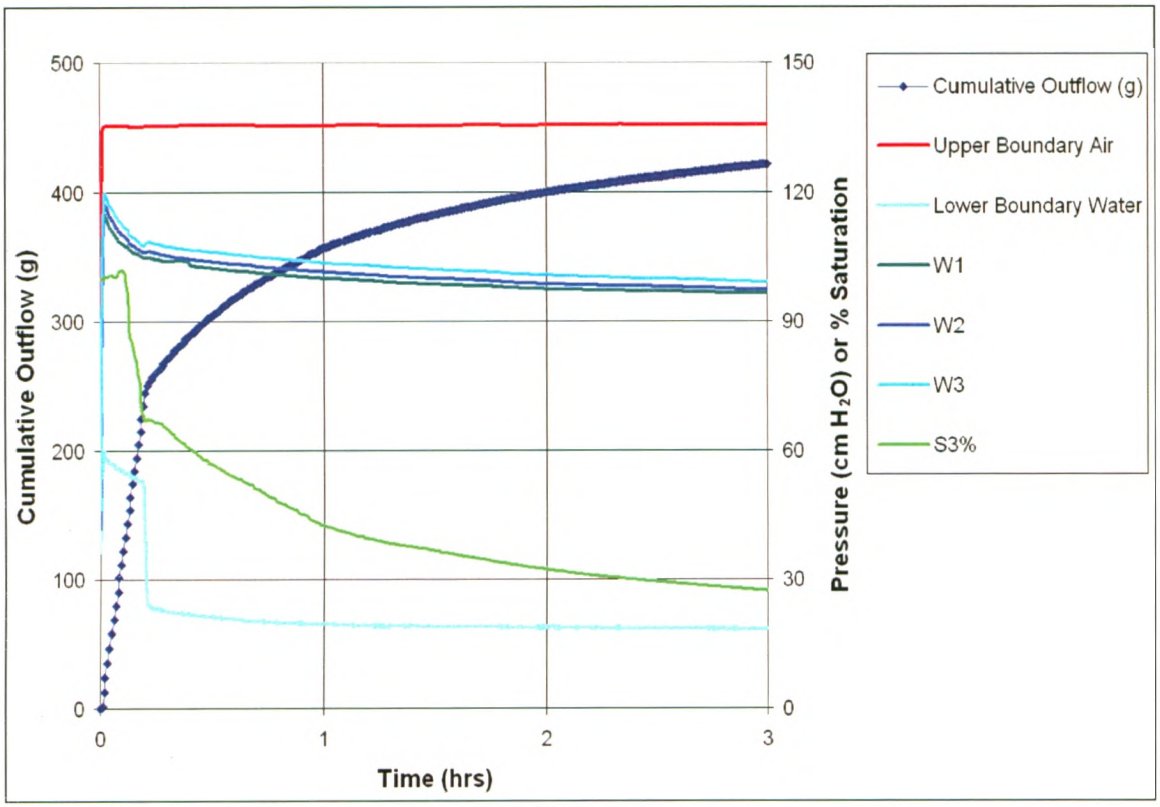

Figure A.3. Measured experimental parameters for F32-F50 Dynamic Experiment 2: cumulative outflow, air pressures (A1 and A3), water pressures (W1, W2 and W3) and saturation (S3) vs. time

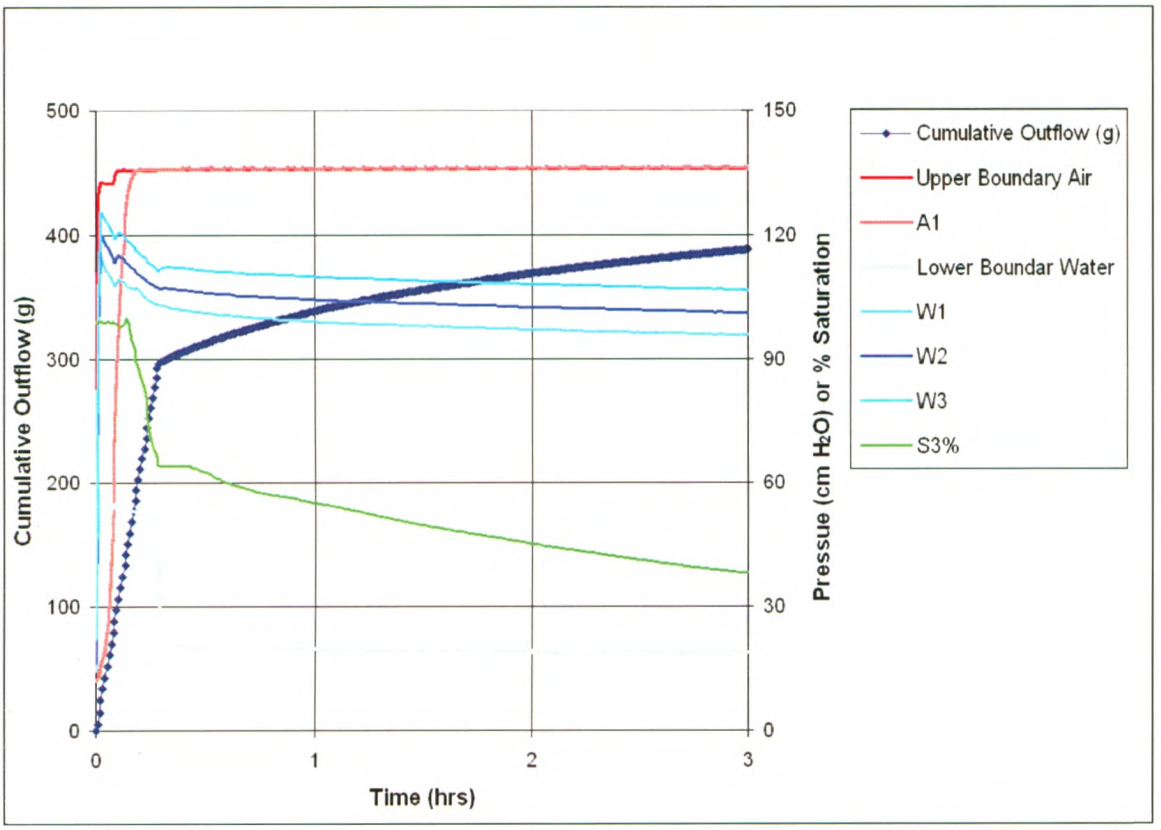

Figure A.4. Measured experimental parameter for F32-F50 Dynamic Experiment 3: cumulative outflow, air pressure (A1), water pressures (W1, W2 and W3) and saturation (S3) vs. time.

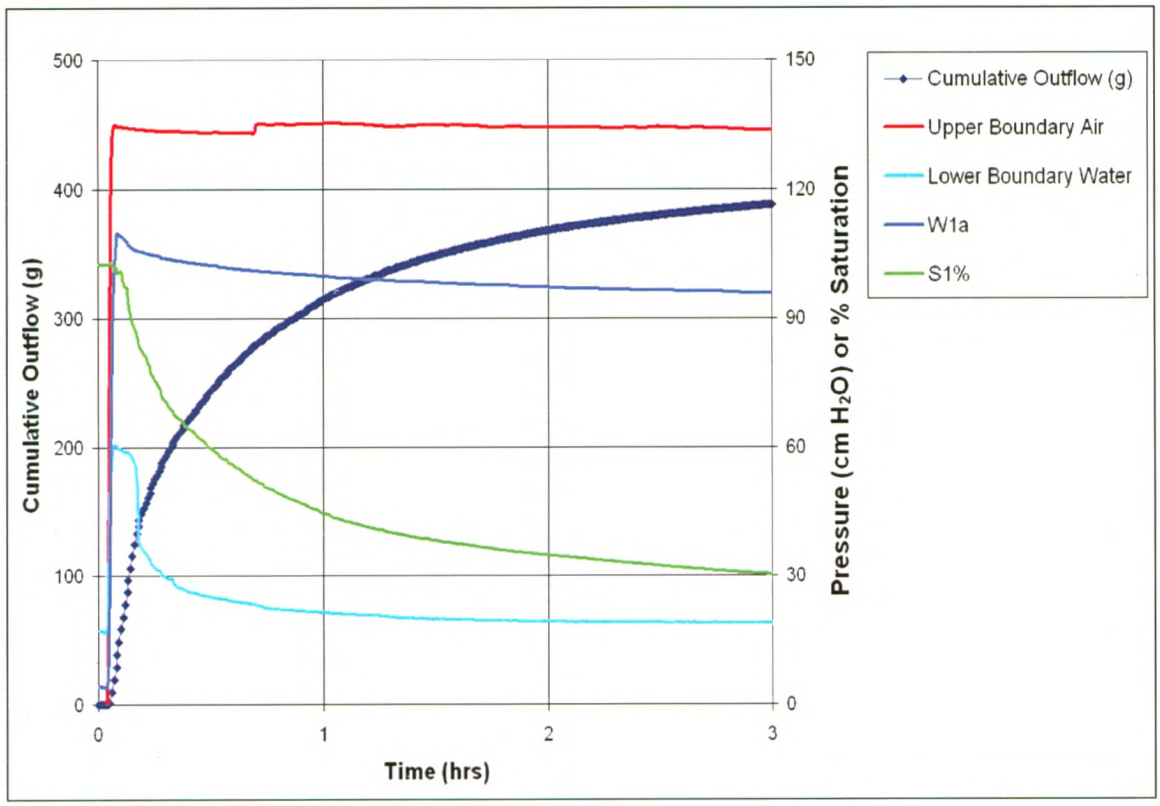

Figure A. 5. Measured experimental parameters for F32-F50 Dynamic Experiment 4: cumulative outflow, upper boundary air, water pressure (W1) and saturation (S1) vs. time

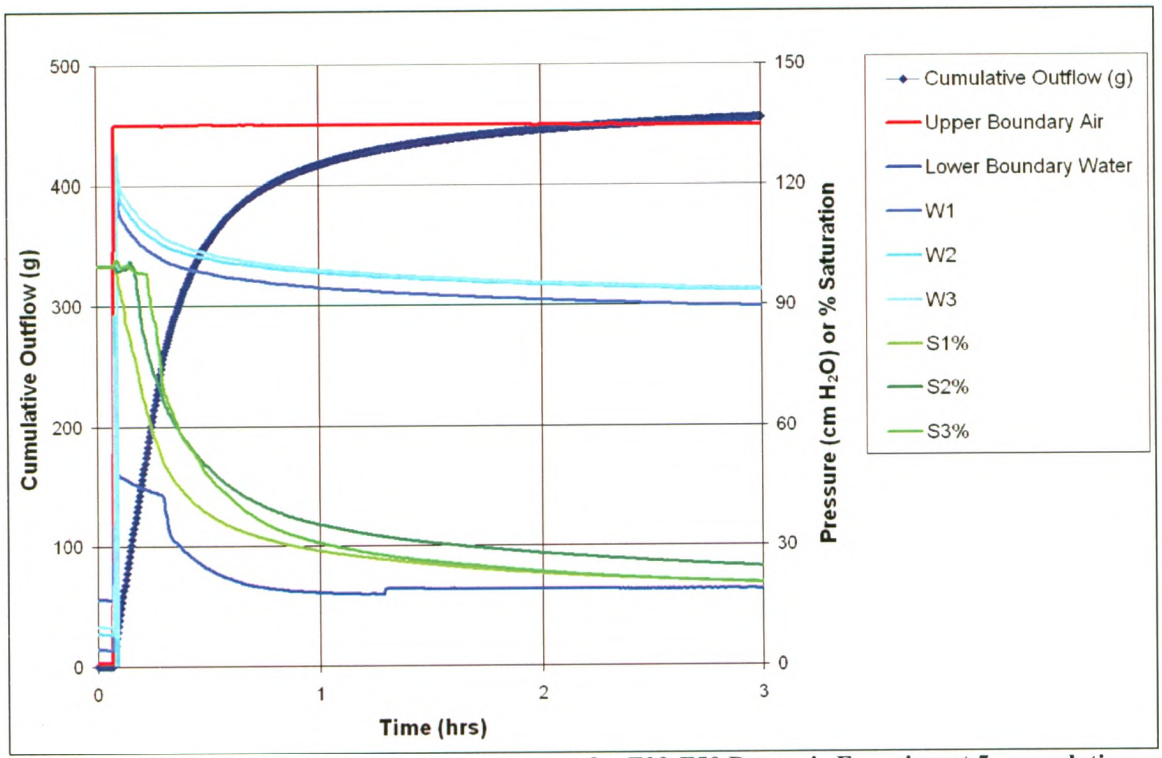

Figure A.6. Measured experimental parameters for F32-F50 Dynamic Experiment 5: cumulative outflow, air pressures (A2 and A3), water pressures (W1, W2 and W3) and saturations (S1, S2 and S3) vs. time.

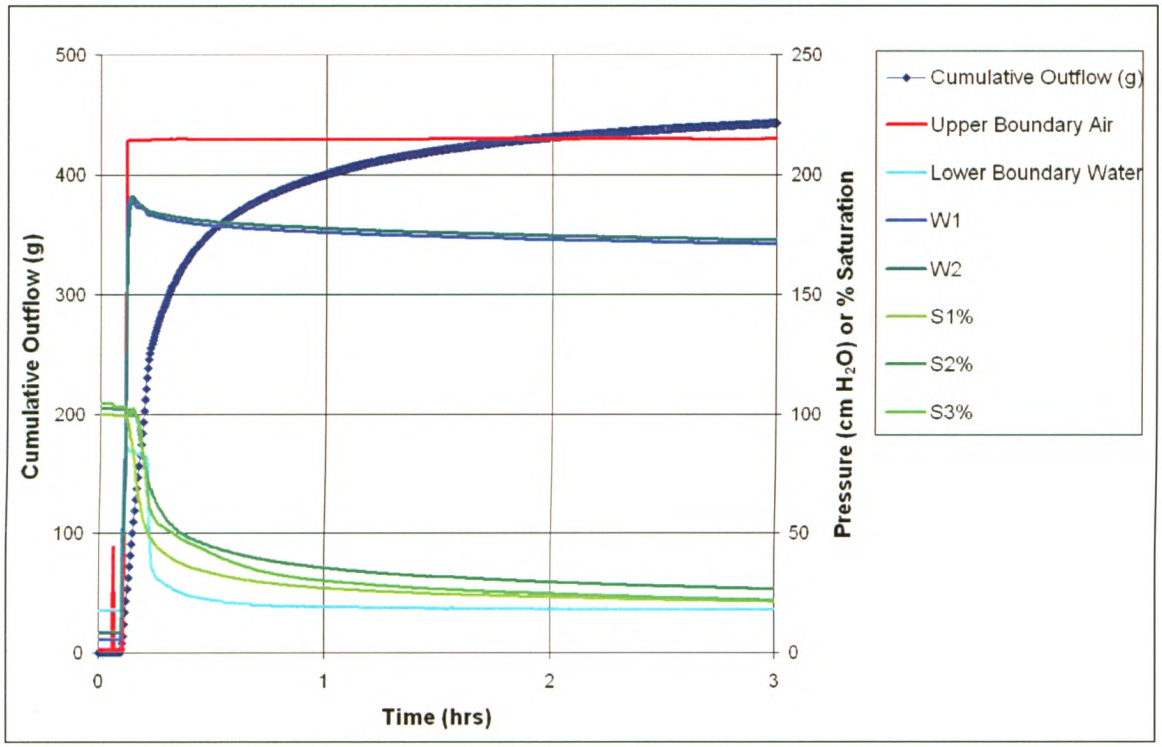

Figure A.7. Measured experimental parameter for F32-F50 Dynamic Experiment 6: cumulative outflow, upper boundary air, water pressures (W1, W2 and W3) and saturations (S1, S2 and S3) vs. time.

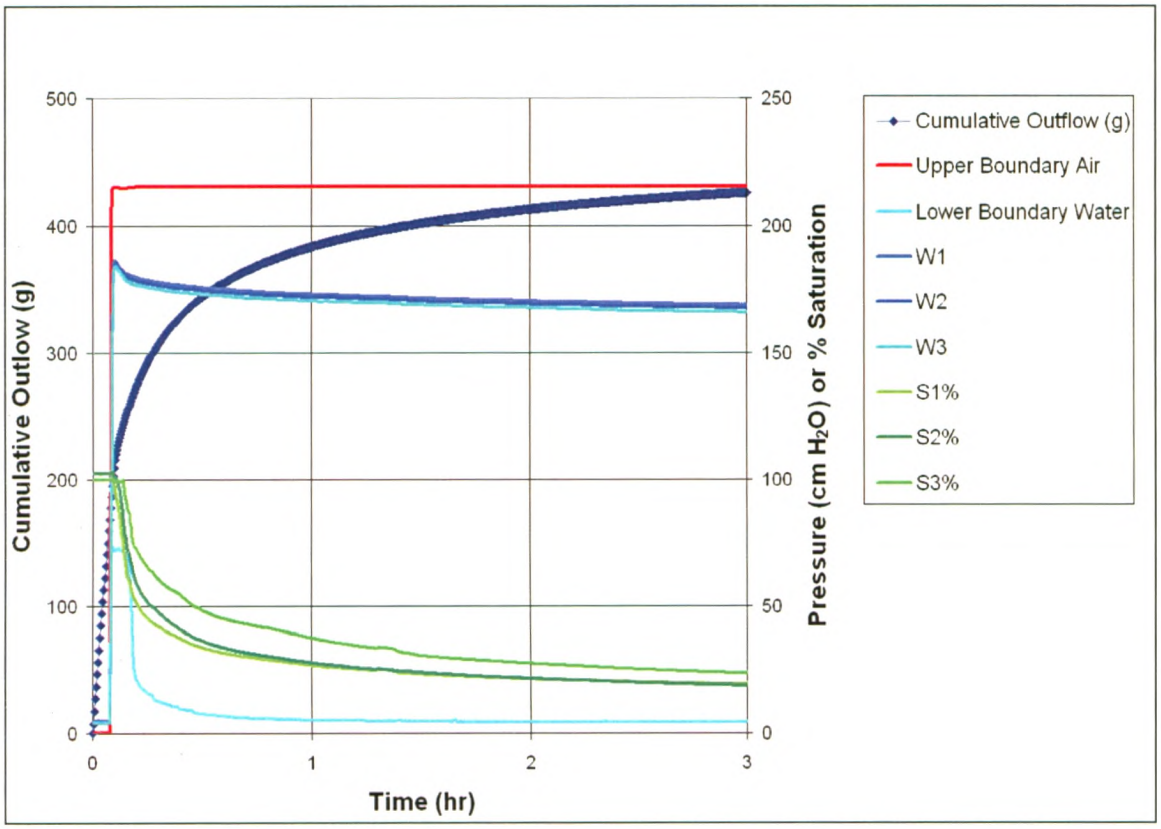

Figure A.8. Measured experimental parameter for F323-F50 Dynamic Experiment 7: cumulative outflow, upper boundary air, water pressures (W1, W2 and W3) and saturations (S1, S2 and S3) vs. time.

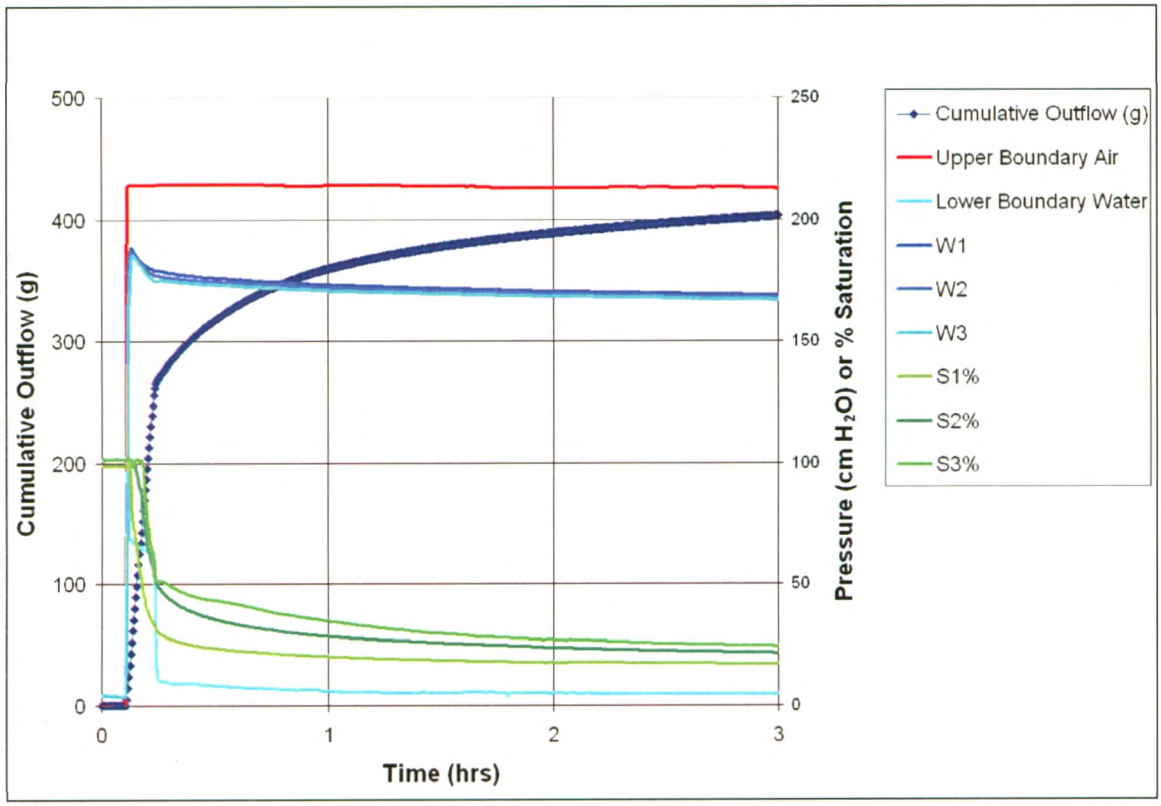

Figure A.9. Measured experimental parameter for F32-F50 Dynamic Experiment 8: cumulative outflow, upper boundary air, water pressures (W1, W2 and W3) and saturations (S1, S2 and S3) vs. time.

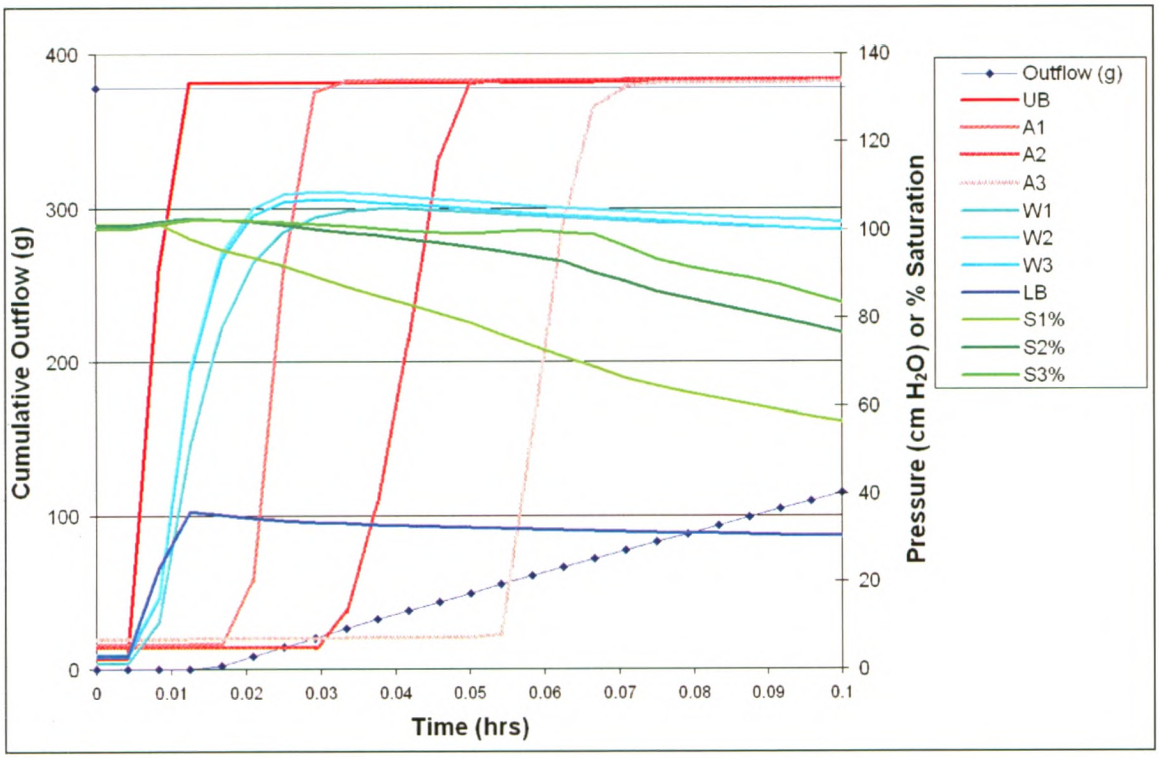

Figure A.10. Measured experimental parameter for F32-F50 Dynamic experiment 9: cumulative outflow, air pressures (A1, A2 and A3), water pressures (W1, W2 and W3) and saturations (S1, S2 and S3) vs. time.

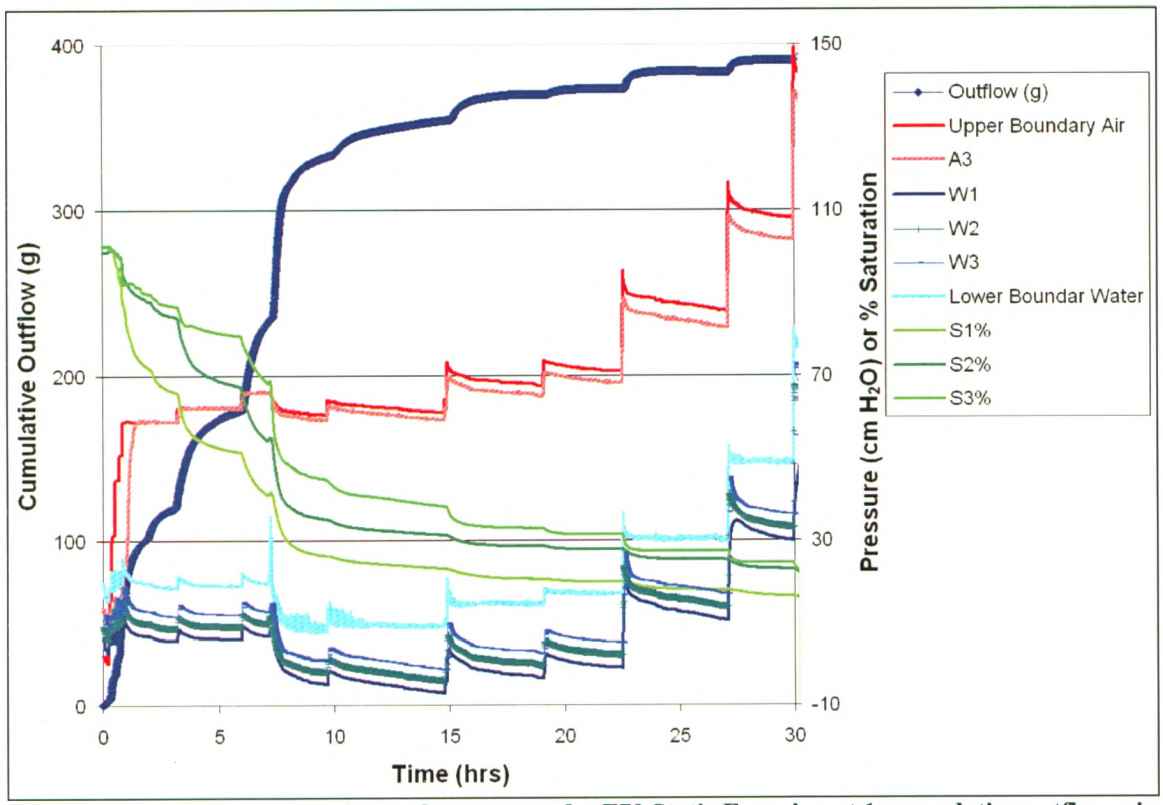

Figure A.11. Measured experimental parameter for F70 Static Experiment 1: cumulative outflow, air pressure (A3), water pressures (W1, W2 and W3) and saturations (S1, S2 and S3) vs. time.

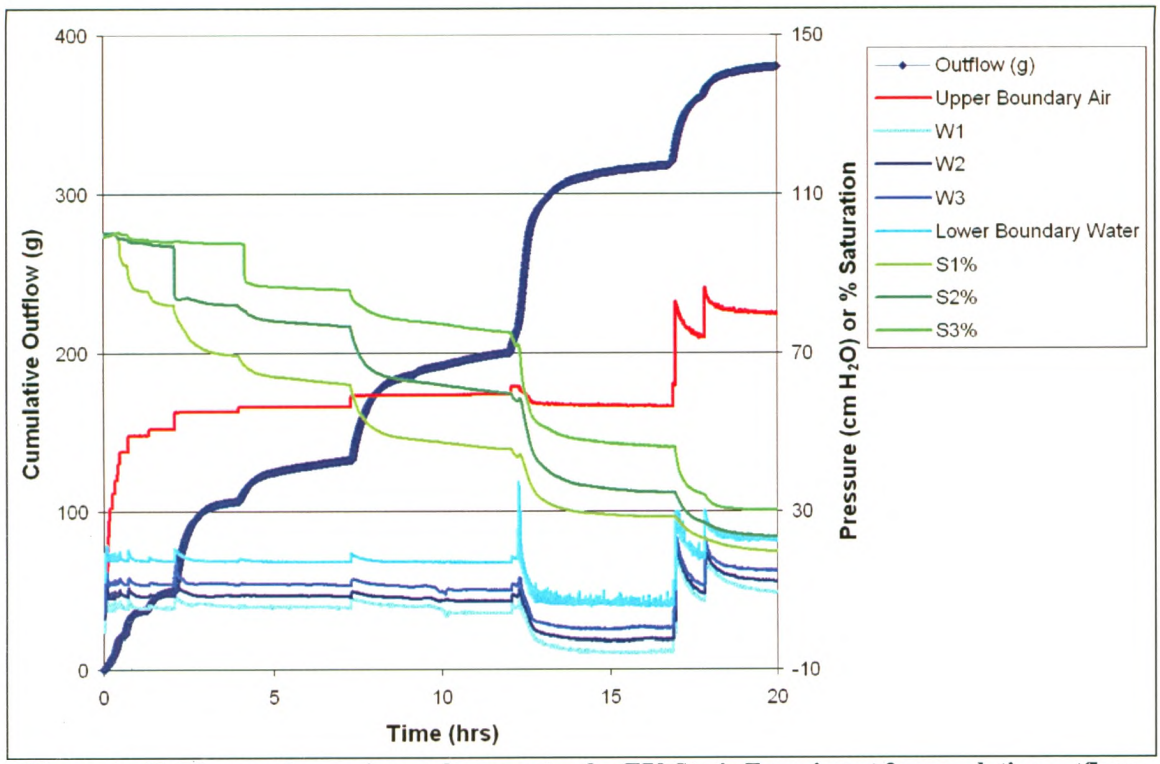

Figure A. 12. Measured experimental parameter for F70 Static Experiment 2: cumulative outflow, upper boundary air, water pressures (W1, W2 and W3) and saturations (S1, S2 and S3) vs. time.

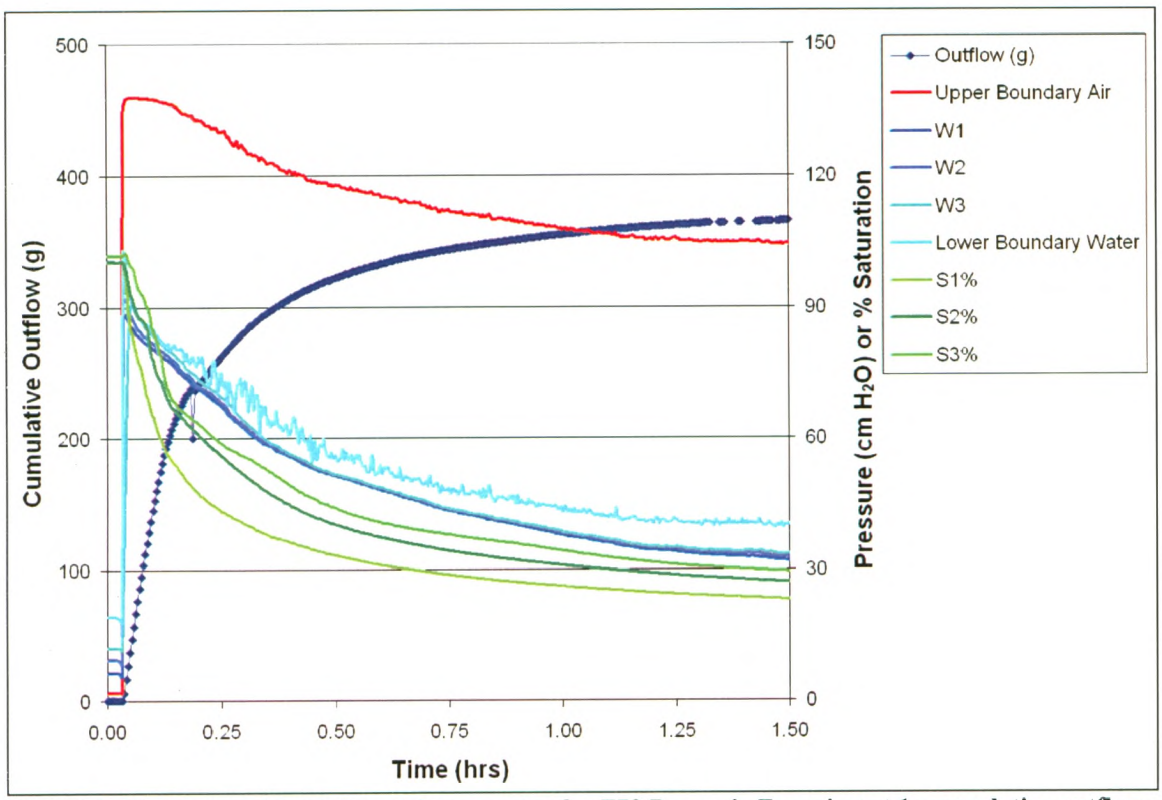

Figure A.13. Measured experimental parameter for F70 Dynamic Experiment 1: cumulative outflow, upper boundary air, water pressures (W1, W2 and W3) and saturations (S1, S2 and S3) vs. time.

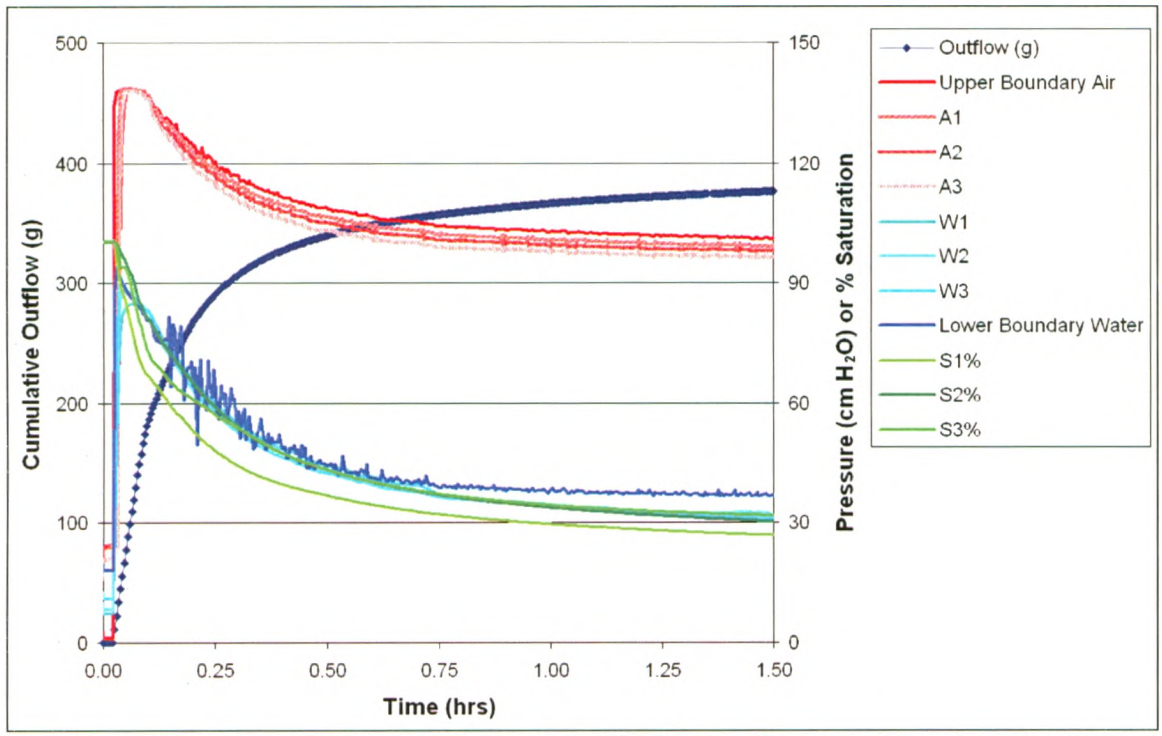

Figure A.14. Measured experimental parameter for F70 Dynamic Experiment 2: cumulative outflow, air pressures (A1, A2 and A3), water pressures (W1, W2 and W3) and saturations (S1, S2 and S3) vs. time.

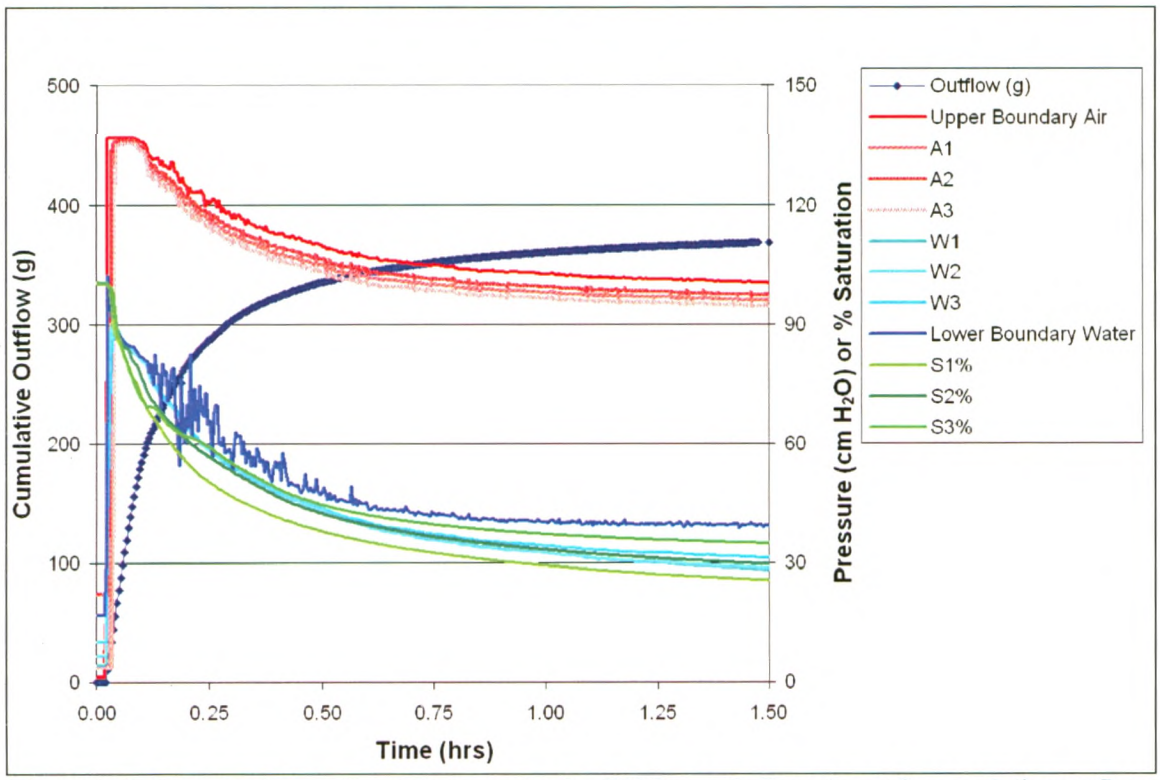

Figure A.15. Measured experimental parameter for F70 Dynamic Experiment 3: cumulative outflow, air pressures (A1, A2 and A3), water pressures (W1, W2 and W3) and saturations (S1, S2 and S3) vs. time.

Appendix B: Investigating the Relationship between dP_c and dS_w/dt

This section presents results from the analysis of the linear relationship between dP_c and dS_w/dt. Figures B.1 to B.2 shows the linear fits to experimentally determined dP_c vs. dS_w/dt for dynamic experiments. Table B.1 to B.3 show the linear fit parameters i.e. the gradient (τ) and the offset. Figures B.7 to B.10 show a comparison of dP_c vs. S_w and dS_w/dt vs S_w for measured and averaged parameters for F32-F50 Dynamic experiments 7 and 8. These graphs show that the averaged parameters were a good estimate of measured parameters.

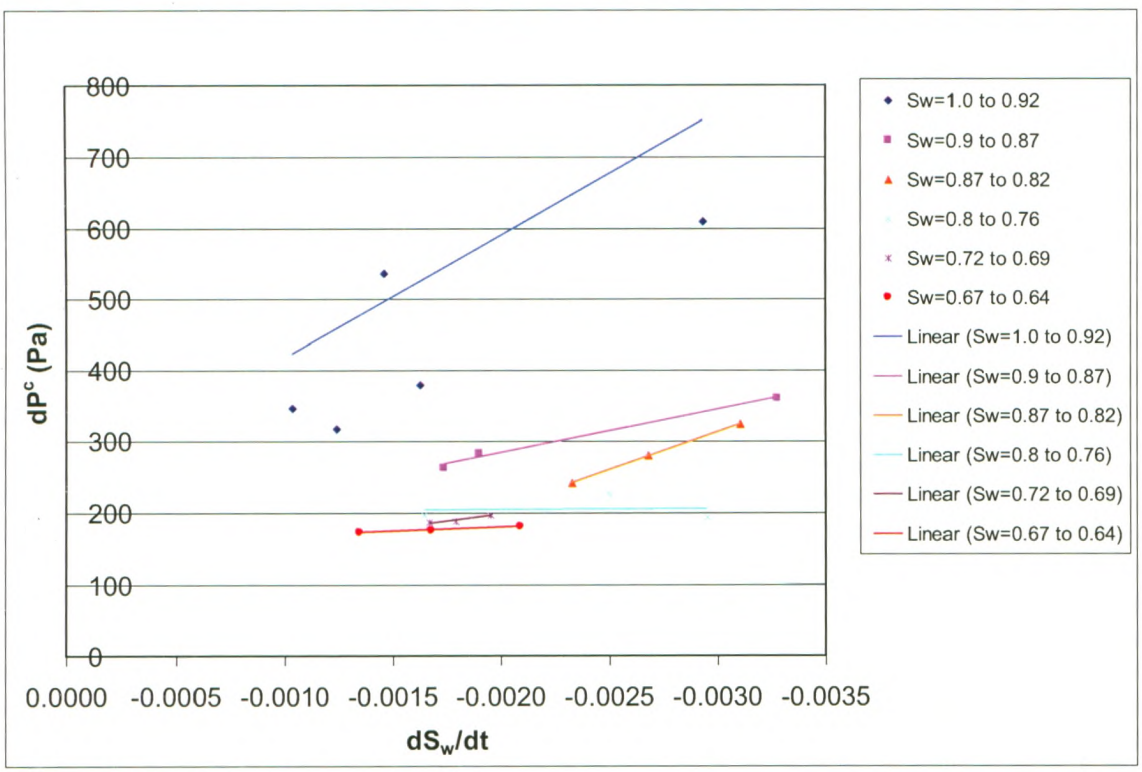

Figure B.1. Linear fits to experimentally determined dPc vs. dSw/dt for F32-F50 Dynamic Experiment 8.

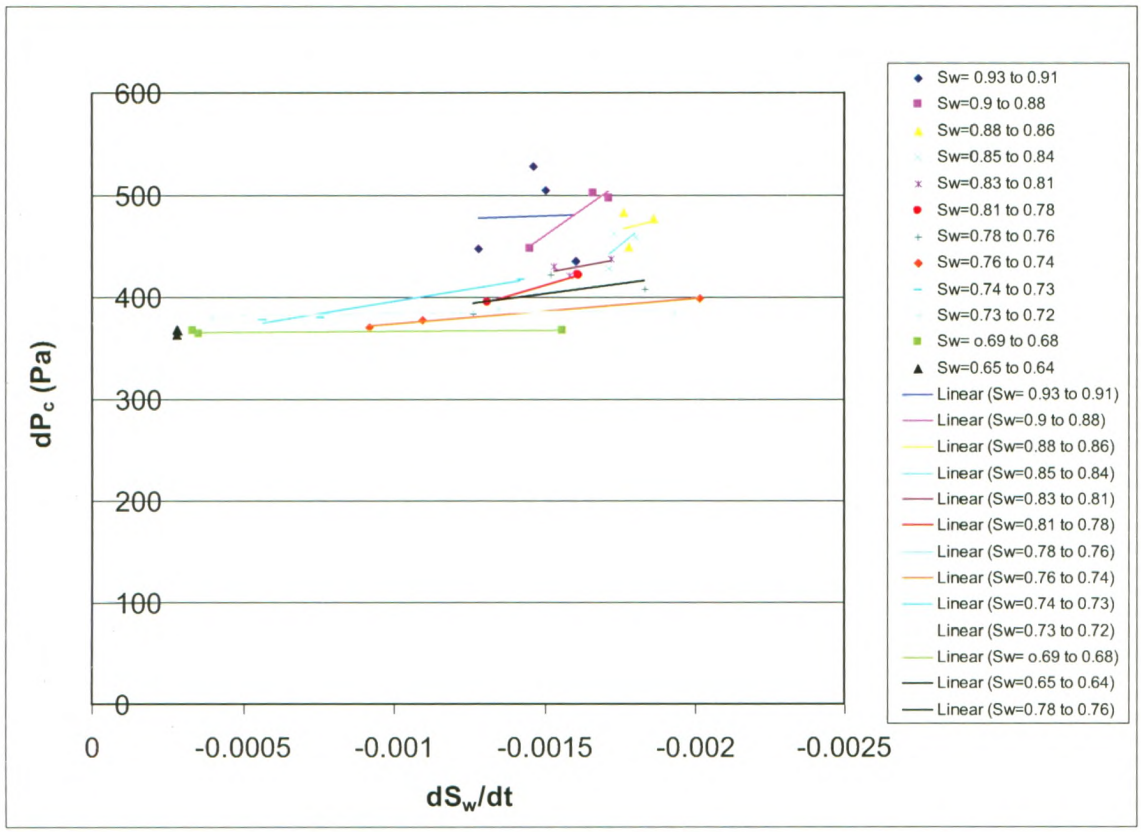

Figure B.2. Linear fits to experimentally determined dPc vs. dSw/dt for F32-F50 Dynamic Experiment 7.

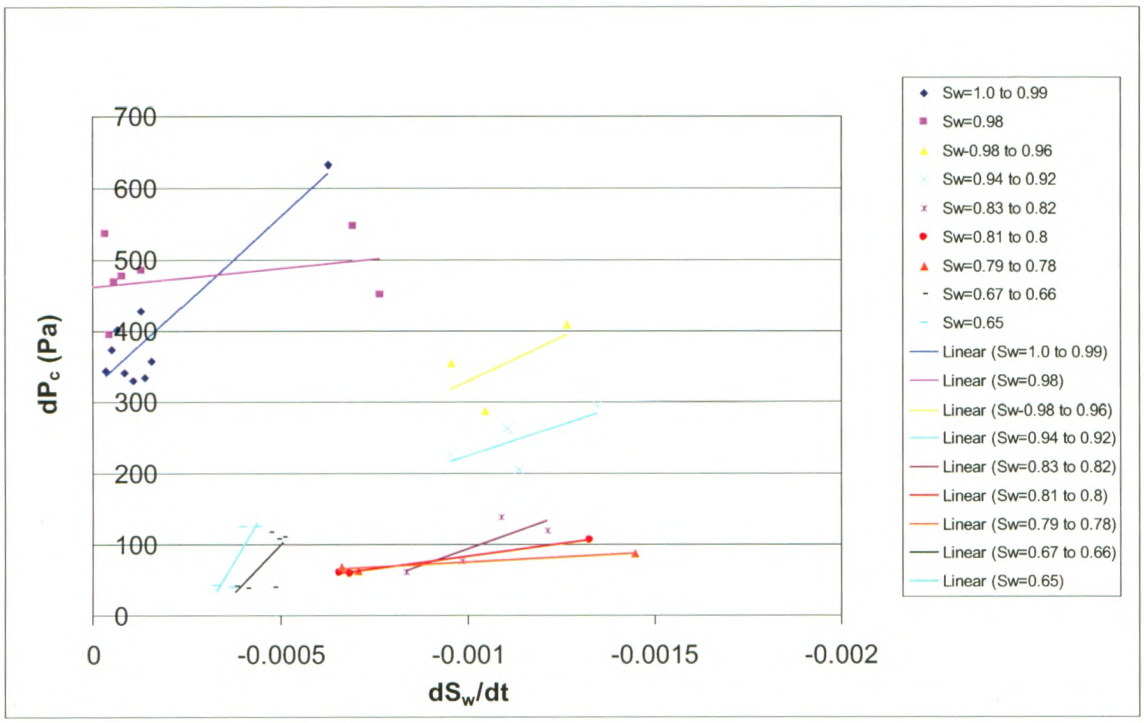

Figure B.3. Linear fits to experimentally determined dPc vs. dSw/dt for F32-50 Dynamic Experiment 5.

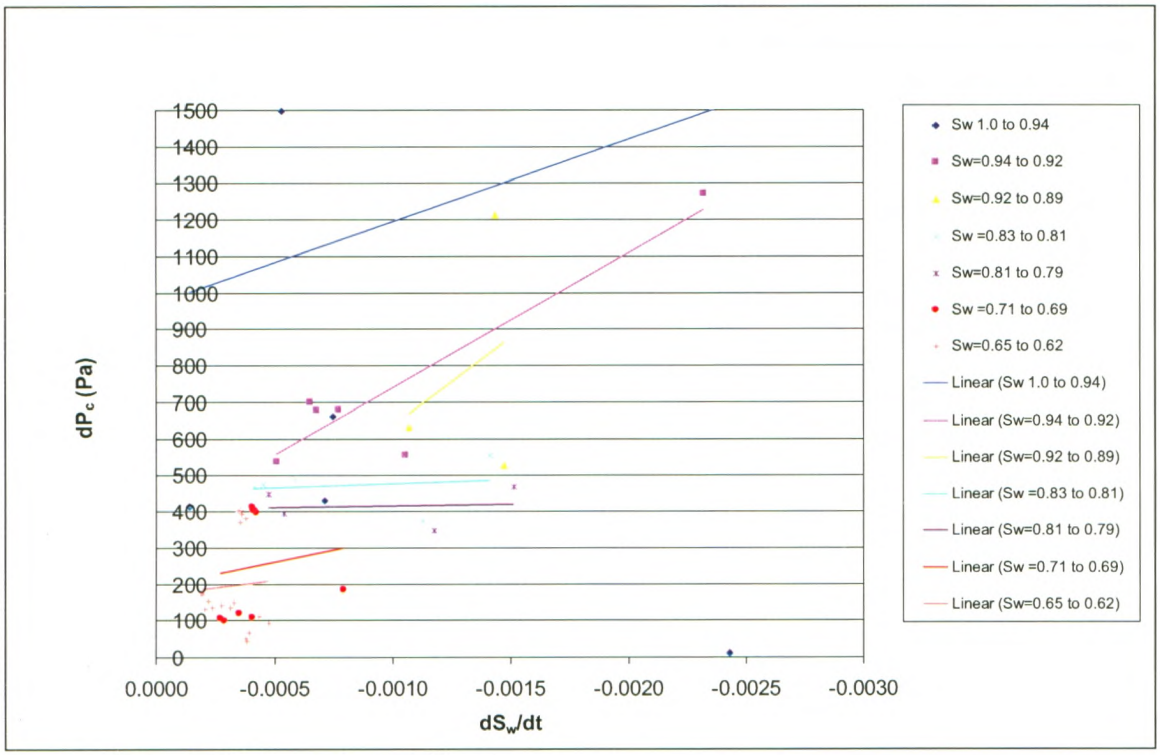

Figure B.4. Linear fits to experimentally determined dPc v.s. dSw/dt for F70 Dynamic Experiment 2.

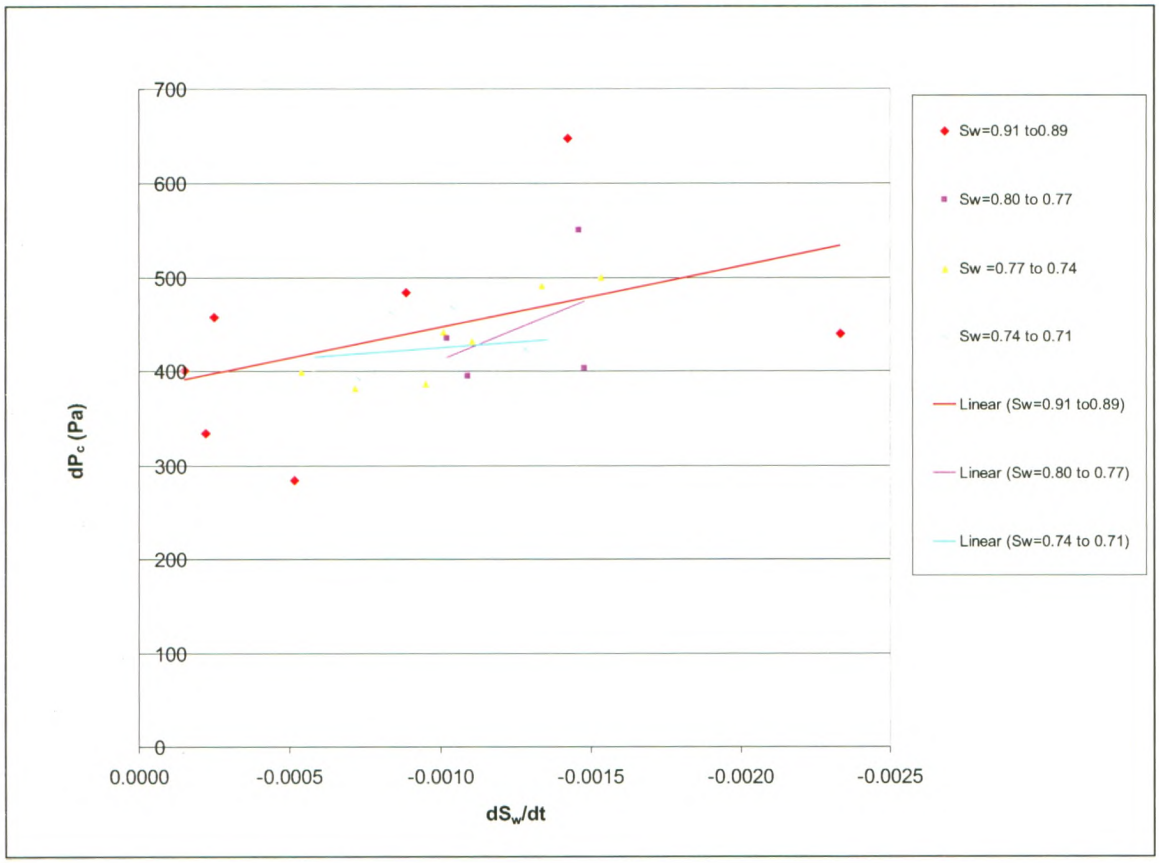

Figure B.5. Linear fits to experimentally determined dPc v.s. dSw/dt for F70 Dynamic Experiment 1.

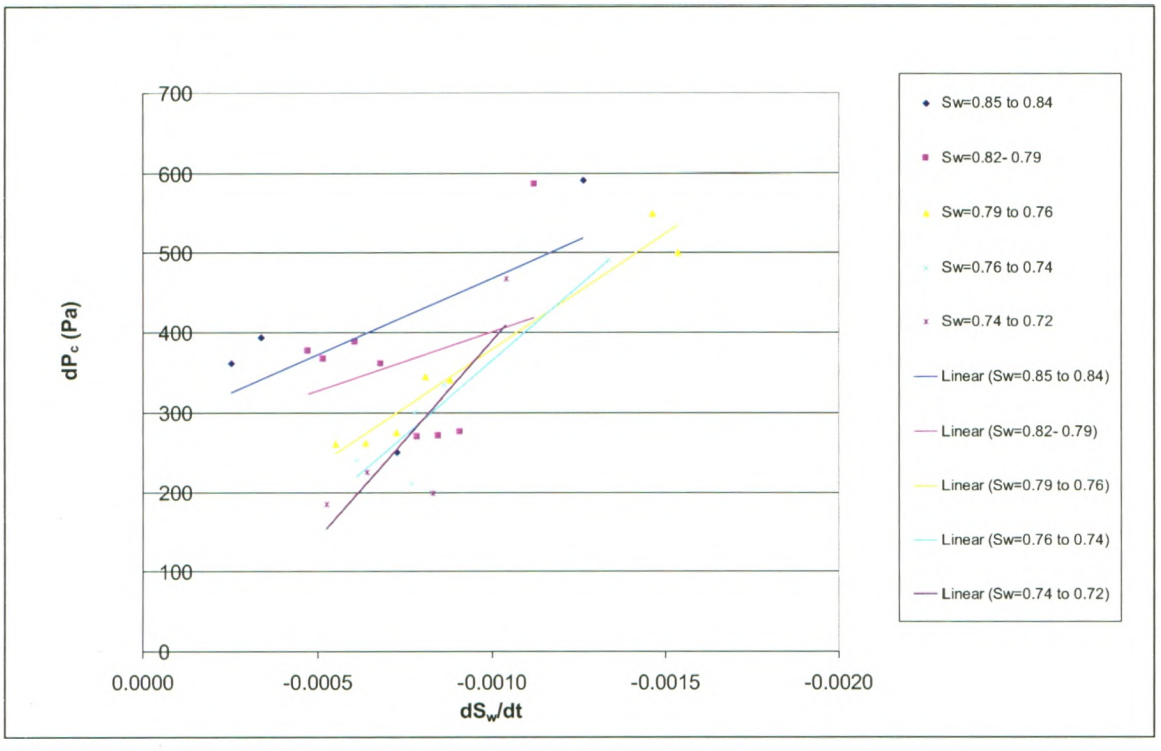

Figure B.6. Linear fits to experimentally determined dPc v.s. dSw/dt for F70 Dynamic Experiment 3.

Table B.1. Linear fit parameters for F32-F50 Dynamic Experiments at Pair=135 cm water

Experiment Name	Saturation Range		τ (kg(ms-1) or slope	Intercept	RSQ	No. of data points
	Upper Limit	Lower Limit				
F32-F50 Dynamic experiment 5 (L2 and L3)	1.00	0.99	480287.00	320.12	0.84	10
	0.99	0.98	38347.53	467.01	0.06	9
	0.98	0.96	242695.17	86.72	0.41	3
	0.96	0.94	170054.95	55.19	0.48	4
	0.84	0.82	187487.97	-94.06	0.69	4
	0.82	0.80	72154.91	10.58	0.79	3
	0.80	0.78	28150.35	38.82	0.54	3
	0.68	0.66	546595.41	-174.42	0.49	6
	0.65	0.65	891643.98	-259.65	0.74	4

Table B.2. Linear fit parameters for F32-F50 Dynamic Experiments at Pair= 214cm water

Experiment Name	Saturation Range		τ ($kg.m^{-1}.s^{-1}$) or slope	Intercept (Pa)	RSQ	No. of data points
	Upper Limit	Lower Limit				
F32-F50 Dynamic experiment 7 (L1, L2 and L3)	0.93	0.91	11628.45	462.41	0.00	4
	0.90	0.88	207724.34	148.88	0.93	3
	0.88	0.86	71609.29	341.75	0.04	3
	0.86	0.84	241864.33	27.55	0.35	3
	0.83	0.81	55633.27	340.49	0.40	3
	0.81	0.78	89230.38	278.06	1.00	3
	0.78	0.76	39736.34	343.41	0.33	3
	0.76	0.74	24817.05	348.92	0.99	3
	0.74	0.73	49108.82	346.88	0.96	3
	0.73	0.72	3302.91	380.31	0.33	3
	0.69	0.68	1869.19	364.86	0.39	3
	0.66	0.65	1077716.15	65.46	0.38	3
F32-F50 Dynamic experiment 8 (L2 and L3)	1.00	0.92	173689.67	241.49	0.19	6
	0.89	0.87	60895.51	161.21	0.99	3
	0.87	0.82	107159.65	-8.27	1.00	3
	0.80	0.76	1571.48	200.79	0.00	3
	0.72	0.69	38697.33	118.98	0.90	3
	0.67	0.64	11459.98	155.95	0.97	3

Table B.3. Linear fit parameters for F70 Dynamic Experiments at Pair = 135cm water

Experiment Name	Saturation Range		τ ($kg.m^{-1}.s^{-1}$) or slope	Intercept (Pa)	RSQ	No. of data points
	Upper Limit	Lower Limit				
F70 Dynamic experiment 1 (L1, L2 and L3)	0.89	0.86	65293.23	381.67	0.20	7
	0.80	0.77	130025.04	281.51	0.19	4
	0.76	0.74	126298.76	302.07	0.80	7
	0.74	0.71	23258.91	401.93	0.05	7
F70 Dynamic experiment 2 (L1, L2 and L3)	1.00	0.94	224866.19	970.65	0.01	6
	0.94	0.92	370698.36	367.87	0.85	6
	0.91	0.89	481096.28	155.68	0.08	3
	0.83	0.81	21305.63	454.14	0.02	5
	0.81	0.79	8746.52	405.17	0.01	4
	0.71	0.69	132161.74	192.19	0.02	9
	0.65	0.62	83570.00	166.75	0.00	18
F70 Dynamic experiment 3 (L1, L2 and L3)	0.85	0.84	193530.79	274.66	0.39	4
	0.82	0.79	148225.43	251.74	0.10	8
	0.79	0.76	291235.24	87.97	0.95	7
	0.76	0.74	376211.74	-11.42	0.88	5
	0.74	0.72	498575.89	-109.50	0.71	4

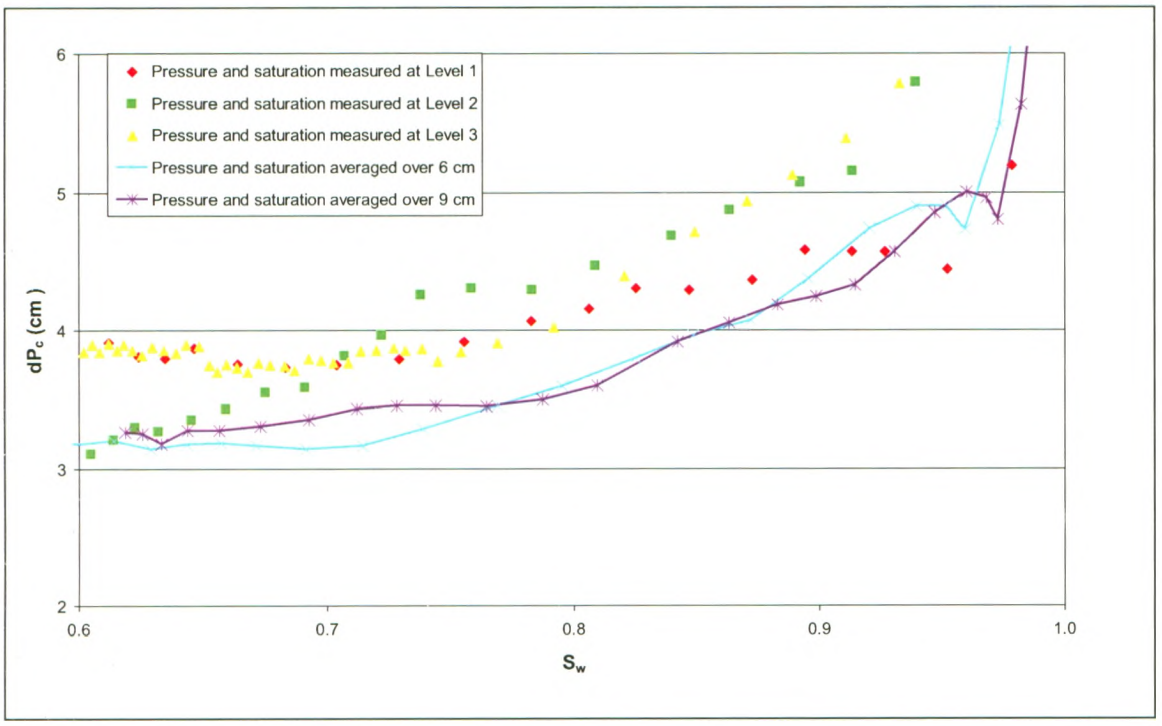

Figure B.7. A comparison of dPc v.s. Sw determined from either point measurements or from averaged pressures and saturations for F32-F50 Dynamic Experiment 7.

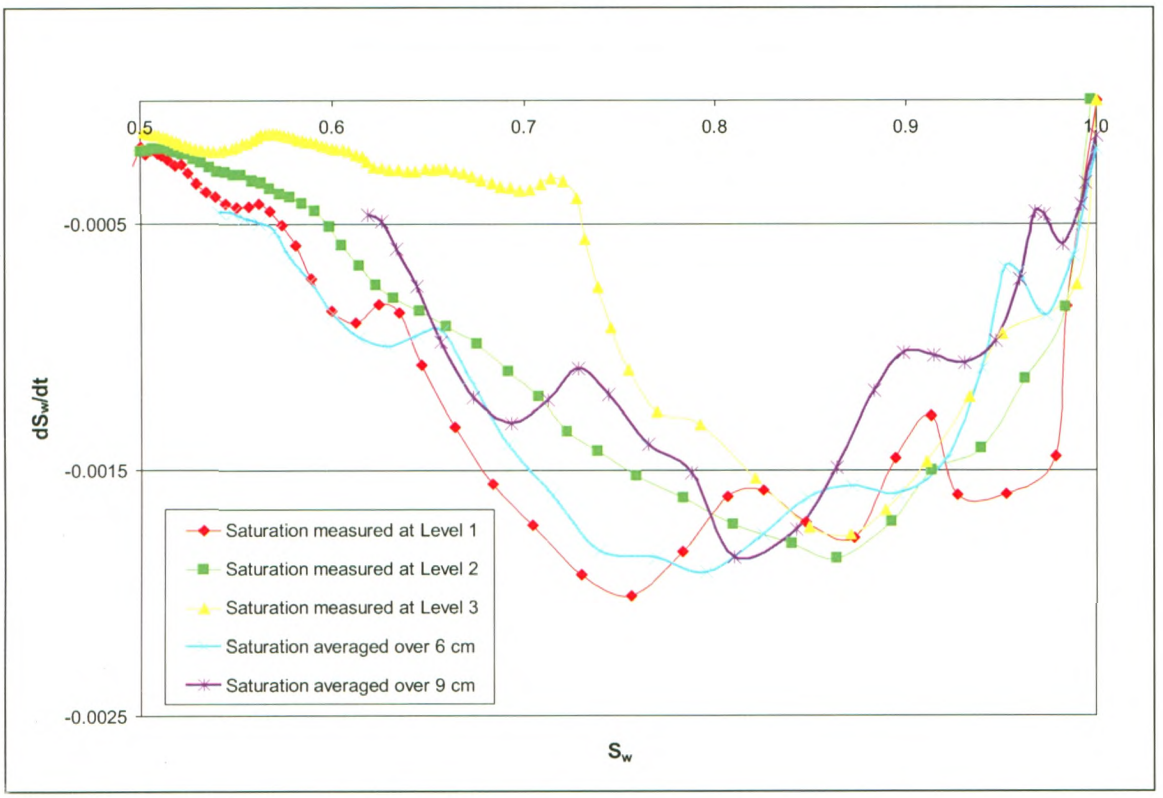

Figure B. 8. A comparison of dSw/dt v.s. Sw determined from either point measurements or from averaged saturations for F32-F50 Dynamic Experiment 7.

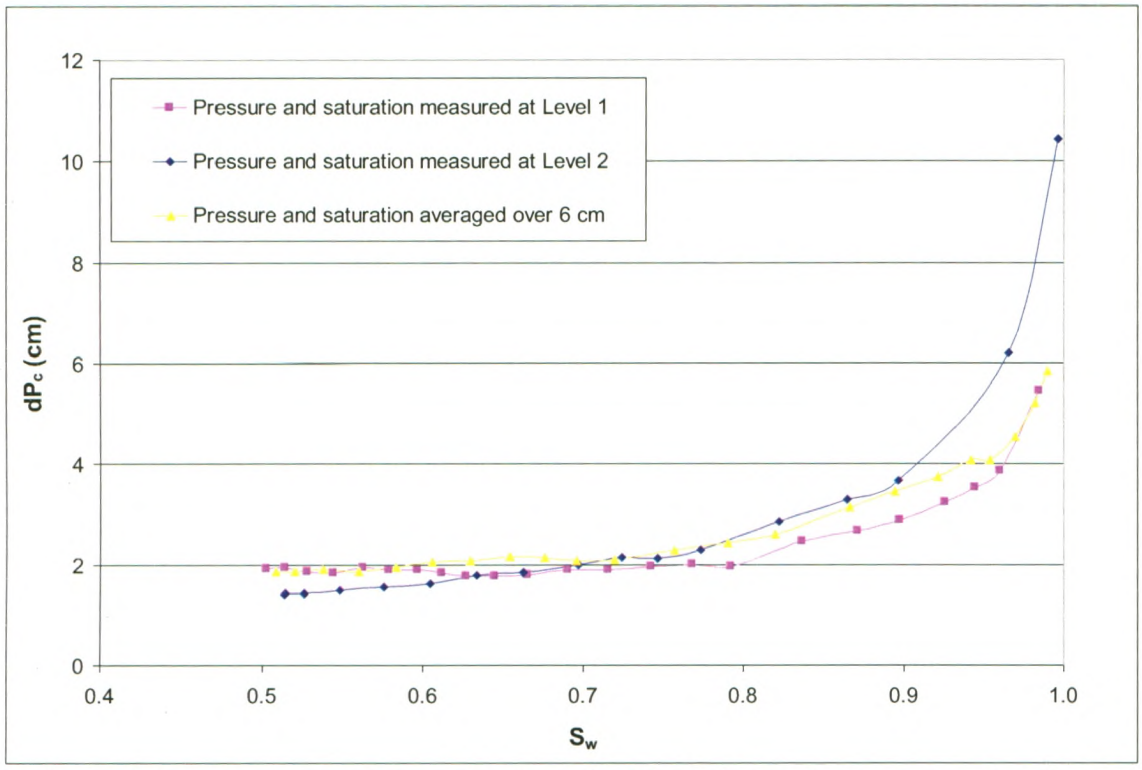

Figure B.9. A comparison of dPc v.s. Sw determined from either point measurements or from averaged pressures and saturations for F32-F50 Dynamic Experiment 8.

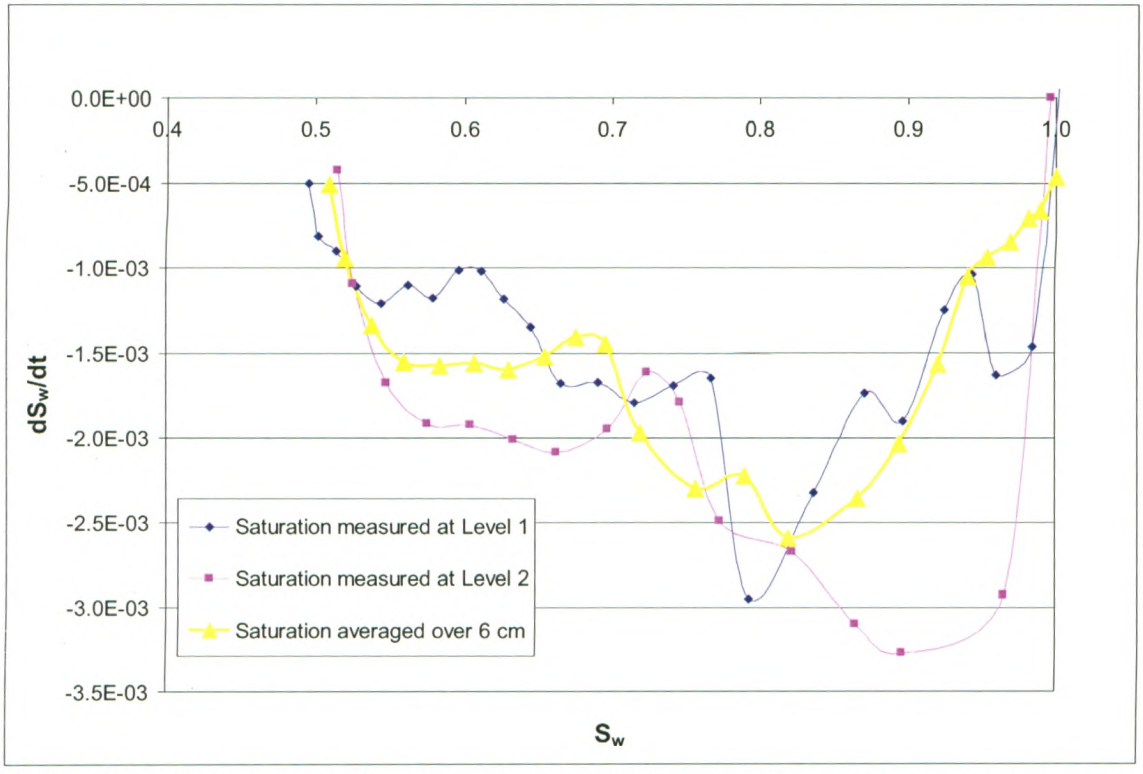

Figure B.10. A comparison of dSw/dt v.s. Sw determined from either point measurements or from averaged saturations for F32-F50 Dynamic Experiment 8.

Appendix C: EC-5 Soil Moisture Probe Calibration Comparison

To enhance the accuracy of the EC-5 probes, to capture the full saturation range and to factor in any interference which may have been caused by the probes close proximity to an aluminum surface (pressure cell), two soil specific calibration procedures were investigated.

C.2 Linear Fit to Multi-Step Outflow Experimental Data

A multi-step primary drainage experiment was first conducted. During the experiment, air was introduced to the column at the upper boundary in a step-wise manner, allowing the system to equilibrate between pressure steps. Once the entry pressure of the sand is achieved, de-saturation of the soil sample begins. The experiment ends when the system reaches the irreducible water saturation.

Water outflow occurs at the lower boundary. Cumulative outflow was measured with a balance (Ohaus Adventure Pro). Air pressure was measured at the upper boundary while water pressure was measured at the lower boundary. Saturation was measured by ec-5 probes positioned at three levels (7cm, 10cm and 13cm from lower boundary). Next the van Genuchten capillary pressure saturation relationship [41] was used to fit the experimental outflow data. To do this the column domain was divided into 20 horizontal

slices with Δx = 1cm. At each equilibrium point, the volume of water in the column (V) is calculated by

$$V = \int_0^L \phi . S_w . A . \delta x \qquad \textbf{(C.2)}$$

Where L is the length of the column, A is the cross-sectional area of the column, S_w is wetting phase saturation and ϕ is the porosity. S_w is given by

$$S_w = S_{eff}(1 - (S_{rw} + S_{rnw}) \qquad \textbf{(C.3)}$$

Where S_{eff} is the effective water saturation, S_{rw} is the residual water saturation and S_{rnw} is the residual non-wetting phase saturation. S_{eff} is given by

$$S_{eff} = [1 + (\alpha . P_c)^n]^{-m} \qquad \textbf{(C.4)}$$

α, n and m are the van Genuchten fit parameters. m is given by m = 1-2/n. Here P_c is the difference between non-wetting and wetting fluid pressures taken at equilibrium. For each equilibrium point, outflow volume was given by the difference in V between two consecutive equilibrium points.

The MS Excel Solver function was used to minimize the difference between the experimental equilibrium outflow volume and the calculated equilibrium outflow volume by fitting α, n and S_{rw}. The measured cumulative outflow from the multi-step outflow experiment, along with the van Genuchten fit to this outflow data is presented in Figure

C1. The van Genuchten fit parameter α, n and S_{rw} were determined to be $3.8x10^{-02}$, 8.0 and 0.12 respectively.

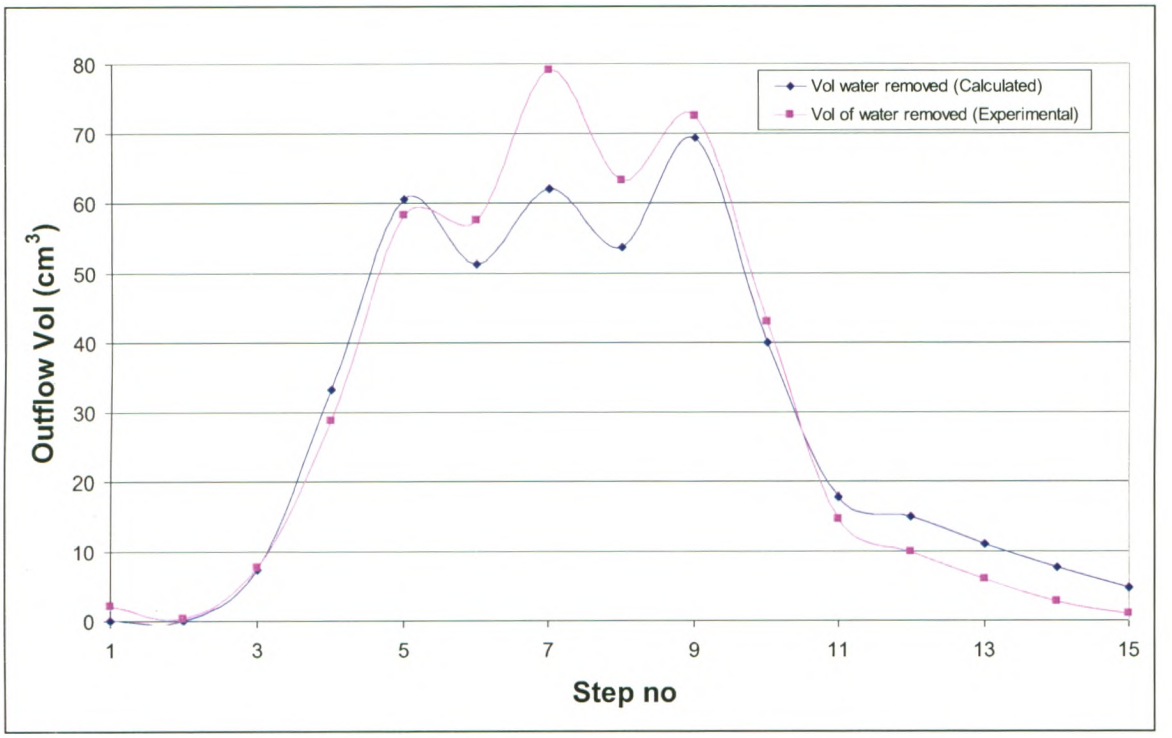

Figure C. 1. Comparison of the measured and fitted outflow volume for the multi-step primary drainage experiment.

Since a relationship between VWC and experimental EC-5 readings was required for calibration, saturation data from the domain location of each EC-5 probe was converted to VWC using the following formula.

$$VWC = \phi S_w \qquad \textbf{(C.5)}$$

where ϕ is porosity (determined to be 0.31, see Dry Packing and Saturation Procedure). Next the VWC was plotted against the corresponding experimental equilibrium EC-5 readings (raw mV). The linear fit of VWC v.s. raw mV for each probe yields the required linear calibration curve (see Figure C.2). The linear calibration equations provided a

reasonable fit to experimental EC-5 data. However, they fail to accurately represent the moisture content in the near dry and near saturated regions (see Figure C.3).

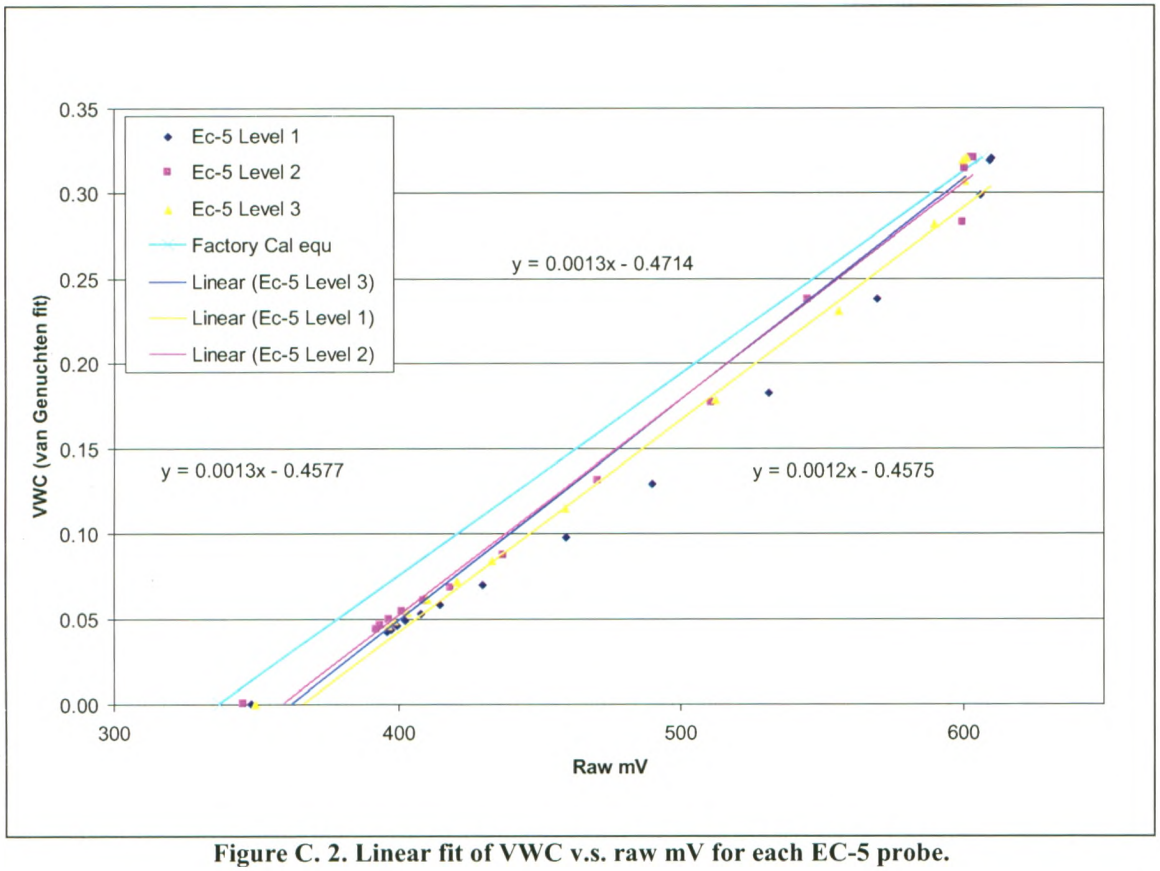

Figure C. 2. Linear fit of VWC v.s. raw mV for each EC-5 probe.

C.3 Two Point Calibration Procedure

An alternate calibration procedure developed by Sakaki et al; 2008, can be used to calibrate the EC-5 probes so that moisture content in the near dry and near saturated ranges are accurately predicted. In this procedure, raw EC-5 readings are taken at 0% saturation i.e. dry sand and at 100% saturation i.e. after saturating the column. Raw EC-5 readings (mV) were recorded by the Campbell Scientific data logger. These readings were first converted to ADC counts using the following equation:

$$ADC = mV * 1.6384 \qquad \textbf{(C.6)}$$

Saturation is then given by

$$S_w = \frac{(ADC^{2.5} - ADC_{dry}^{2.5})}{(ADC_{sat}^{2.5} - ADC_{dry}^{2.5})} \quad \textbf{(C.7)}$$

Where *ADC* is the experimental readings (converted using Eq.3.5) taken during an outflow experiment, ADC_{dry} is the reading taken at 0% saturation (dry soil) and ADC_{sat} is the reading taken at 100% saturation.

C.4 Comparison of EC-5 Calibration procedures

The root mean square error (RMSE) was used to quantitatively compare van Genuchten fit saturations to saturations calculated from EC-5 experimental data at the 15 equilibrium points obtained from the multi-step outflow experiment.

For each equilibrium point, EC-5 experimental saturation values were calculated by applying either the linear (see Figure C.2) or the quadratic calibration procedure (see Figure C.4). Results indicate that the saturation calculated at level 1, 2 and 3 using the quadratic equation yielded RMSE values that were 73.7 %, 95.1% and 49.0% lower than saturation calculated with the linear calibration equation at each respective level.

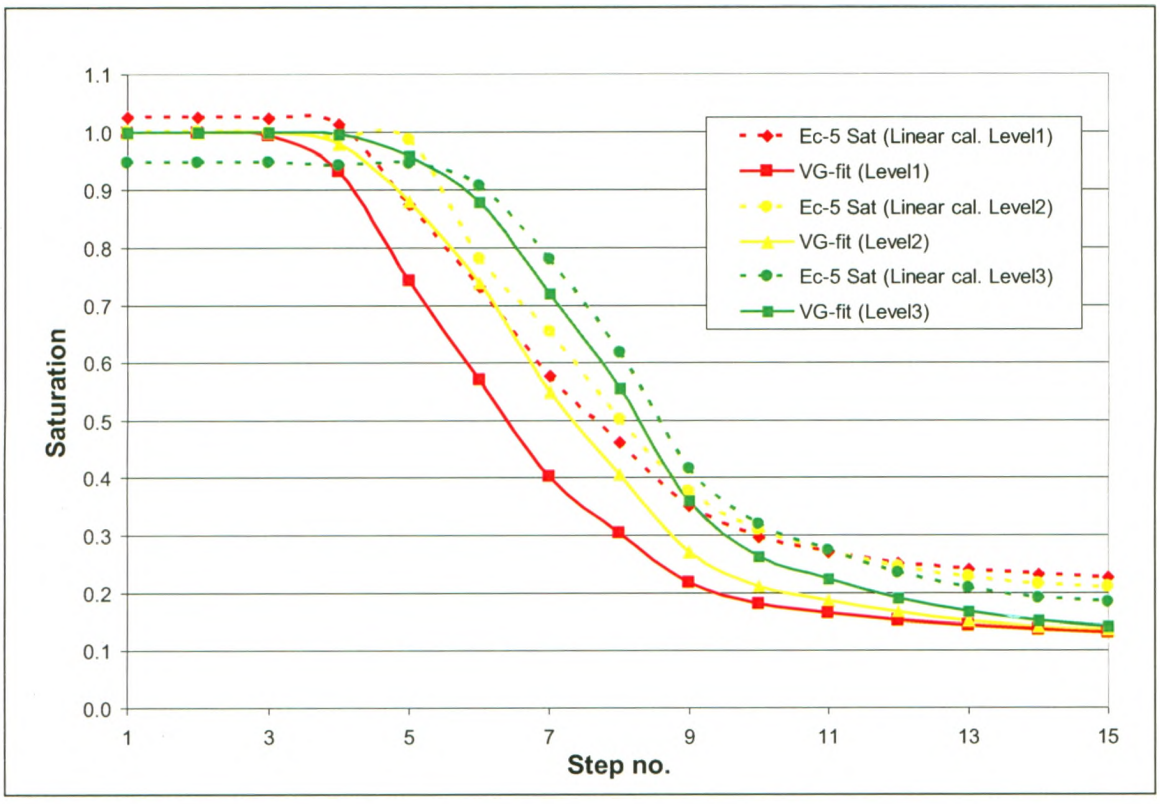

Figure C. 3. A comparison of the linear calibration and the V.G. fit to experimental data.

An examination of Figure C.4 reveals that in addition to having lower RMSE values for each level, the quadratic equation is capable of an accurate determination of the saturation at $S_w = 1$ and at S_{rw}. At 100% saturation, the linear calibration procedure over predicts saturation at level1 while at level 3 it under predicts the saturation. At residual saturation, the linear equation over predicts the saturation for all three levels.

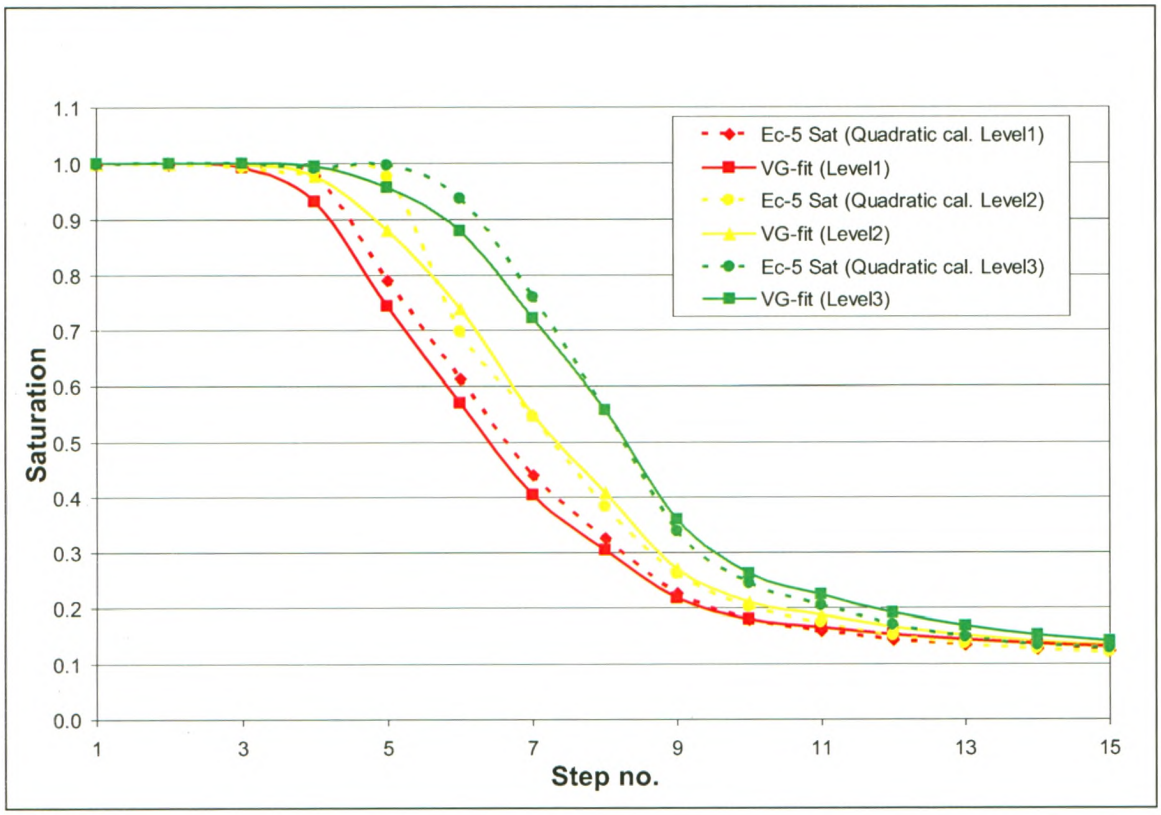

Figure C. 4. A comparison of the quadratic calibration and the V.G. fit to experimental data.

The two point calibration procedure has been shown to significantly improve the accuracy of the saturation predictions and is capable of capturing saturation over the full range of saturation values i.e. 0 to 100%. Therefore the quadratic calibration procedure was chosen to determine the saturation from EC-5 experimental data for all experiments presented in this study.

Appendix D: Saturated Hydraulic Conductivity Example

In this section, a representative example of the linear relationship between delta H and flow rate is provided. Here the gradient of the linear fit gives the saturated hydraulic conductivity according to Darcy's law.

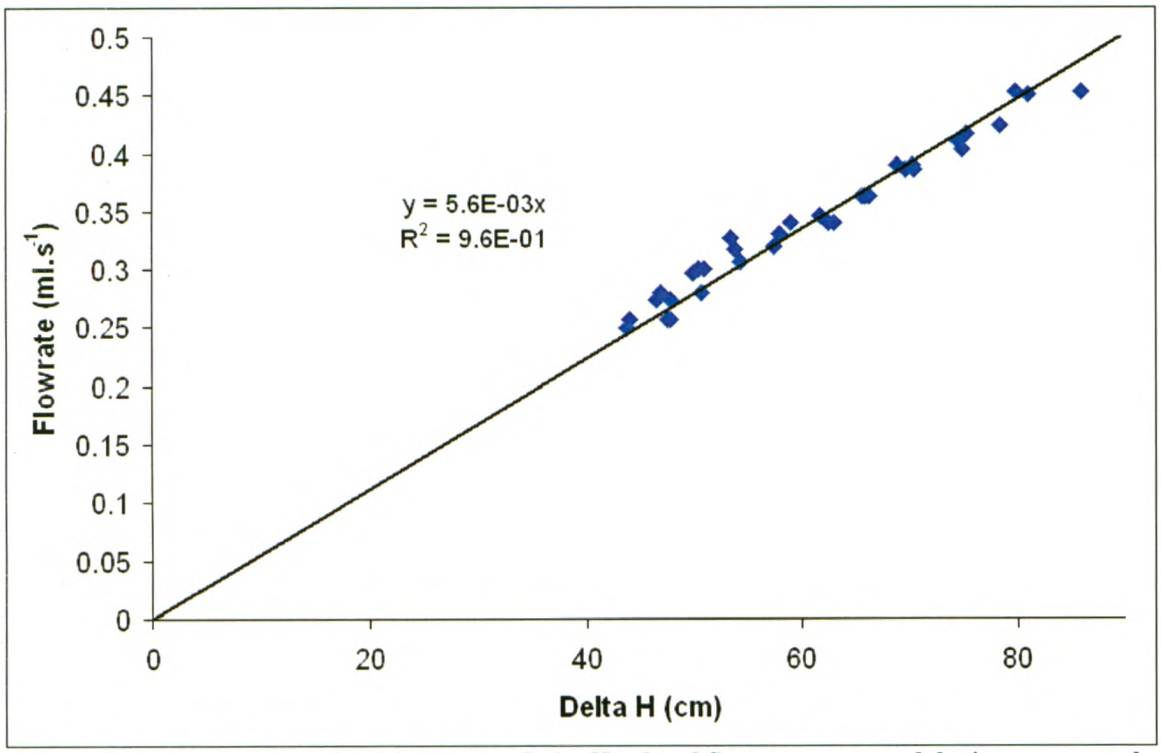

Figure D.1. The linear relationship between Delta Head and flow rate measured during a saturated hydraulic conductivity experiment.